National Library of Canada
Acquisitions and Bibliographic Services Branch
395 Wellington Street
Ottawa, Ontario
K1A 0N4

Bibliothèque nationale du Canada
Direction des acquisitions et des services bibliographiques
395, rue Wellington
Ottawa (Ontario)
K1A 0N4

Your file Votre référence

Our file Notre référence

NOTICE

The quality of this microform is heavily dependent upon the quality of the original thesis submitted for microfilming. Every effort has been made to ensure the highest quality of reproduction possible.

If pages are missing, contact the university which granted the degree.

Some pages may have indistinct print especially if the original pages were typed with a poor typewriter ribbon or if the university sent us an inferior photocopy.

Reproduction in full or in part of this microform is governed by the Canadian Copyright Act, R.S.C. 1970, c. C-30, and subsequent amendments.

AVIS

La qualité de cette microforme dépend grandement de la qualité de la thèse soumise au microfilmage. Nous avons tout fait pour assurer une qualité supérieure de reproduction.

S'il manque des pages, veuillez communiquer avec l'université qui a conféré le grade.

La qualité d'impression de certaines pages peut laisser à désirer, surtout si les pages originales ont été dactylographiées à l'aide d'un ruban usé ou si l'université nous a fait parvenir une photocopie de qualité inférieure.

La reproduction, même partielle, de cette microforme est soumise à la Loi canadienne sur le droit d'auteur, SRC 1970, c. C-30, et ses amendements subséquents.

Canada

UNIVERSITY OF ALBERTA

A BIDIRECTIONAL OPTICAL COMMUNICATION SYSTEM USING FABRY-PEROT LASER DIODES AS TRANSCEIVERS

BY

DINO JOHN CORAZZA

A thesis submitted to the Faculty of Graduate Studies and Research in partial fulfillment of the requirements for the degree of **Master of Science**.

DEPARTMENT OF **ELECTRICAL ENGINEERING**

Edmonton, Alberta
Fall 1993

National Library
of Canada

Acquisitions and
Bibliographic Services Branch

395 Wellington Street
Ottawa, Ontario
K1A 0N4

Bibliothèque nationale
du Canada

Direction des acquisitions et
des services bibliographiques

395, rue Wellington
Ottawa (Ontario)
K1A 0N4

Your file Votre référence

Our file Notre référence

The author has granted an irrevocable non-exclusive licence allowing the National Library of Canada to reproduce, loan, distribute or sell copies of his/her thesis by any means and in any form or format, making this thesis available to interested persons.

L'auteur a accordé une licence irrévocable et non exclusive permettant à la Bibliothèque nationale du Canada de reproduire, prêter, distribuer ou vendre des copies de sa thèse de quelque manière et sous quelque forme que ce soit pour mettre des exemplaires de cette thèse à la disposition des personnes intéressées.

The author retains ownership of the copyright in his/her thesis. Neither the thesis nor substantial extracts from it may be printed or otherwise reproduced without his/her permission.

L'auteur conserve la propriété du droit d'auteur qui protège sa thèse. Ni la thèse ni des extraits substantiels de celle-ci ne doivent être imprimés ou autrement reproduits sans son autorisation.

ISBN 0-315-88165-8

Canada

UNIVERSITY OF ALBERTA

RELEASE FORM

NAME OF AUTHOR: **Dino John Corazza**

TITLE OF THESIS: **A Bidirectional Optical Communication System Using Fabry-Perot Laser Diodes as Transceivers**

DEGREE: **Master of Science**

YEAR THIS DEGREE GRANTED: **Fall 1993**

Permission is hereby granted to the University of Alberta Library to reproduce copies of this thesis and to lend or sell such copies for private, scholarly or scientific research purposes only.

The author reserves all other publication and other rights in association with the copyright in the thesis, and except as hereinbefore provided neither the thesis nor any substantial portion thereof may be printed or otherwise reproduced in any material form whatever without the author's prior written permission.

Dino Corazza

10130 - 73 Street
Edmonton, Alberta
T6A 2W9

DATE: August 24/93

I dedicate this thesis to my grandparents.

UNIVERSITY OF ALBERTA

FACULTY OF GRADUATE STUDIES AND RESEARCH

The undersigned certify that they have read, and recommend to the Faculty of Graduate Studies and Research for acceptance, a thesis entitled **A BIDIRECTIONAL OPTICAL COMMUNICATION SYSTEM USING FABRY-PEROT LASER DIODES AS TRANSCEIVERS** submitted by **DINO JOHN CORAZZA** in partial fulfillment of the requirements for the degree of **MASTER OF SCIENCE.**

G. D. Cormack, Supervisor

B. P. Keyworth, Internal Examiner

J. N. McMullin, Internal Examiner

D. J. Harrison, External Examiner

DATE: August 24/93

ABSTRACT

A novel bidirectional optical communication system using Fabry-Perot laser diodes as transceivers is evaluated for suitability in cost sensitive short haul applications. The transceivers are switched between transmitting and detecting states in this half duplex system. The system differs from other half duplex arrangements as the detection function is achieved by monitoring diode junction voltage changes while the device is biased just below lasing threshold.

The detection properties of Fabry Perot laser diodes biased just below threshold are discussed. Responsivity, sensitivity and detector response time are predicted by modifying existing theory for traveling wave laser detectors from Gustavsson [22]. Responsivity is also verified experimentally.

Switching times between transmitting and receiving states are predicted by solving the laser rate equations and the laser turn off time is experimentally verified. It is found that the system switching time is much faster than switching times for other half duplex transceiver systems that have a zero or negative applied bias voltage for detection.

The proposed system is also compared with other configurations for bidirectional optical communication. It is found that a major problem in implementing this proposed system is maintaining a close match of the wavelength dependent responsivity of the receiving laser to the emission wavelength of the transmitting laser.

ACKNOWLEDGEMENTS

I would like to express my most sincere thanks to my supervisor, Dr. George Cormack, for his investment of time and constant support throughout the duration of this project. In addition, I would like to thank Dr. Barrie Keyworth and Dr. Ian MacDonald for their helpful advice and discussions. I would also like to thank the members of my examining committee, Dr. George Cormack, Dr. Barrie Keyworth, Dr. Jim McMullin, and Dr. Jed Harrison for reviewing this thesis.

I wish to extend special thanks to many of my colleagues for their helpful advice and perspective, including Eric Cauchon, Chris Janz, Dobby Lam, Greg May, Tim Neufeld and Kinh Pham. Special thanks also goes to Chris Janz and Kevin Robbie for proofreading a first draft of this thesis. In addition, I would like to thank David Clegg for numerous practical suggestions and helpful comments provided in the lab.

Finally, I would like to acknowledge the Natural Sciences and Engineering Research Council, Telecommunications Research Laboratories, and the University of Alberta for their generous financial support without which this work would not have been possible.

TABLE OF CONTENTS

1. INTRODUCTION 1
- 1.1 SHORT HAUL SYSTEM CONFIGURATIONS 1
  - 1.1.1 System #1: Two Unidirectional systems 2
  - 1.1.2 System #2: Use of a single fibre and directional couplers 2
  - 1.1.3 System #3: Switching the laser between transmitting and detecting states 3
  - 1.1.4 System #4: Self Heterodyne full duplex system 4
  - 1.1.5 System #5: Full duplex system using traveling wave laser amplifiers 5
- 1.2 FAST SWITCHING HALF DUPLEX SYSTEM-INTRODUCTION 6
- 1.3 SYSTEM PERFORMANCE GOALS 6

2. THE FAST SWITCHING HALF DUPLEX (FSHD) SYSTEM 7
- 2.1 SYSTEM OPERATION 7
- 2.2 LASER AS A TRANSMITTER 10
- 2.3 LASER AS A DETECTOR 10
  - 2.3.1 Responsivity of a Fabry-Perot laser diode 11
    - 2.3.1.1 Introduction 11
    - 2.3.1.2 Theoretical predictions 13
    - 2.3.1.3 Experimental setup 24
    - 2.3.1.4 Experimental results and reconciliation with theory 25
  - 2.3.2 Sensitivity of a Fabry-Perot laser diode 39
    - 2.3.2.1 Introduction to theoretical model 39
    - 2.3.2.2 Noise calculation of a Fabry-Perot amplifier 39
    - 2.3.2.3 Results 43
- 2.4 SYSTEM CONSIDERATIONS 51
  - 2.4.1 Switching time between states 52
    - 2.4.1.1 The rate equations 52
    - 2.4.1.2 Transmitting to receiving turn-off time 53

2.4.1.3 Experimental turn-off time results 57
2.4.1.4 Turn-on delay time and relaxation oscillations 59
2.4.1.5 Concluding remarks on switching time 63
2.4.2 Response time of a Fabry-Perot laser diode 63
2.4.3 Synchronization of the two laser transceivers 64
2.4.4 System impairments 65
2.4.5 Power budget calculation 67
3. POSSIBLE IMPROVEMENTS TO THE FSHD SYSTEM 69
3.1 USE OF DIFFERENT LASER DIODES FOR TRANSCEIVERS 69
3.1.1 The effect of using a different laser diode on responsivity 69
3.1.2 The effect of using a different laser diode on sensitivity 70
3.2 ULTRAFAST SWITCHING POTENTIAL 71
3.3 THERMAL STABILITY PROBLEMS AND POSSIBLE SOLUTIONS 72
4. COMPARISON WITH OTHER BIDIRECTIONAL SYSTEMS 75
4.1 A COMPARISON OF THE FSHD SYSTEM WITH DIRECTIONAL COUPLER SYSTEM 75
4.2 A COMPARISON OF THE FSHD SYSTEM WITH SWITCHED SYSTEM TO ZERO BIAS 75
4.3 A COMPARISON OF THE FSHD SYSTEM WITH FULL DUPLEX LASER AMPLIFIER SYSTEM 76
5. CONCLUSIONS 79
REFERENCES 81
APPENDIX 1: RELATIONSHIP BETWEEN DIODE VOLTAGE AND CARRIER DENSITY 86
APPENDIX 2: LISTING OF MATHEMATICA PROGRAM MODEL.M 89
APPENDIX 3: LISTING OF MATHEMATICA PROGRAM NOISEFPA.M 93
APPENDIX 4: LISTING OF MATHEMATICA PROGRAM AGRAWAL.M 101

LIST OF TABLES

Table 1	Theoretical responsivity values.	21
Table 2	Measured responsivity of Fabry-Perot laser diode detectors.	37
Table 3	Cavity gain at various sidelobes.	51
Table 4	Comparison of turn-off times with [11].	58
Table 5	Calculated detector bandwidth.	64
Table 6	Power budget calculation.	68

LIST OF FIGURES

Figure 1 Simple full duplex link. 2

Figure 2 Full duplex system using directional couplers. 3

Figure 3 Simple half duplex system. 3

Figure 4 FSHD block diagram. 7

Figure 5 Transmission and detection bias points for FSHD. 7

Figure 6 Electrical and optical RZ formats. 8

Figure 7 Alternate coding scheme for asymmetric bit rates. 9

Figure 8 Voltage and current responsivity. 12

Figure 9 Change in carrier density versus frequency detuning- model. 14

Figure 10 Carrier density versus diode voltage. 15

Figure 11 Detector equivalent circuit from [21]. 18

Figure 12 Illustration of responsivity dependence on detector cavity gain.
12A: Dependence on different detector bias currents. 22
12B: Dependence on individual detector resonant gains. 22

Figure 13 Responsivity versus peak cavity gain for different sidelobes. 23

Figure 14 Experimental setup. 25

Figure 15 Responsivity results.
15A: Using source laser #3 and detect laser #5. 29
15B, 15C: Using source laser #4 and detect laser #5. 30-31
15D: Using source laser #4 and detect laser #1. 32
15E, 15F: Using source laser #1 and detect laser #5. 33-34
15G: Using source laser #3 and detect laser #1. 35

15H: Using source laser #5 and detect laser #1. 36

Figure 16 Theoretical and experimental voltage responsivity as a function of cavity gain. 38

Figure 17 Sensitivity results.
17A: BER curves for varying cavity gain with 30 MHz electrical bandwidth. 43
17B: BER curves for varying cavity gain with 10 MHz electrical bandwidth. 44
17C: Mean square noise current for 5.75 dB cavity gain. 45
17D: Mean square noise current for 9.16 dB cavity gain. 46
17E: Mean square noise current for 14.68 dB cavity gain. 47

Figure 18 BER curves for off peak gain resonances.
18A: Cavity gain = 14.68 dB, electrical bandwidth = 30 MHz. 48
18B: Cavity gain = 9.16 dB, electrical bandwidth = 30 MHz. 49
18C: Cavity gain = 14.68 dB, electrical bandwidth = 10 MHz. 50

Figure 19 Simple laser diode equivalent circuit from [11]. 54

Figure 20 Laser diode diffusion capacitance versus carrier density. 56

Figure 21 Experimental setup to measure turn-off time. 57

Figure 22 Calculated internal recombination turn-off times and observed turn-off times for different external time constants. 59

Figure 23 Laser diode transients as a result of a step increase in laser injection current from zero to 112% of the threshold current.
23A: Carrier density transient. 60
23B: Photon number transient. 61

Figure 24 Laser diode transients as a result of a step increase in laser injection current from 92% to 112% of the threshold current.
24A: Carrier density transient. 62
24B: Photon number transient. 62

Figure 25 Ultrafast switching of laser diodes. 71

Figure 26 Possible feedback control system to stabilize laser detector responsivity. 73

CHAPTER 1. INTRODUCTION

In today's telecommunications industry the need for communication systems with increased capacity has resulted in glass fibre competing with conventional twisted pair or coaxial cable as the preferred communication medium. A fibre optic communication system, as opposed to a conventional communication system utilizing a copper wire link, offers immunity to electromagnetic interference as well as a significant increase in bandwidth or bit rate. The vast potential of fibre optic communication systems was first utilized in long-haul systems, where large amounts of data are to be transported over long distances using a minimum number of repeaters. In recent years, a strong effort has been made to extend the reach of optical communications into short-haul applications, especially in the local loop of the existing telephone network. Initiatives such as "fibre to the home" (FTTH) or "fibre to the curb" (FTTC) will ultimately result in replacement of the twisted pair local loop with a fibre based local loop. With FTTH, services can be offered to subscribers that are not possible in the present system, such as remote access to libraries or data banks, ISDN, and a host of other interactive video services. The successful deployment of FTTH or any other short-haul fibre application requires a system that can adequately meet performance requirements and is cost effective for mass deployment. This thesis will focus on a novel half-duplex bidirectional scheme suitable for short-haul applications using Fabry-Perot semiconductor laser diodes as both the transmitter and receiver, or "transceiver", in the system, and will compare this novel scheme with several other different schemes that have already been suggested.

1.1 Short-haul system configurations

Many different system configurations are possible for bidirectional optical communication links. Regardless of configuration, any short-haul optical link targeted for mass deployment must be simple, inexpensive, and meet all targeted performance specifications. The first five systems discussed in Sections 1.1.1 through 1.1.5 are bidirectional links proposed by other authors and have appeared in the literature. After these systems are discussed, the system that is the main focus of this thesis is introduced in Section 1.2.

1.1.1 System #1: Two unidirectional systems

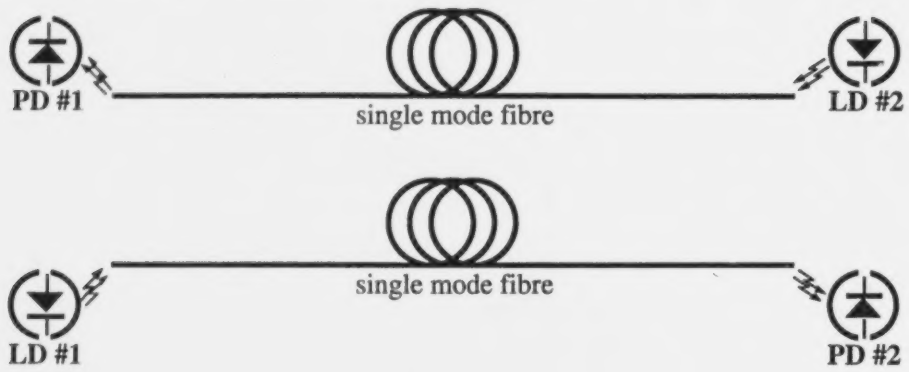

Figure 1. Simple full-duplex link. LD = laser diode, PD = photodiode.

This simplistic approach to a bidirectional optical link consists of two laser diodes as transmitters, two photodetectors as receivers, and two separate fibres, one for upstream information and one for downstream information, as illustrated in Figure 1. Attractive features of this system are its full-duplex operation, which means that information can be exchanged simultaneously in both directions, and the absence of crosstalk between the upstream and downstream channels. However, since this system has two laser diodes, two photodetectors, and two fibres, the high component cost is undesirable for widespread short-haul applications.

1.1.2 System #2: Use of a single fibre and directional couplers

The second system involves taking the two separate fibres from the first system and replacing them with a single fibre and a coupler at each end of the system, as shown in Figure 2. Operation of a bidirectional optical communication system using couplers has been demonstrated previously and reported by many authors [1-6]. Again, this system operates in full-duplex mode by simultaneously transmitting and detecting data. The system uses less fibre compared with the previous system, but the component count has increased with the addition of couplers at each end of the link. This system would also be unattractive for

widespread short-haul deployment primarily due to the additional cost of the extra components at both ends of the link.

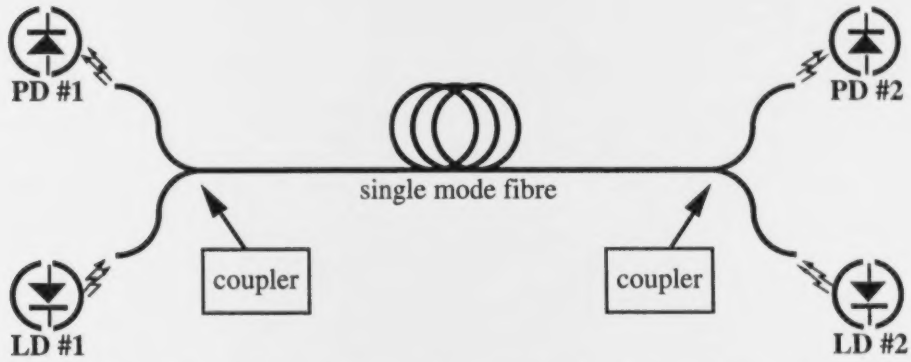

Figure 2. Full-duplex system with couplers. LD = laser diode, PD = photodiode.

1.1.3 System #3: Switching the laser between transmitting and detecting states

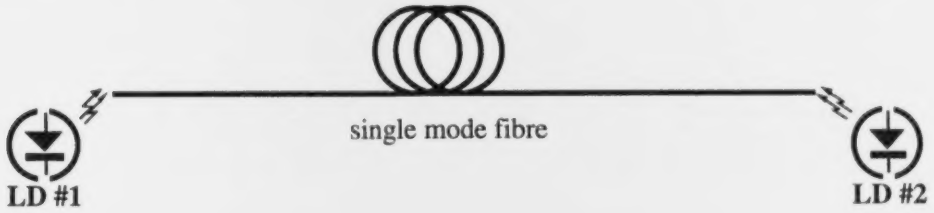

Figure 3. Simple half-duplex system. LD = laser diode.

The third system makes use of the fact that a semiconductor laser diode can operate as both a transmitter and receiver. The diode is switched between a transmitting state (forward biased above threshold) and a detecting state (zero or reverse biased). Since no other components are needed, this system is very simple, as shown in Figure 3. When a laser diode is in the detecting state, any light injected into the laser cavity from the distant source will be absorbed and create free electron hole pairs which generate a photocurrent. In other words, the detecting laser acts as a conventional photodetector. Many authors [7-12] have investigated the detection properties of Fabry-Perot laser diodes at zero or reverse bias, and performances of 100 Mb/s over 500 m [10] and 46 Mb/s over 7.5 km [9] have been demonstrated.

This method of light detection has a significant cost advantage over more complex systems since only one active element is needed at each end of the link. On the other hand, the system is half-duplex, which necessitates some kind of synchronization between the two laser diodes. Another disadvantage of this system involves the time needed to switch between the laser transmitting state above threshold and the detecting state at zero or reverse bias. This process can be slow, with reported times needed to switch from transmitting to detecting ranging from 20 ns to 500 ns [11] depending on the external drive circuitry of the laser diode. This "turn-off" time can represent a major limitation on the system bit rate and hence the possibility of a long delay is the main drawback of this bidirectional system.

1.1.4 System #4: Self-Heterodyne full-duplex system

The fourth system involves the use of a single fibre and a laser diode at each remote end as with the previous "switching between transmitting and detecting states" laser system. This system operates in full-duplex mode since the laser diodes remain biased above threshold. The detection function, proposed by Linke et al [13], is based on one laser diode, emitting light at a wavelength λ, receiving light from another laser operating at a wavelength $\lambda + \Delta\lambda$. The receive laser diode will then produce an electrical current proportional to the input optical power at the beat frequency corresponding to $\Delta\lambda$. This current could then be amplified and detected to reproduce the incoming signal.

A major attraction of the self-heterodyne full-duplex system is that only one active component is required at each end of the fibre. However, significant difficulties must be overcome to implement this system, such as the need for semiconductor lasers with very stable emission spectra. The peak wavelengths of the lasers must be very stable and close together to obtain an electrical current at a beat frequency in the GHz range. This factor alone renders the self-heterodyne technique for light detection impractical for use in any system designed for widespread commercial application.

In addition, the authors of [13] neglect the fact that injection locking may occur at the detect laser. Injection locking occurs when a laser output spectrum is "locked" to a peak reference wavelength while injecting photons of peak

wavelength λ_p in a laser cavity that oscillates near this peak wavelength [14-17]. The laser will "lock-on" to the reference wavelength under certain conditions, which would cause the laser cavity to oscillate at the peak emission wavelength λ_p. If this lock-on effect occurred in the self-heterodyne system, the electrical current produced by the return light signal would be present at dc rather than at an intermediate frequency, and would be masked by the much larger dc injection current. This would severely impair the noise performance of the laser detector and would complicate the reception of the incoming signal. Hence the self-heterodyne full-duplex system appears to be impractical for any widespread short-haul application.

1.1.5 System #5: Full-duplex system using traveling wave laser amplifiers

The fifth system again involves the use of a single fibre and a laser diode at each remote end as shown in Figure 3. This system also operates full-duplex since the transmitting and receiving functions are performed simultaneously by the laser diodes, which have antireflection (AR) coatings on their facets and function as near traveling wave laser amplifiers. Each laser amplifier acts as an optical source by emitting light through spontaneous emission similar to a light emitting diode (LED). Detection takes place by monitoring the laser amplifier junction voltage [18]. The external optical signal injected into the laser cavity depletes the carrier density which in turn modifies the quasi-Fermi levels of the diode. The fluctuation of the quasi-Fermi levels can then be detected by monitoring the voltage across the junction of the diode.

A major advantage of detection by quasi-Fermi level fluctuation comes from its full-duplex operation and system simplicity. Reported performance is 50 Mb/s over 5.5 km [18].

A major disadvantage of this system is the impact of back reflections on the transceivers, since light pulses can be partially reflected from optical connectors on the fibre link. If a reflection occurs close to one end of the system the intensity of the reflection could be sufficient to degrade system performance. In

addition, the application of multilayered AR coatings on laser diode facets can be expensive.

1.2 Fast switching half-duplex (FSHD) system-introduction

The system that will be the main focus of this thesis involves a hybrid of the system which switches the laser between transmitting and detecting states (System #3) and the full-duplex traveling wave amplifier system (System #5), which will be called the Fast Switching Half-Duplex (FSHD) system. This system uses Fabry-Perot laser diodes as transceiver elements where the laser is switched between a transmitting state above threshold and a detecting state just below threshold. Detection is achieved by monitoring the junction voltage across the laser diode in a fashion similar to the diode laser amplifier scheme. The FSHD system offers a distinct advantage over the conventional switched laser system since the diode need only be switched from the transmitting point to a detection point just below threshold rather than switching to zero or reverse bias. By operating in such a fashion, the overall system dead time over one complete switching cycle (the sum of the transmitting to detecting and detecting to transmitting times) can be reduced.

Since the remote lasers in the FSHD system require switching between transmitting and receiving states, synchronization is needed to ensure that the individual lasers are ready to transmit or receive at the correct time. This feature will be discussed in Chapter 2, along with many other important characteristics of the FSHD system.

1.3 System performance goals

The goal of the research reported here was to determine the technical feasibility of the FSHD system for a user bit rate of at least 50 Mb/s for distances beyond 12 km. This performance goal corresponds to a bit rate distance product of at least 600 Mb km/s. A cost effective system meeting these performance goals would be a very strong candidate for FTTH or other short-haul applications.

CHAPTER 2. THE FAST SWITCHING HALF-DUPLEX (FSHD) SYSTEM

2.1 System operation

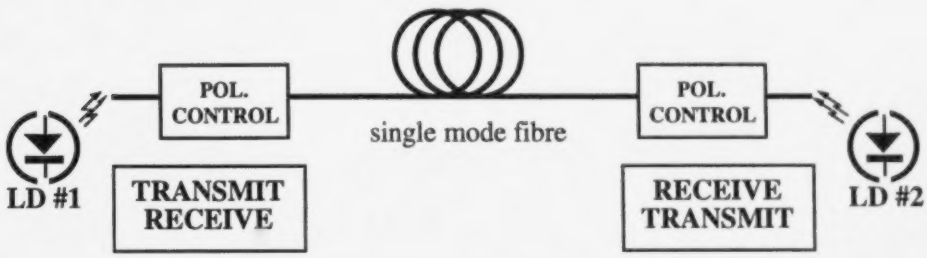

Figure 4. FSHD block diagram.

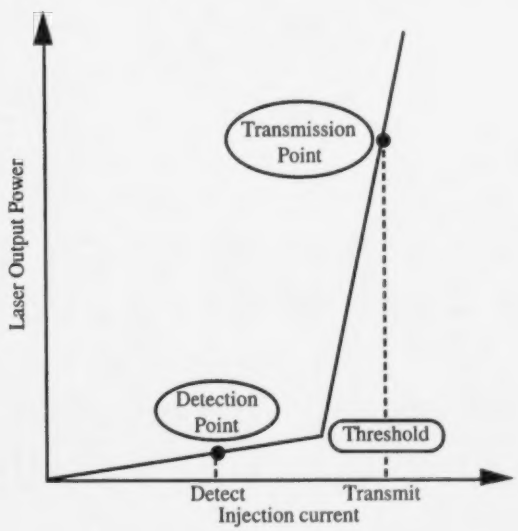

Figure 5. Transmission and detection bias points for FSHD.

A pictorial representation of the proposed fast switching half-duplex bidirectional optical communication system using a laser diode as a transceiver is shown in Figure 4. This system represents a novel approach to short-haul bidirectional optical communication, the description of which has not appeared previously in the literature. The basic building blocks of the system are the laser diodes and the electronic drive circuitry needed to switch the diodes between

transmitting and receiving operating regimes. Polarization controllers are placed directly in front of each transceiver to ensure the detected light is TE polarized. The laser diodes to be used at both ends of the optical link are InGaAsP Fabry-Perot type lasers operating at a peak wavelength corresponding to the fibre dispersion minimum wavelength of 1.3 μm. When the laser diode is in the transmitting mode, the bias point for the laser will be located above threshold, as illustrated in Figure 5. When the laser diode is reconfigured for the receiving mode, this bias point is switched from above threshold to just below threshold.

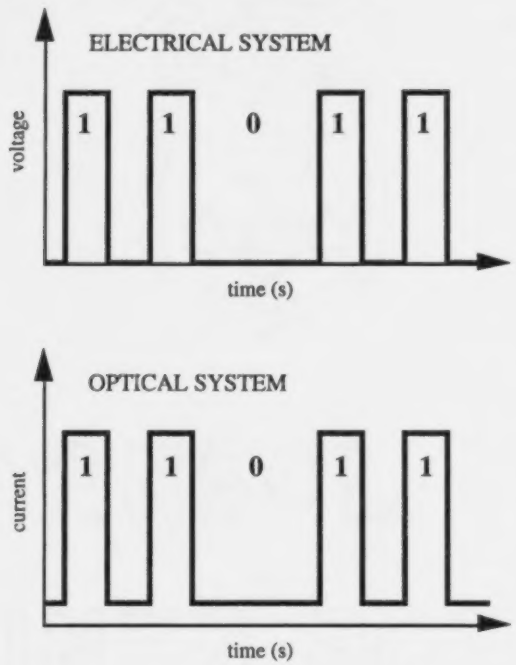

Figure 6. Electrical and optical RZ formats.

The coding scheme proposed for the FSHD system is a return to zero digital format. This format is shown in Figure 6 for both an electrical and optical signal. In the electrical signal, the digital zero is represented by a zero voltage, while the zero for an optical signal would correspond to a low optical power. The zero and one bits take up exactly one half of the total bit time. During the second half of the bit time, the device would be in receiving mode. Hence the

two remote lasers could easily retain synchronization using this coding scheme by transmitting a bit of information after one bit has been detected.

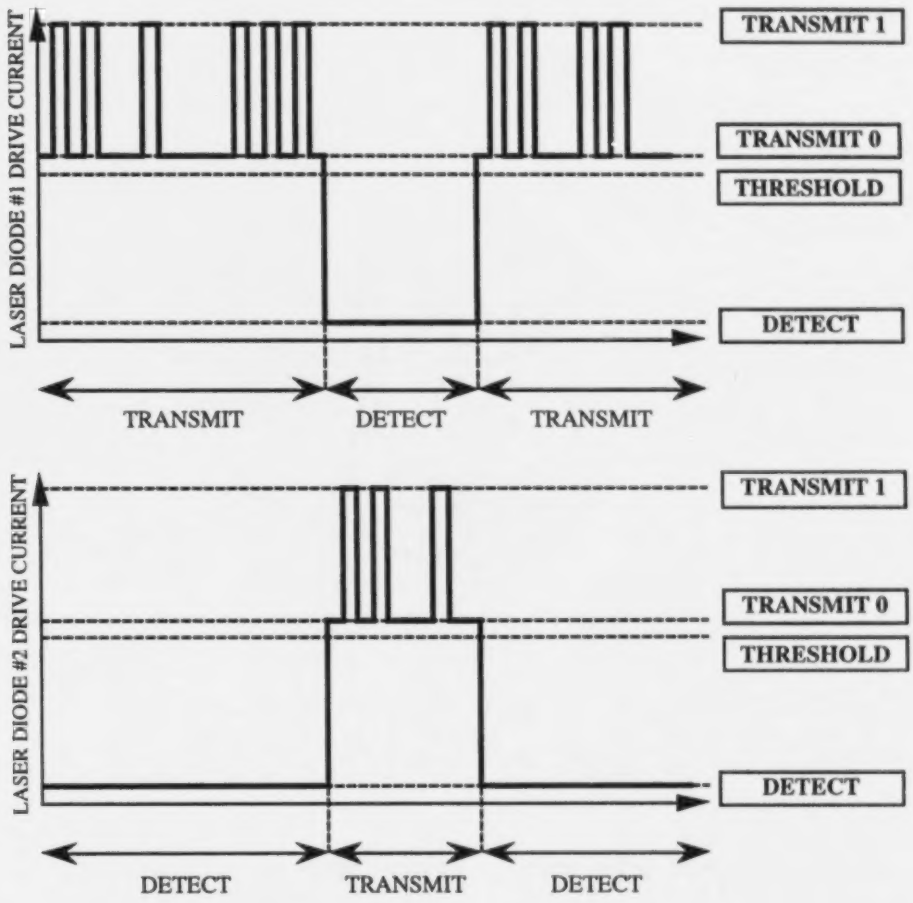

Figure 7. Alternate coding scheme for asymmetric bit rates.

In addition to the previous coding scheme, an alternate implementation could be used that would allow for more flexibility in the rate of information transfer. The need for an alternative coding scheme comes from the fact that the laser must constantly be switched between transmission and detection points after every bit time. With the coding scheme illustrated in Figure 7, the need to switch the lasers after every bit period is eliminated by the transmission of long uninterrupted bit groupings or "packets" in one direction. Switching information for the laser transceivers can come in the form of overhead bits at the end of each

group. This allows the system to have different bit rates in either direction and for the directional bit rates to change in order to meet varying capacity requirements. In addition, two important advantages are realized by using this alternate coding scheme. First, the line coding can be changed to a more efficient non-return to zero (NRZ) format, since the synchronization provided by the RZ format is no longer needed. Second, the time delay previously encountered after every bit when switching the lasers between states is now encountered less frequently after every bit group. Hence the user data rate is greater in this system than in the system where the lasers are switched after the transmission of every bit.

2.2 Laser as a transmitter

The laser diode is biased above lasing threshold when acting as the source of light in the FSHD system. The injection current required for the transmission of ones and zeros depends on desired noise performance and the operating life of the laser diode. First, to minimize the chance of a bit error as well as maximizing the transmission distance of the link, the logical one point and the logical zero point should be located as far apart as possible, or in other words, the logical one pulse should contain much more optical energy than a logical zero pulse. The logical zero point is usually taken to be at or near the threshold point, which necessitates that the logical one point be far above threshold.

However, there are other limitations on the choice of the logical one point. Repeatedly driving a laser diode with an injection current which is much larger than the threshold current results in a steady decrease in optical power output and advances the onset of device failure. To offset this concern, an injection current of 1.3 to 1.5 times the device threshold current is usually a good choice for the transmission of a logical one.

2.3 Laser as a detector

In categorizing the performance of a laser diode as a detector, two important factors must be considered. The laser detector must have adequate responsivity, or convert the incoming optical signal to an output electrical signal efficiently, and the detector must have good sensitivity, or require a minimum

amount of optical power to achieve a given bit error rate. These two factors will be discussed individually in the sections to follow.

2.3.1 Responsivity of a Fabry-Perot laser diode

2.3.1.1 Introduction

Responsivity is a measure of the conversion efficiency of an input optical signal to an output electrical signal. For conventional photodetection, such as with a pin photodiode, responsivity R_O is the ratio of the output photocurrent to the input optical power, or

$$R_O = \frac{I_{out}}{P_{in}} \tag{1}$$

where I_{out} is the output photocurrent, P_{in} = the input optical power, and R_O has the units of mA/mW. The observed responsivity R of a detector is the product of the actual responsivity R_O and the coupling factor η. The coupling factor is the ratio of the actual amount of power from the source laser that is coupled into the photosensitive region to the total optical power available at the input of the detector. Since a photocurrent is produced in the process, this can be called a "current responsivity", since this responsivity is a measure of the generated photocurrent per input photon.

The definition of responsivity for a semiconductor laser diode depends on the bias voltage across the laser diode. At zero or reverse bias voltage, the laser diode acts just like a photodetector, and thus can be characterized by a current responsivity. As the bias point of the laser is increased from zero volts, a forward current will start to flow through the diode. This forward bias causes a buildup of electrons in the conduction band and holes in the valence band. An incoming photon will now see a reduced probability of causing an electron transition upward into the conduction band (absorption) and an increased probability of causing an electron hole recombination (stimulated emission). These two competing processes degrade the laser current responsivity until the laser has zero current responsivity at material transparency, the point where the two processes are in balance.

Above material transparency, the laser diode acts as an amplifier of incoming light, since stimulated emission is now dominant over absorption and a net optical gain exists in the laser cavity. The increased stimulated emissions caused by incoming photons cause a depletion of the carrier density in the active region. This depletion of carrier density is manifested as a drop in quasi-Fermi level gap, which in turn can be observed as a drop in the diode voltage. The equations that link carrier density to quasi-Fermi level gap and diode voltage are given in Appendix 1.

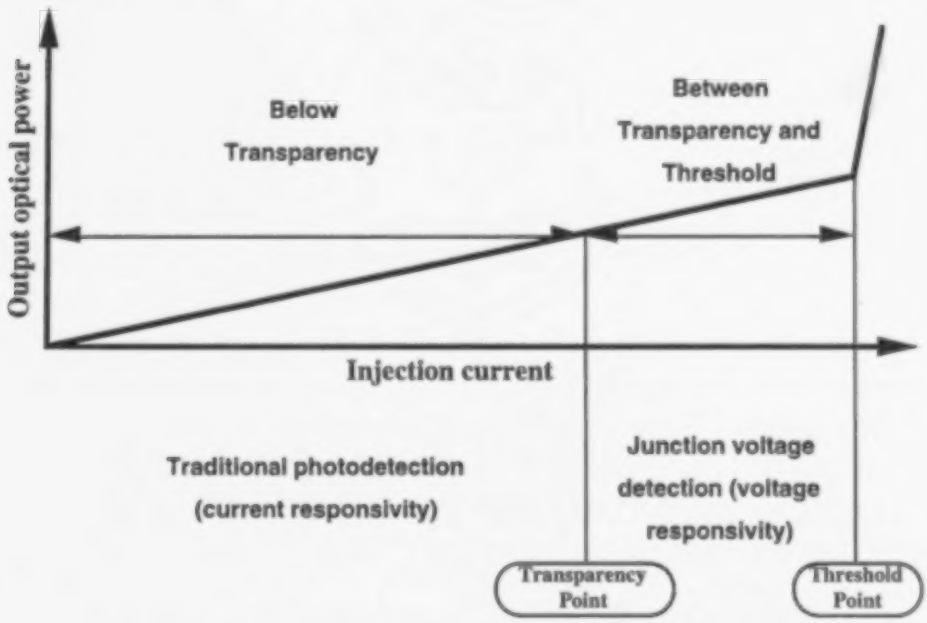

Figure 8. Voltage and current responsivity.

Thus the responsivity above transparency must be defined as a voltage responsivity since the laser detector produces a voltage deviation from the dc bias voltage that is proportional to the input optical power, or

$$R_O = \frac{V_{sig}}{P_{in}} \tag{2}$$

where V_{sig} is the detected voltage change, P_{in} = the input optical power, and R_O has the units of mV/mW. The different responsivity definitions as a function of bias current are shown on a typical laser light current (LI) graph in Figure 8.

2.3.1.2 Theoretical predictions

When the laser diode is biased between transparency and threshold, the change in carrier density, and hence the voltage responsivity, can be enhanced if the incoming photon can pass several times through the active region (optical cavity) since the photon experiences a net gain for every pass through the cavity. Thus the responsivity can be expected to peak at a certain point between transparency and threshold if the peak wavelength of the injected light coincides with a wavelength that gives substantial optical gain inside the laser cavity. In other words, a maximum responsivity point should be present where the input signal wavelength closely matches a Fabry-Perot resonant wavelength of the laser detector. When this condition is satisfied, a standing wave pattern is formed in the optical cavity, and the carrier density in the active region experiences a larger decrease from the bias condition, resulting in an increased responsivity.

To predict device responsivity requires an accurate model of a Fabry-Perot laser diode. Okada et al [19] introduced a model which can predict the change in carrier density in a Fabry-Perot amplifier as a function of the light injected into the active region of the cavity. To simulate this, a computer program model.m was written for *Mathematica* based on this model. The listing of this program along with a description is found in Appendix 2. The program outputs data which shows the deviation in carrier density versus the frequency difference between the injected light ν_I and the nearest cavity resonance without optical injection ν_O, with input power as a parameter. Sample output from model.m is shown in Figure 9, with the four different traces corresponding to four different input optical powers. Notice that the change in carrier density (and hence the responsivity) peaks at a point where the incoming light is slightly detuned from the spectral location of the cavity resonance without optical injection. Also notice the distinct asymmetry that exists when plotting against the frequency detuning $\nu_O - \nu_I$. This asymmetry is due to the carrier dependent refractive index in the active region of laser diodes and has been predicted and observed previously [15, 16, 19-21]. When light is injected into the

laser cavity, the resulting depletion of carrier density causes a shift of the Fabry-Perot resonances due to the dependence of refractive index on carrier density. This shift away from the zero frequency difference becomes more pronounced with an increase in input optical power.

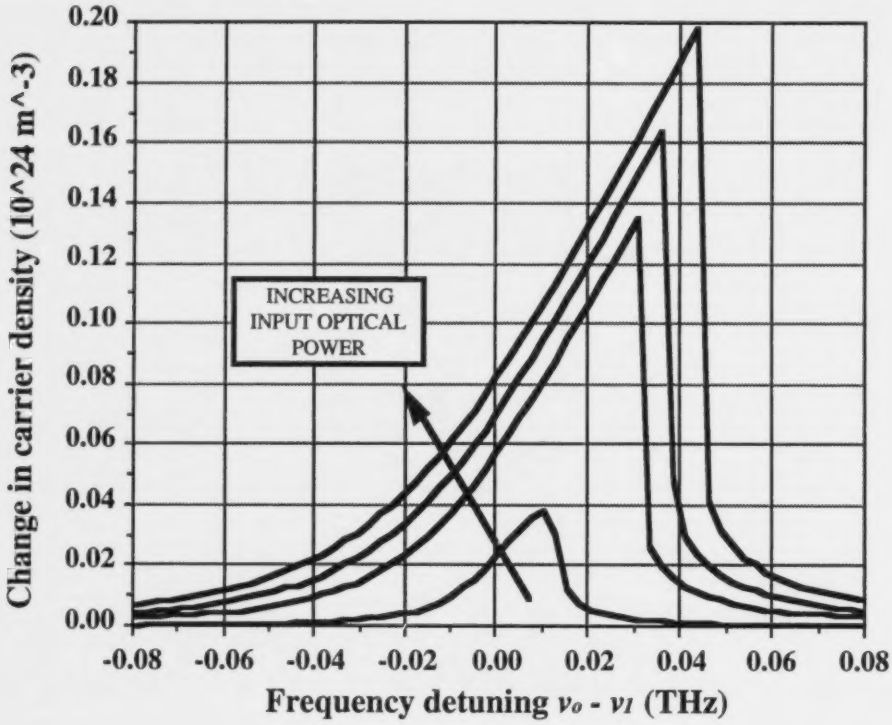

Figure 9. Change in carrier density versus frequency detuning-model

Another important feature of the curves in Figure 9 is the fact that the true Fabry-Perot resonance of the detector cavity and the input signal wavelength coincide at the point where the change in carrier density is maximum. The frequency ν_O is the cavity resonant frequency in the absence of optical injection. The actual cavity resonant frequency will decrease due to the decrease in carrier density caused by the light injection. In fact, the difference between the actual resonant frequency of the cavity and the frequency of the input signal decreases until the change in carrier density is at a maximum. The sharp peak in the responsivity, and thus a sharp peak in the amplified light output of the amplifier

detector, allows for the possibility of employing a simple feedback circuit to keep the Fabry-Perot laser detector biased at a point which will maximize the device responsivity. The back facet monitor found in most commercially available laser packages could be used in a feedback loop to fine tune the detection bias point. If the input signal wavelength was close enough to a cavity resonant wavelength such that a change in output power from the back facet of the laser could be detected, the feedback circuit could increase or decrease the detector injection current slightly to maximize the responsivity. When the peak of the curve is reached and the light output from the back facet drops, the feedback circuit could again change the injection current slightly to compensate. This feedback circuit, along with conventional temperature stabilization of the laser diode, could add to the robustness of the detector, making it relatively immune to fluctuating responsivity over time. The possibility of implementing this feedback circuit to increase laser detector stability is discussed further in Section 3.3.

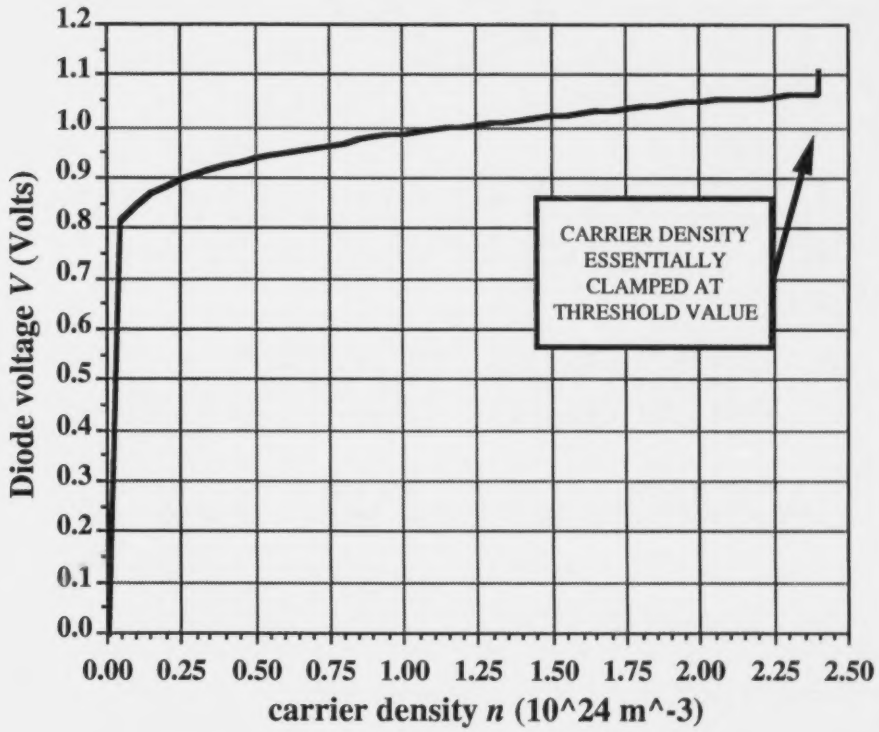

Figure 10. Carrier density versus diode voltage.

If the bias current of the detect laser is increased to the point where laser oscillation occurs, the carrier density in the active layer becomes "clamped" at a threshold value. This clamping phenomenon is shown in Figure 10, where carrier density n is plotted against diode voltage V. If light injection were to occur in this regime, the resulting change in carrier density would be quite small due to the clamping effect. However, it is also apparent from Figure 10 that a small change in carrier density can translate into a noticeable change in diode voltage above threshold. This is indeed the case, but for reasons that will be explained later, observing a noticeable voltage change when injecting light into a lasing optical cavity does not guarantee that biasing the detect laser above threshold is feasible for adequate signal detection.

Before the analysis of laser diode responsivity is continued, the differences between the injection of light in a Fabry-Perot laser amplifier detector and the process of injection locking a laser diode as described in Section 1.1.4 must be noted. Injection locking occurs when a strong light signal is injected in an optical cavity that is biased above threshold, or in a lasing state. The peak resonant wavelength of the optical cavity will then be locked on to the input signal wavelength if the two wavelengths are within close proximity, or within "locking range". In the case where the laser is biased below threshold, the Fabry-Perot resonant frequency of the laser detector is not locked to coincide with the signal frequency; rather, the resonant cavity wavelength is increased (or the resonant frequency is decreased) as a result of the optical injection. The optical injection causes a depletion of carrier density, which in turn causes an increase in the refractive index of the active region. The reduction in cavity resonant frequency results from the decrease in the optical path length of the cavity due to this increase in active layer refractive index. Injection locking also creates a depletion of carrier density, but the magnitude of this difference would be much smaller than the difference created when the cavity is operated as an amplifier, due to the clamping effect of the carrier density above threshold.

Unfortunately, the predicted change in carrier density from Figure 9 cannot be directly expressed as a change in voltage to compare with experimental measurements. The theoretical results shown in Figure 9 only serve as an illustration of the shape of the expected responsivity curve over a particular

frequency detuning range. Ultimately, a quantitative prediction of laser detector responsivity cannot be made from this model due to the unknown value of the device gain. However, a more thorough model can be used to predict the responsivity of a Fabry-Perot laser diode detector. Gustavsson et al [22] introduced a model valid for traveling wave laser amplifier detectors. These traveling wave amplifiers are simply Fabry-Perot laser diodes which have antireflection coatings on the device facets, which reduce the natural facet reflectivity to a small fraction of one percent. Otherwise, they function the same as Fabry-Perot laser detectors by producing a change in diode junction voltage when light is injected in the device.

To modify the traveling wave amplifier theory to make it valid for Fabry-Perot devices, two important modifications must be made. First, the reflectivity of the facets of the device must be changed from a fraction of one percent to the reflectivity of an air semiconductor boundary. This power reflectivity for uncoated devices is given as [23]

$$R_1 = R_2 = \left(\frac{n_{eff} - 1}{n_{eff} + 1} \right)^2 \tag{3}$$

where $R_1 = R_2$ = power reflectivity of facets 1 and 2. Using n_{eff} = the index of refraction of the active layer ≈ 3.6 gives $R_1 = R_2 = 0.32$ as the natural facet power reflectivity. In addition, the cavity gain of a traveling wave must be modified to take into account Fabry-Perot resonances in the optical cavity. In a true traveling wave amplifier with zero facet reflectivity, the cavity gain of the device would be equal to the single pass gain, or

$$G_{c,twa} = G_{s,twa} = e^{(\Gamma g_m - \alpha_s)l} \tag{4}$$

where $G_{c,twa}$ = cavity gain of a traveling wave amplifier, $G_{s,twa}$ = single pass gain of a traveling wave amplifier, Γ = mode confinement factor for TE polarization, g_m = material gain of active layer (m^{-1}), α_s = scattering losses in active layer (m^{-1}), and l = length of optical cavity (m).

The single pass gain of a Fabry-Perot device is equal to the single pass gain of a traveling wave amplifier, but the Fabry-Perot cavity gain can be much larger if the length of the optical cavity corresponds to an integral number of half wavelengths of the input signal. The relations for the Fabry-Perot device then become [34]

$$G_{s,fpa} = G_s = e^{(\Gamma g_m - \alpha_s)l} \tag{5a}$$

and

$$G_{c,fpa} = \frac{G_s(1-R_1)(1-R_2)}{(1-\sqrt{R_1R_2}G_s)^2 + 4G_s\sqrt{R_1R_2}\,\sin^2\left[\dfrac{2\pi n_{eff}(\nu-\nu_0)l}{\lambda}\right]} \tag{5b}$$

where $G_{s,fpa}$ = single pass gain of a Fabry-Perot device, $G_{c,fpa}$ = cavity gain of a Fabry-Perot device, R_1 = power reflectivity of facet 1, R_2 = power reflectivity of facet 2, ν = optical frequency of the input signal (Hz), ν_0 = any cavity resonant frequency (Hz), Γ = mode confinement factor for TE, g_m = material gain of active layer (m^{-1}), and α_s = scattering losses of the active layer (m^{-1}). With the incorporation of the above two changes to the traveling wave amplifier theory, an accurate model of Fabry-Perot laser detectors can be used to predict device responsivity.

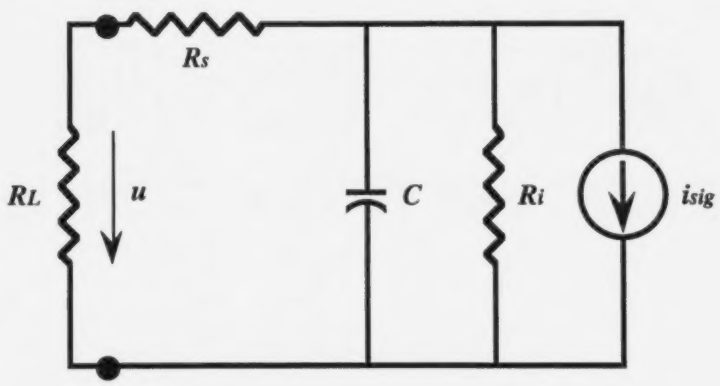

Figure 11. Detector equivalent circuit from [22].

The Fabry-Perot laser detector is modeled with the equivalent circuit [22] shown in Figure 11. An electrical current i_{sig} is produced due to the injected light signal. This current i_{sig} is related to the input optical power by [22]

$$i_{sig} = \eta \frac{q\lambda}{hc} P_{in} \tag{6a}$$

where

$$\eta = \frac{(1-R_1)(1+R_2G_s)(G_s-1)}{(1-\sqrt{R_1R_2}G_s)^2 + 4\sqrt{R_1R_2}G_s \sin^2\left[\frac{2\pi n_{eff}(\nu-\nu_0)l}{\lambda}\right]} \frac{\Gamma g_m}{\ln[G_s]} \tag{6b}.$$

Here h = Planck's constant (J s) and P_{in} = the input optical power (W). The carrier density dependent diffusion capacitance of the detector is given as C, and has the value [22]

$$C = \frac{qlwd}{\left(\frac{dU_f}{dn}\right)} \tag{7a}$$

where

$$U_f(n) = \frac{E_{fc}(n) - E_{fv}(n)}{q} \tag{7b}$$

where n = carrier density in the active region (m^{-3}), E_{fc} = conduction band quasi-Fermi level (J), E_{fv} = valence band quasi-Fermi level (J), and U_f = quasi-Fermi level separation = diode junction voltage (see Appendix 1). The detector series resistance R_S is estimated at 3 Ω. R_i is given as an effective differential diode resistance, and has the value [22]

$$R_i = \frac{\left(\frac{dU_f}{dn}\right)}{(qlwd)\left(\frac{dR(n)}{dn} + \Gamma \frac{dg_m}{dn} S_{sig}\right)} \tag{8a}$$

where

$$S_{sig} = \kappa \frac{\lambda P_{in}}{\ln[G_s] hclwd} \tag{8b}$$

and

$$\kappa = \frac{(1-R_1)(1+R_2G_s)(G_s-1)}{(1-\sqrt{R_1R_2}G_s)^2 + 4\sqrt{R_1R_2}G_s \sin^2\left[\frac{2\pi n_{eff}(\nu-\nu_0)l}{\lambda}\right]} \tag{8c}$$

Here $R(n)$ = total radiative and nonradiative recombination rate (m^{-3} s^{-1}). Notice that R_i is dependent on both the carrier density in the active region and the input optical power. Part of the equivalent signal current will flow through the external load resistance R_L (see Figure 11) and generate a small signal voltage u given by [22]

$$u = \frac{R_i R_L}{[R_i + R_L + R_s]\left[1 + j\omega \frac{R_i(R_L+R_s)}{R_i+R_L+R_s} C\right]} i_{sig} \tag{9}.$$

The 3 dB cutoff frequency in the above relation is

$$f_{3dB} = \frac{R_i + R_s + R_L}{2\pi C R_i (R_L + R_s)} \tag{10}.$$

At a typical bias carrier density of 2.15 10^{24} m^{-3} and an input power of -20 dBm, $R_i \approx 0.932\ \Omega$. Making an approximation that the change in Fermi level with respect to carrier density is constant at 5 10^{-26} V/m^{-3} for all points between transparency and threshold (from Figure 9), $C \approx 1728$ pF, which makes the 3 dB cutoff

frequency equal to about 100 MHz. For frequencies far below this cutoff frequency, the voltage u is given approximately by

$$u = \frac{R_i R_L}{(R_i + R_L + R_s)} i_{sig} \qquad (11).$$

This voltage change u is the detected voltage signal across the junction of the laser diode. Thus the responsivity of the Fabry-Perot laser detector can be estimated by the use of Equations (5) through (11) above. The results of this calculation are given in Table 1.

Table 1. Theoretical responsivity values.

Input power (dBm)	Cavity gain (dB)	Approximate bias point, as a % of threshold	Responsivity (mV/mW)
-20.0	3.25	80	3.44
-20.0	4.42	82	4.86
-20.0	5.75	84	7.08
-20.0	7.30	87	10.75
-20.0	9.16	90	17.43
-20.0	11.50	96	31.31
-20.0	14.68	98	67.07
-20.0	19.71	99	203.26

The responsivity values in Table 1 have been calculated assuming that the peak input wavelength coincides with Fabry-Perot resonance with the most gain, so that

the input signal sees the maximum gain of the detector. Hence these values represent an upper bound for responsivity as a function of peak detector gain or bias point.

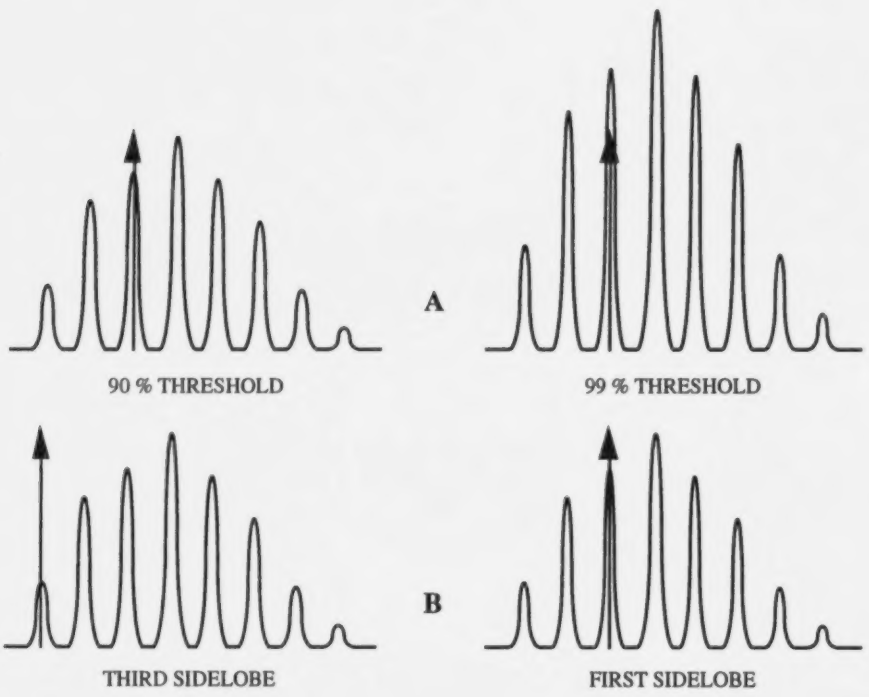

Figure 12. Input signal wavelength is shown as an arrow. A: Input signal sees more gain at 99% threshold than at 90% threshold on same resonance. B: Input signal sees more gain at first sidelobe than at third sidelobe with same bias point.

As stated previously, if the laser is to perform well as a detector, the change in voltage for a given input optical power must be maximized. Unfortunately, the responsivity of a laser diode varies depending on the peak wavelength of the source used to measure detector responsivity. To understand this concept, consider the illustration shown in Figure 12. The magnitude of the induced voltage change (and hence responsivity) will depend on the optical gain seen by the input signal. This gain is controlled by the bias point of the laser. As the laser bias current is increased, the optical gain profile will increase and shift to shorter wavelengths (higher frequencies). If the source wavelength and a cavity resonance coincide far away from threshold, the optical gain seen by the input

signal will be much smaller than if the two wavelengths coincide when the detect laser is biased close to threshold, as shown in Figure 12A. In addition, a resonant peak gain closer to the peak material gain will be stronger than the resonant gains on either side, and thus more optical gain is present at the main cavity resonance than at any sidelobes, as shown in Figure 12B. Thus the responsivity of a laser diode is a strong function of the optical gain seen by the input signal at a particular cavity resonant wavelength.

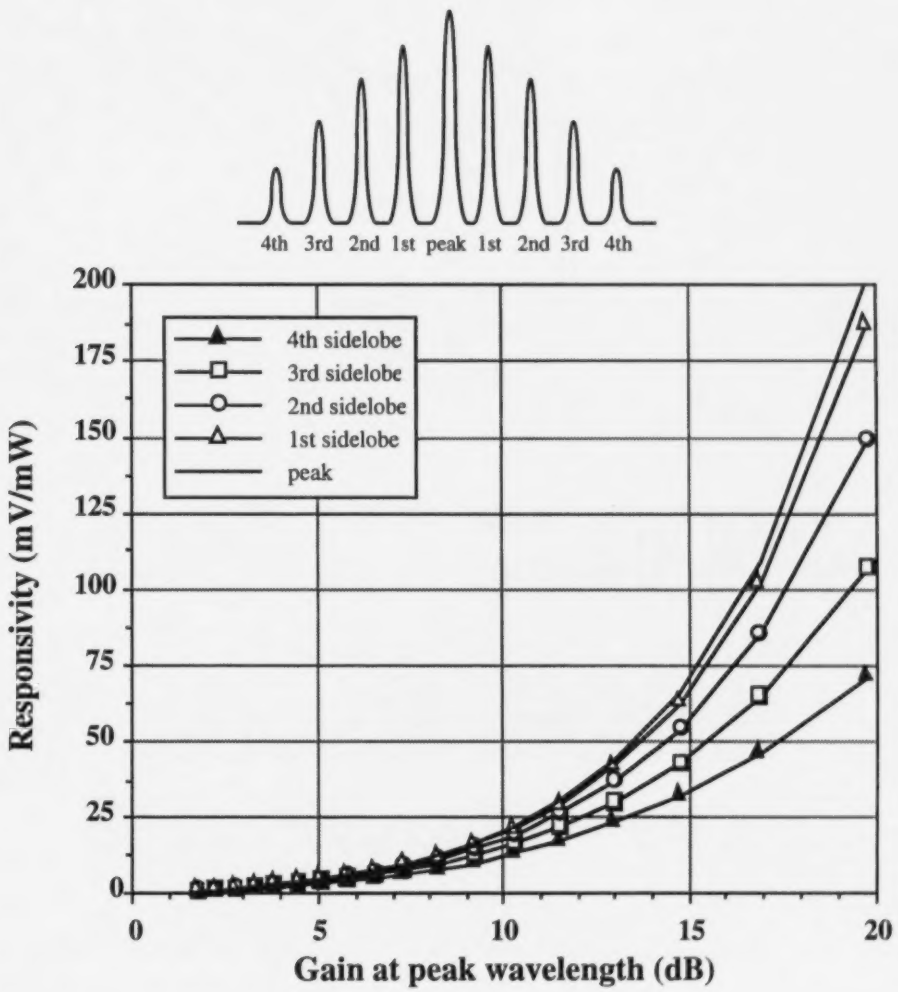

Figure 13. Responsivity versus peak cavity gain for different sidelobes

The optical gain of a Fabry-Perot laser amplifier is also dependent on the polarization of the input light [24]. The cavity gain of the device can be substantially lower for a TM polarized input signal than for a TE polarized input. This is due to the fact that the facet reflectivity and mode confinement factor for TE modes are larger than those for TM modes. Knowing this, it is evident from Equation (5) that TE polarized input light would see a higher cavity gain in a Fabry-Perot amplifier. This polarization dependent gain is the reason for the placement of polarization controllers in front of the laser diode transceivers in the FSHD system block diagram (Figure 4).

To illustrate the responsivity dependence on cavity gain, a calculation using the model of Gustavsson [22] modified for Fabry-Perot devices was performed for four different scenarios. The calculation was performed for the signal wavelength coinciding with the peak gain Fabry-Perot resonant wavelength of the detector as well as for the signal wavelength coinciding with the first, second, third, and fourth sidelobe resonances. For simplicity, the material gain profile of the laser detector was assumed to be parabolic about the peak wavelength. The results of this calculation are shown in Figure 13. The theoretical responsivity is plotted against the peak cavity gain of the Fabry-Perot laser detector. Notice that the responsivity of the device at the sidelobes is smaller than the responsivity at the peak cavity gain, with the responsivity at the fourth sidelobe being about 30 % of the peak responsivity at a cavity gain of 20 dB. Thus the experimentally observed responsivity values can be expected to vary significantly due to the fact that the gain at the actual detector resonant wavelength which coincides with the input signal wavelength is unknown.

2.3.1.3 Experimental setup

An experiment was devised to try to measure the responsivity of Fabry-Perot laser diodes to compare with values predicted by the model described in the previous section. The arrangement consisted of two InGaAsP Fabry-Perot lasers from Northern Telecom (type NT8J42BB) with one acting as a source and the other acting as a detector, as illustrated in Figure 14. The light from the source laser was modulated by a chopper and focused into the detect laser diode. The voltage across the detect laser diode was then monitored with a lock-in amplifier.

When the bias voltage V_b on the detect laser is varied between zero and threshold, the detect laser carrier density changes which affects the carrier dependent Fabry-Perot resonant frequencies of the detector. Hence by changing the bias point on the detect laser the Fabry-Perot resonant peaks are shifted. Since changing the detector bias current from zero bias to above threshold has the result of sweeping the detector cavity resonances over a range of frequencies, the shape of the resulting voltage signal curve should be similar to the asymmetric shape predicted by Okada [19] and shown in Figure 9.

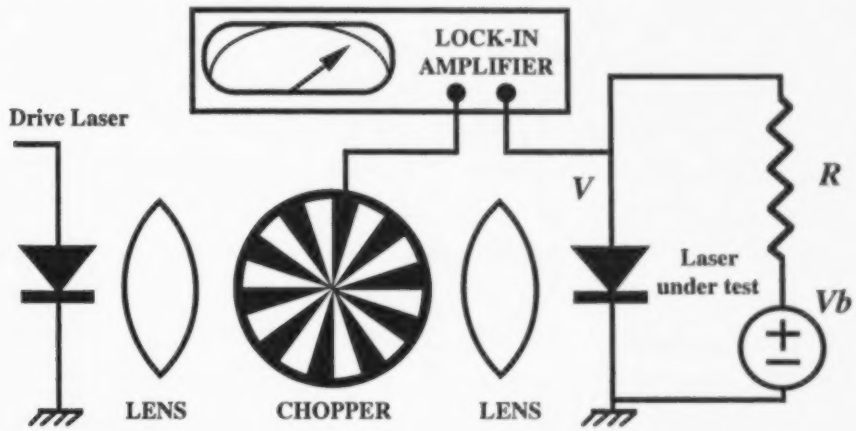

Figure 14. Experimental setup to measure voltage responsivity

2.3.1.4 Experimental results and reconciliation with theory

Results of the responsivity measurements are shown in Figure 15 for five different Fabry-Perot laser diodes, numbered 1 through 5, and six different source detector combinations.

The upper graph in Figure 15A shows the change in voltage due to light injection, ΔV_p, across the detect laser as a function of time. The detect laser is driven with a ramp voltage, which provides an increasing bias voltage from zero volts to a value above the lasing threshold, as shown in the lower graph of Figure 15A. The increase in ΔV_p resulting from an input optical signal is as predicted previously (Section 2.3.1.2) in that a large voltage change ΔV_p is achievable for zero or low bias voltages, and this value drops to zero at the threshold point, as

shown in the upper graph of Figure 15A. The voltage change peaks at a point between transparency and threshold when a Fabry-Perot resonance of the detect laser coincides with the input signal frequency, also as predicted. However, the magnitude and shape of the peak between transparency and threshold is quite different for the various combinations of sources and detectors. In the case of Figure 15B, the peak is smaller although the same detect laser from Figure 15A is used. This proves that the responsivity of a forward biased laser diode is a function of both the individual detector and source used in the measurements. The combination used in Figure 15A resulted in the signal wavelength coinciding with a cavity resonance when the laser was biased closer to lasing threshold than with the combination used in Figure 15B. Therefore, more gain was seen by the signal in Figure 15A and hence a larger voltage change was observed for the same optical input power.

Figure 15C better illustrates the shape of the peak in Figure 15B by focusing in on the area where the peak occurs. Notice that for bias voltages above threshold, the voltage change is very small, indicating no overlap between the signal peak wavelength and a cavity resonant wavelength. In addition, the observed voltage change is starting to show the asymmetric shape predicted by the responsivity model (see Figure 9). Figure 15D shows the voltage change results for a different combination of lasers. The signal wavelength and a detector cavity resonance overlap closer to transparency than threshold in this case, resulting in a reduced voltage change and a trace showing no asymmetry.

Figures 15E and 15F show the voltage change for laser #5 as a detector and laser #1 as the source. Spectral scans of these lasers near their respective threshold points indicated that the two lasers have peak wavelengths within 0.1 nm at room temperature. Based on this information, it was predicted that this combination would have the highest voltage change of any combination since a detector resonant wavelength and the peak signal wavelength would be closely matched near the detector threshold, and thus the input signal would see a substantial optical gain from the detector amplifier. This was indeed the case. The peak between transparency and threshold is very asymmetric, with a shape similar to the shape predicted by the model trace shown in Figure 9. The asymmetric peak occurs at a detector bias point of about 92 % of the threshold value, which indicates

that the input signal sees substantial gain in the detector cavity and causes a significant modulation of carrier density.

Figure 15G is yet another result from a different source detector combination. The asymmetric shape of the responsivity is not evident here indicating a lower detector gain and hence a lower voltage change.

Figure 15H is a unique case in that the peak responsivity occurs just above the threshold point of the detector. A peak above threshold can also be observed looking back to Figures 15E and 15F, where a second lower peak occurs just after the asymmetrical peak response. This lower peak is observed to occur just as the dc light output of the detect laser starts to rapidly increase (the detector threshold point). This observation leads to the conclusion that the detector is experiencing an injection locking effect from the input signal (refer to the description of injection locking in Section 2.3.1.2, starting on page 16). This injection locking effect becomes weaker as the detector resonant wavelength is shifted farther away from the input signal wavelength due to the continuing increase in bias point, which is reflected in the observed signal reduction. This result can be explained by the results obtained by Kobayashi [25] and mentioned previously in Section 2.3.1.2. A noticeable voltage change is possible across a laser diode detector biased above threshold even though the change in carrier density in the active region is quite small. This is evident from the diode voltage versus carrier density curve shown previously in Figure 9. Above threshold, where the curve is quite steep, a small change in carrier density can still produce a substantial change in diode voltage.

The detection of a noticeable voltage change across the diode junction above threshold raises some questions as to the choice of bias voltage for the detector. If the laser detector delivers adequate voltage responsivity above threshold, there seems to be no reason to switch the laser to a point below threshold, as proposed in the FSHD system. In doing so, the transmitting to detecting transition time would be much smaller in a half-duplex arrangement, or even better, both lasers could remain in a lasing state and the bidirectional system would operate full-duplex. Unfortunately, detecting with a laser diode above threshold would decrease the sensitivity of the laser detector. The stimulated

transitions occurring when the diode is biased above threshold dictate that the noise performance of the detector would suffer in both half-duplex or full-duplex arrangements. Moreover, the possibility exists that the magnitude of the input optical signal could make the detector oscillate between stable and unstable states [46]. The boundaries between stable and unstable states are also highly dependent on the linewidth enhancement factor α of the laser diode [46], which is extremely hard to control or identify during the manufacturing process.

For the particular case of a full-duplex system, yet another drawback of operating the laser detector above threshold is the fact that the incoming signal causes a different voltage change depending on the detect laser bias point. This would result in the detector having voltage responsivities that depend on whether the laser is transmitting a one or a zero. This could have a drastic effect on the bit error rate at the detector. More importantly, it has been documented in the literature that under certain conditions optical feedback into a laser cavity can have drastic effects on the coherent output of the device [26-33]. The input signal light from the transmitting laser could be viewed as incoherent feedback into the detect laser if the peak wavelengths of the two devices are closely matched. Incoherent feedback into an active laser cavity will cause the linewidth of the source to broaden, or reduce the coherence of the light output of the device. A broadened source linewidth could severely impact the maximum transmission distance of the system due to chromatic dispersion in the fibre. Hence the utilization of a voltage peak above detector threshold does not appear to be feasible in either a half-duplex or a full-duplex bidirectional system.

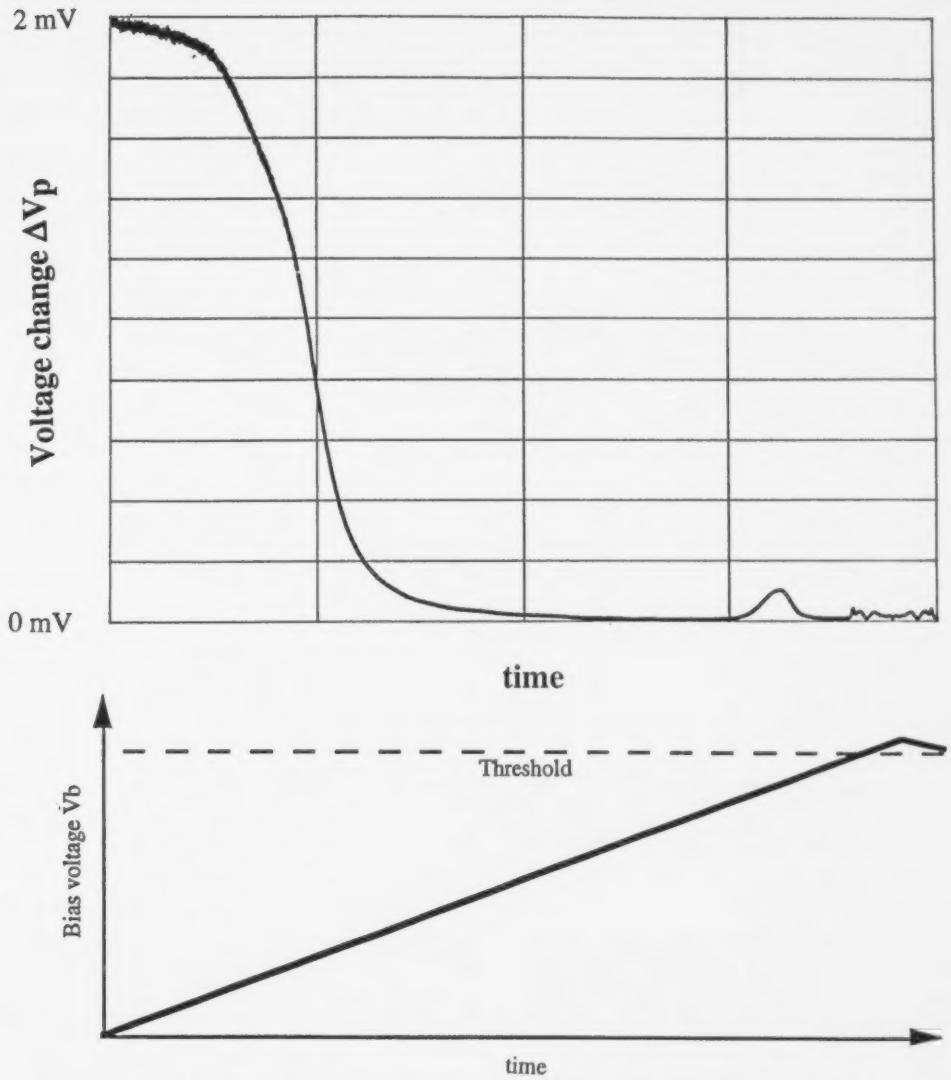

Figure 15A. Results from test using source laser #3, detect laser #5. Input optical power = -17 dBm

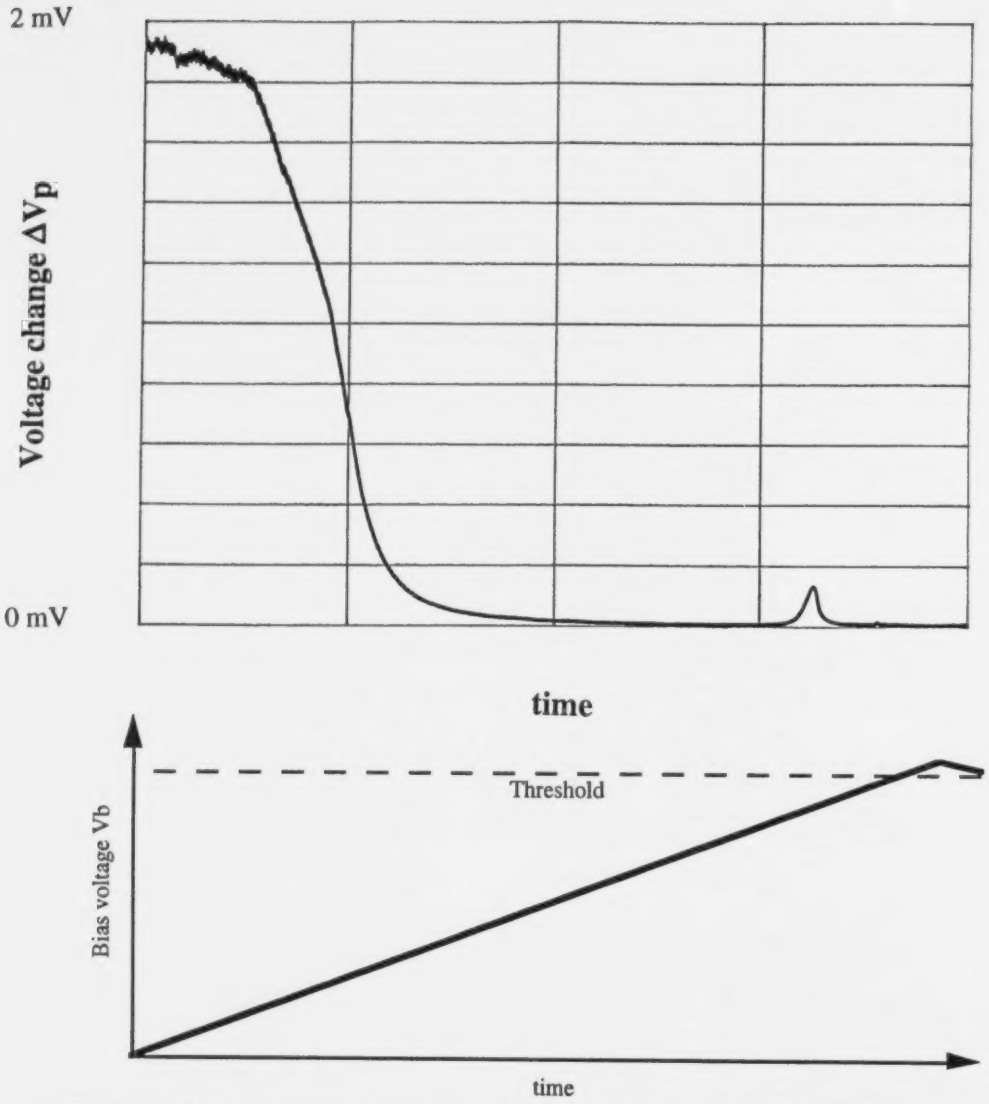

Figure 15B. Results from test using source laser #4, detect laser #5. Input optical power = -13.5 dBm

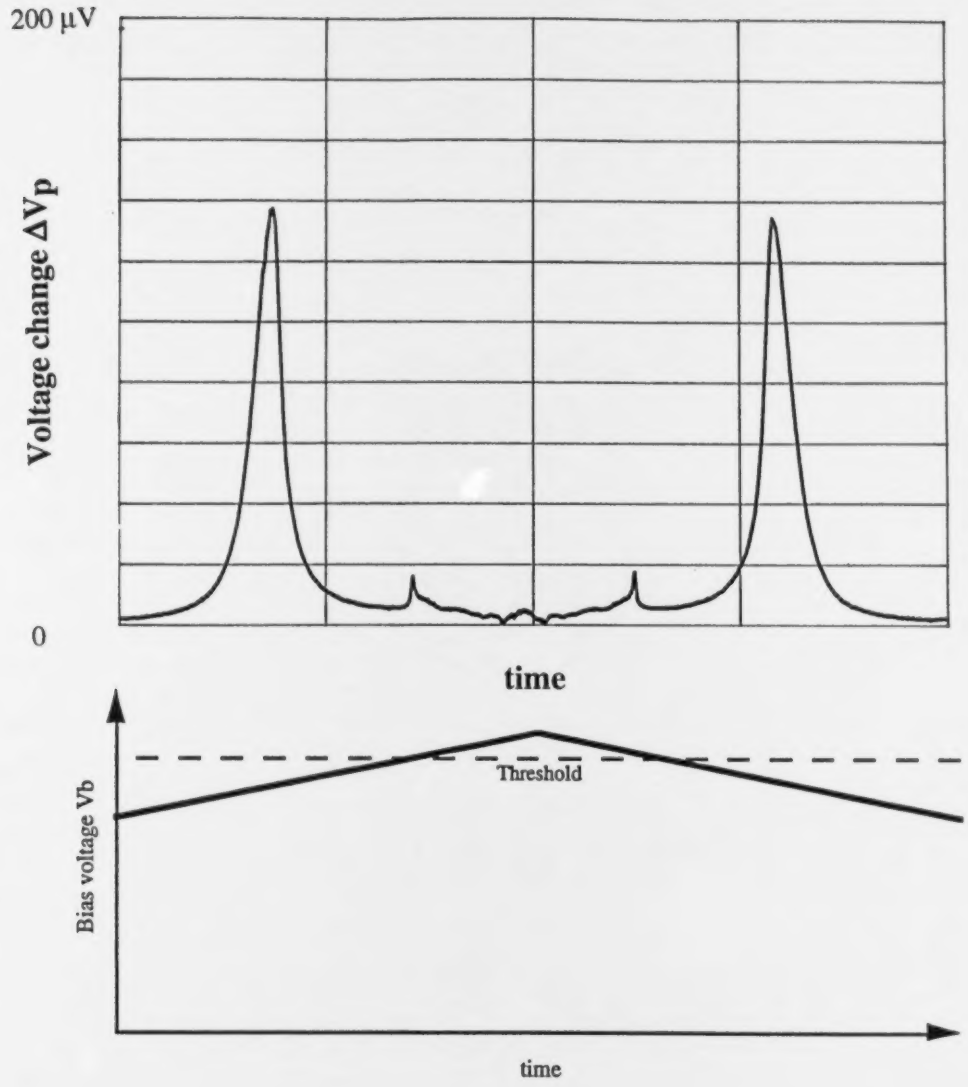

Figure 15C. Results from tests using source laser #4, detect laser #5. Input optical power = -13.5 dBm.

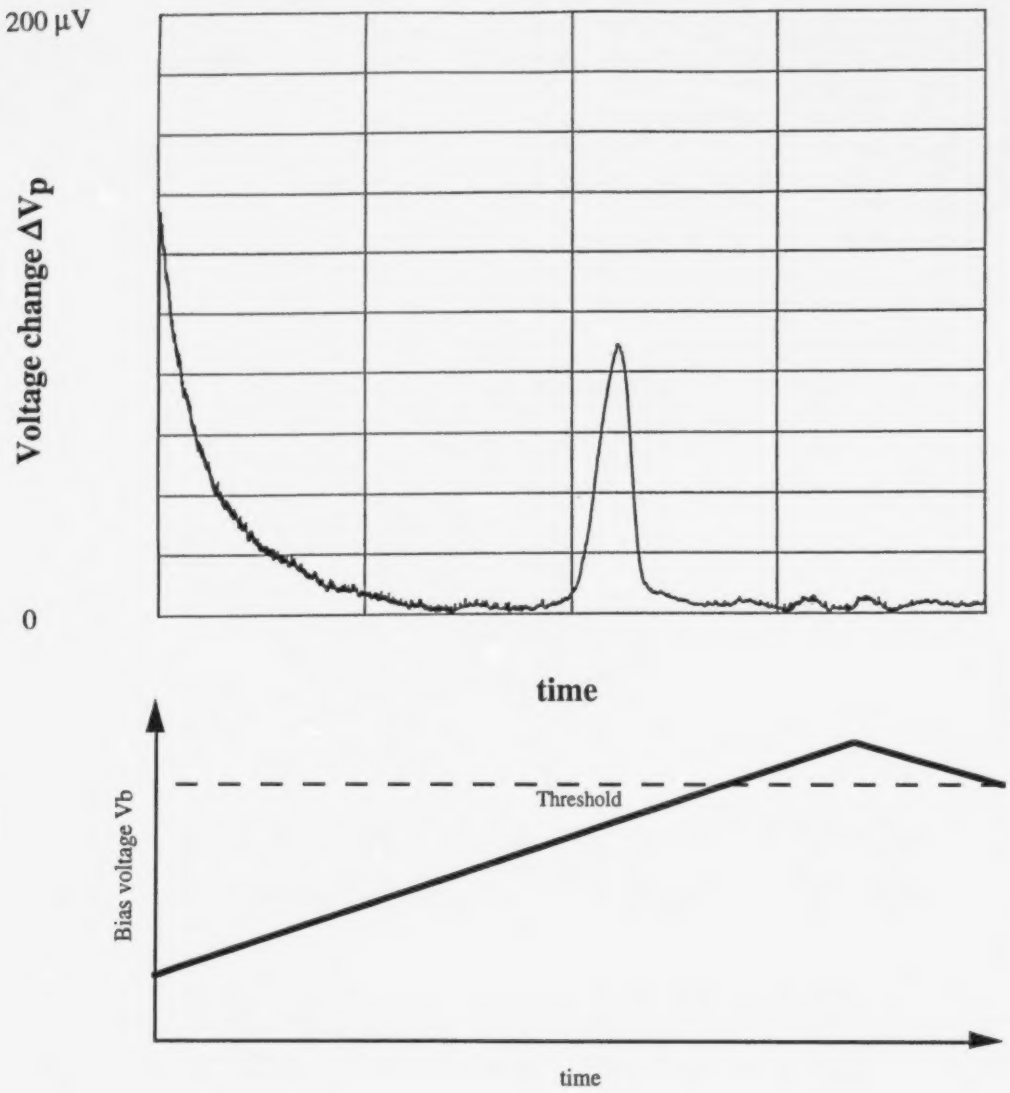

Figure 15D. Results from tests using source laser #4, detect laser #1. Input optical power = -14 dBm.

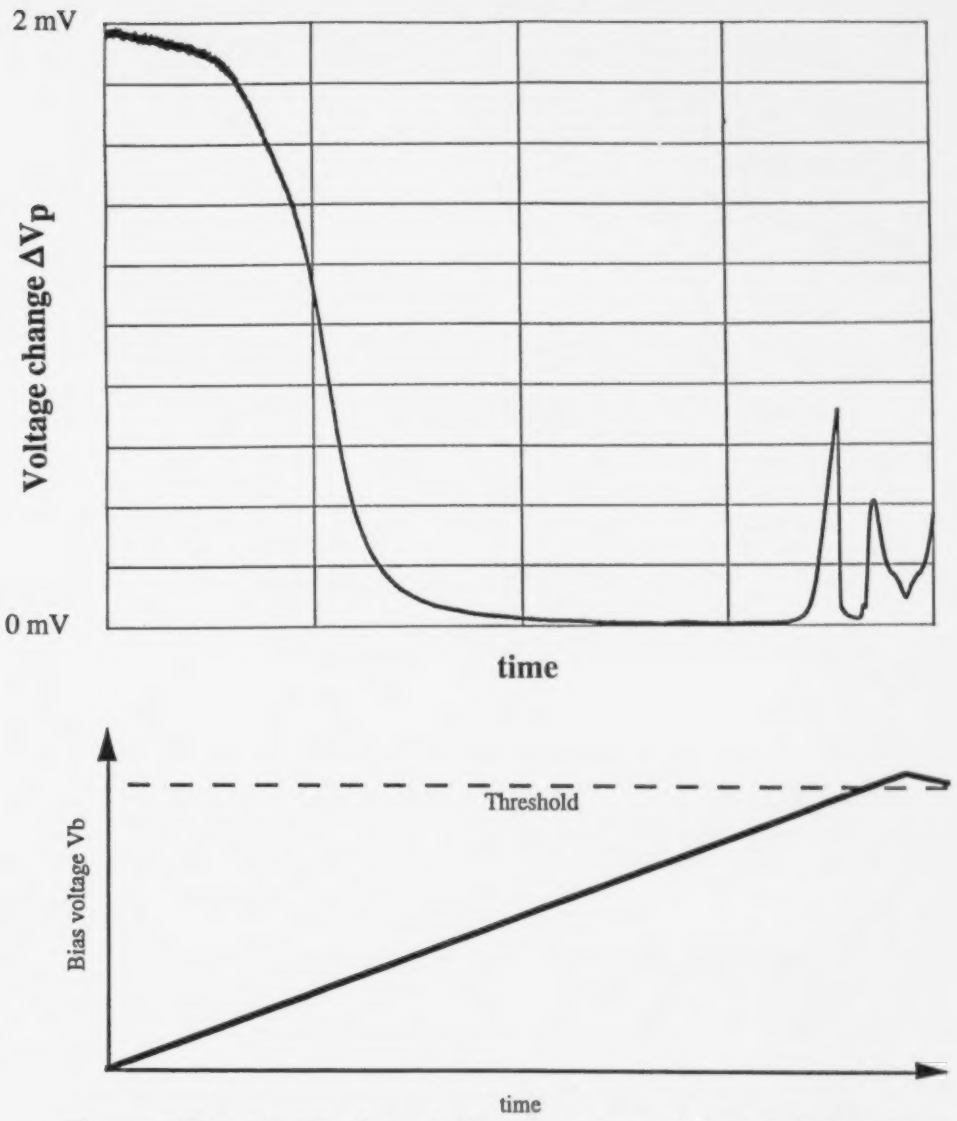

Figure 15E. Results from tests using source laser #1, detect laser #5. Input optical power = -15.5 dBm.

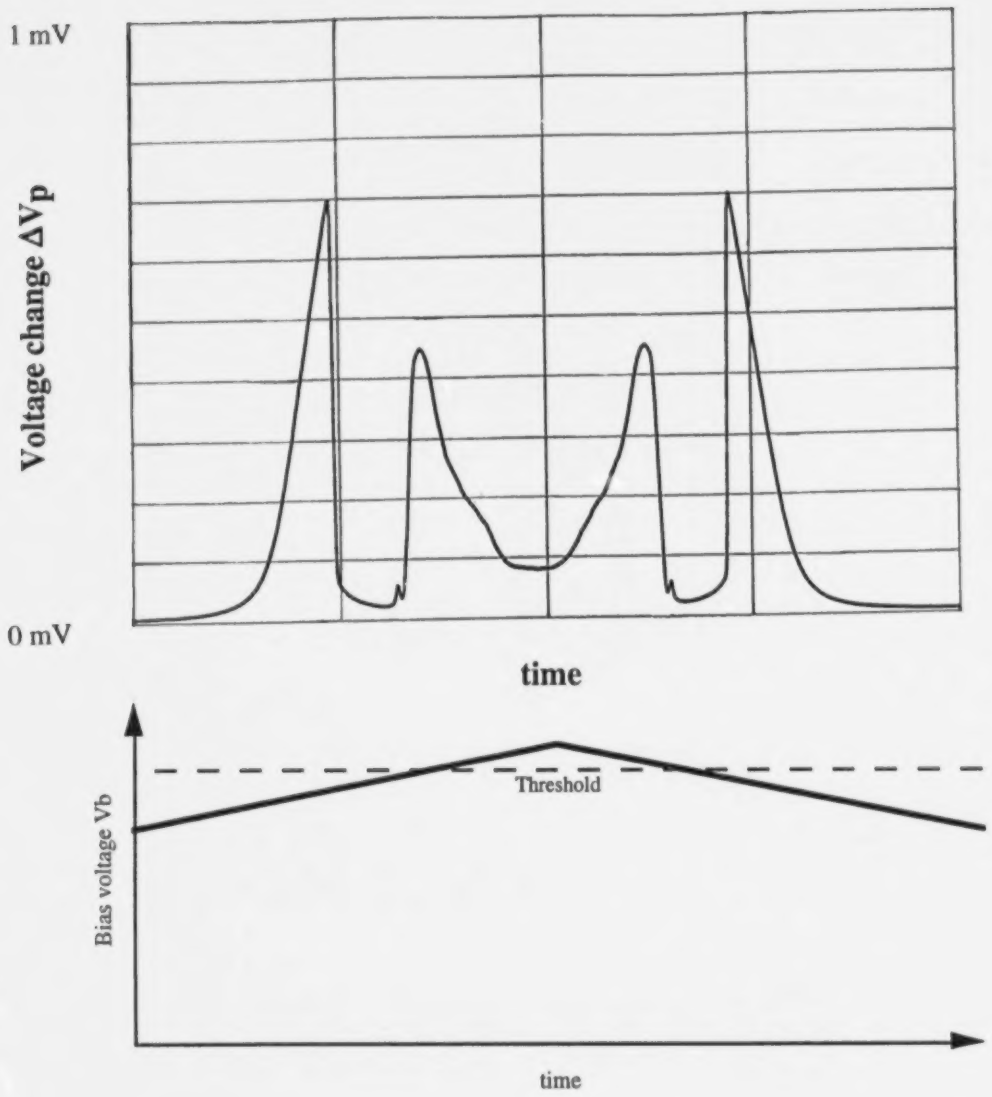

Figure 15F. Results from tests using source laser #1, detect laser #5. Input optical power = -15.5 dBm.

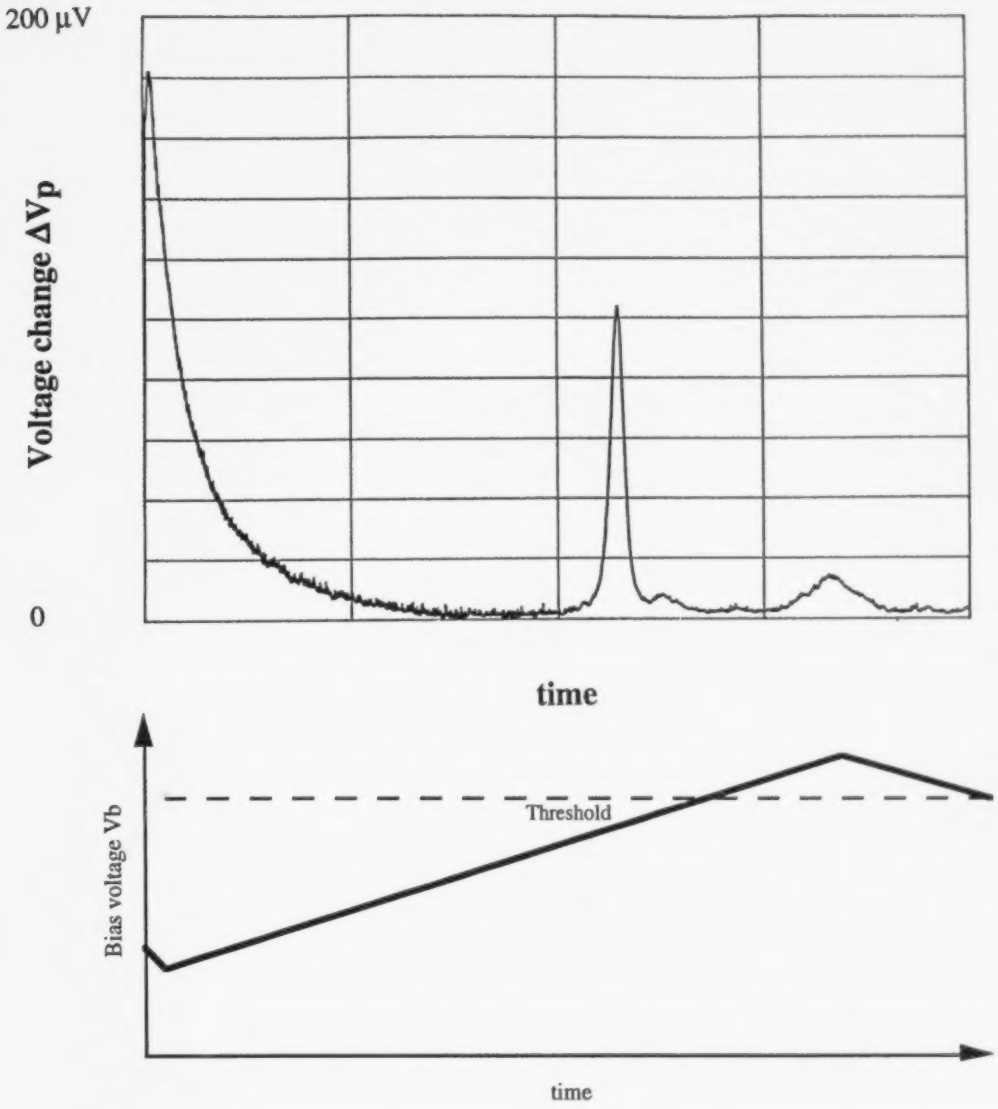

Figure 15G. Results from tests using source laser #3, detect laser #1. Input optical power = -15 dBm.

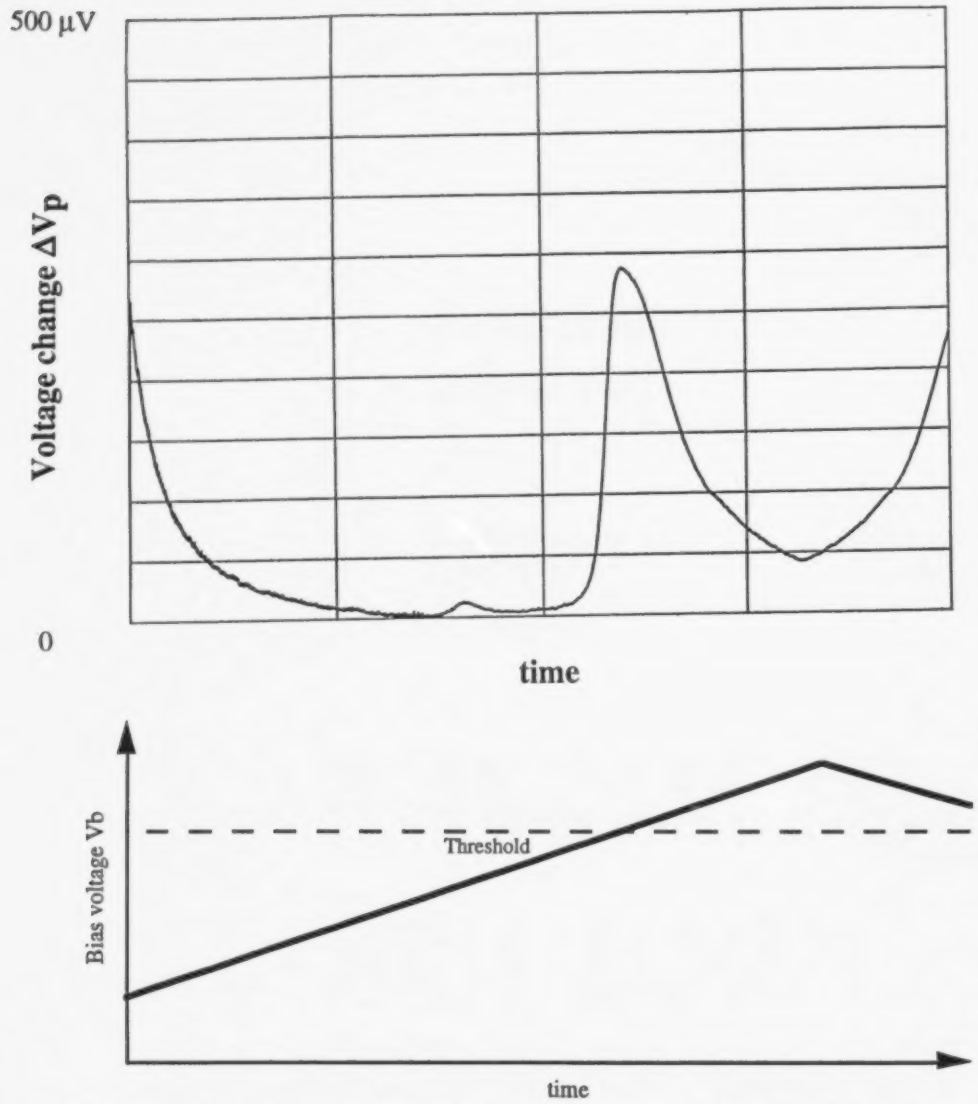

Figure 15H. Results from tests using source laser #5, detect laser #1. Input optical power = -13.5 dBm.

To estimate the responsivity of a Fabry-Perot laser detector, the observed peak voltage deviations in Figure 15 were divided by an estimate of the amount of power actually coupled into the junction region of the detect laser. The coupling loss into the detect laser was estimated at 11 dB (0.08) for all the individual cases. This estimate was determined by comparing observed current responsivities and published current responsivities from [11] at zero bias under identical conditions. This relatively large coupling loss was due to the inability to focus the source beam spot size accurately on the detect laser active region. The results of the responsivity calculations are shown in Table 2.

Table 2. Measured responsivity of Fabry-Perot laser diode detectors

Figure reference	Source laser	Detect laser	Detect Laser Responsivity (with 11 dB coupling loss)	Bias point of detect laser (as a % of threshold)
Fig. 15A	Laser #3	Laser #5	5.0 mV/mW	87
Figs. 15B, C	Laser #4	Laser #5	2.95 mV/mW	89
Fig. 15D	Laser #4	Laser #1	2.25 mV/mW	85
Figs. 15E, F	Laser #1	Laser #5	25.0 mV/mW	93
Fig. 15G	Laser #3	Laser #1	3.13 mV/mW	86
Fig. 15H	Laser #5	Laser #1	6.36 mV/mW	103

A graphical comparison of the observed and predicted responsivities is shown in Figure 16. An estimate of the peak cavity gain for a given bias point as a fraction of threshold is obtained using the first part of the computer program noisefpa.m listed in Appendix 3. This calculation results in the following

conversion: 85% threshold ≈ 4 dB peak cavity gain, 86% ≈ 4.25 dB, 87% ≈ 4.75 dB, 89% ≈ 5.5 dB, and 93% ≈ 11 dB. Notice that the responsivity values vary widely for the observed cases. This is due to the fact that the responsivity peaks for the individual cases occurred at different detector bias points, and thus the optical gain seen by the signal was different in all cases. Comparing these values with the results in Table 1 shows that the observed responsivities are in general agreement with the theoretical values obtained in the 85% to 95% threshold range within experimental error.

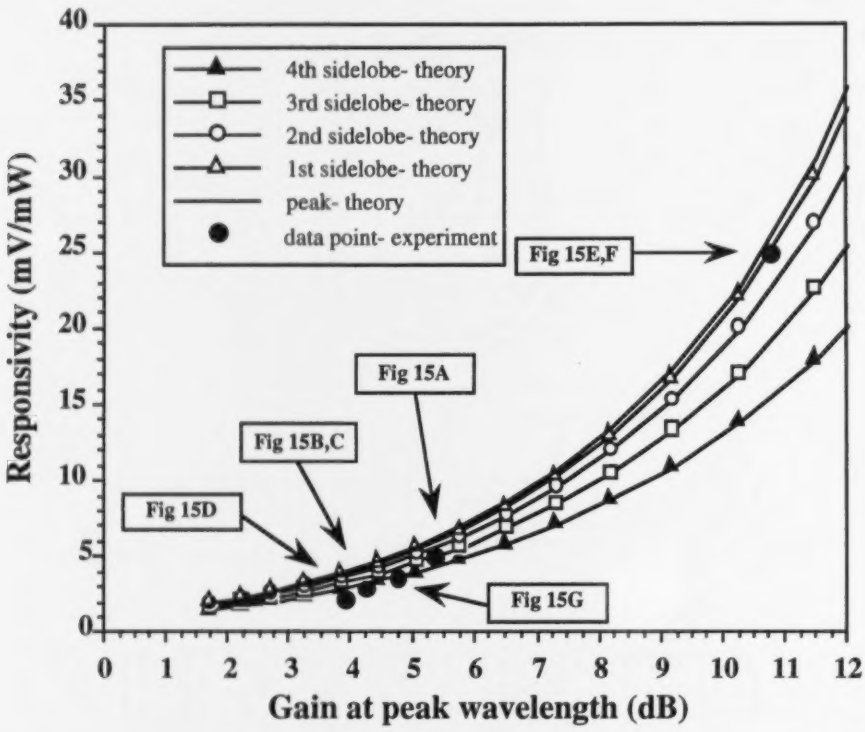

Figure 16. Theoretical and experimental voltage responsivity as a function of cavity gain.

More importantly, the measured responsivity values agree with previous predictions in that the maximum responsivity value (source laser #1, detect laser #5, Figure 15E, F) is obtained when the source wavelength coincides with a detector resonant wavelength when the laser is biased near lasing threshold. Therefore to maximize responsivity of a source detector laser pair, the two devices

should have peak wavelengths in close proximity when near threshold bias currents are applied to the respective laser diodes. This would not guarantee that the responsivities of both lasers would be equal; rather, that the discrepancy between the two responsivities would be minimized. Precise matching could be achieved by adjusting respective device temperatures.

2.3.2 Sensitivity of a Fabry-Perot laser diode

2.3.2.1 Introduction to theoretical model

Sensitivity is defined as the minimum amount of signal power which must be coupled into the detector to achieve a given bit error rate. In optical communication systems, sensitivity is usually quoted in dBm, or decibels below 1 mW optical power, and most often for a bit error rate of 10^{-9}. Although the sensitivity calculation for a Fabry-Perot laser diode detector in a FSHD system has not appeared in the literature as yet, many authors have done sensitivity calculations for other similar detectors and detection schemes. For instance, Kashima [11] reports that the sensitivity of a Fabry-Perot laser diode used as a photodetector at zero bias is -36 dBm for a bit rate of 2 Mb/s and a bit error rate of 10^{-9}. Gustavsson [22] reports the sensitivity of a traveling wave laser amplifier using a junction voltage scheme similar to the FSHD system as -30 dBm to -36 dBm for a bit rate of 200 Mb/s and a bit error rate of 10^{-9}.

2.3.2.2 Noise calculation of a Fabry-Perot amplifier

There are several important sources of noise in a Fabry-Perot laser diode cavity. The traveling wave amplifier detector model of Gustavsson [22] introduced for calculating responsivity can also be applied to the sensitivity calculation by making the appropriate modifications for a Fabry-Perot device explained earlier. The model for the laser detector was shown in Figure 11, with all the appropriate parameter values outlined in Equations (5) - (8). Noise sources at the detector will be modeled as equivalent noise current sources in parallel with the current source i_{sig}. The major sources of noise to be considered in the sensitivity analysis include shot noise and thermal noise from the detector, amplified signal shot noise, spontaneous emission shot noise, beat noise between signal and spontaneous emission, and beat noise between spontaneous emission components.

The first source of noise to be recognized is shot noise from the laser detector itself. This shot noise comes as a result of the inherent randomness in the stimulation of an electron hole pair recombination. The equivalent noise current for detector shot noise is given as [22]

$$i_{shot}^2 = 2qI_{bias}B_e \tag{12}$$

where I_{bias} = detector dc bias current (A), q = electronic charge (C), and B_e = electrical bandwidth of the receiver circuitry (Hz).

The second noise contribution to consider is thermal noise from both the detector and the subsequent electrical amplification of the signal. The equivalent noise current for thermal noise is given by [22]

$$i_{th}^2 = \left[\frac{1}{R_L} + \frac{F-1}{R_L}\right]4kTB_e \tag{13}$$

where R_l = load resistance (50Ω) and F = noise figure of electrical amplifier (8 dB typical). To calculate the remainder of the noise terms mentioned above requires an estimate of the variance in the number of photons output from the optical cavity. This variance is given as [22]

$$\begin{aligned}\sigma_{out}^2 &= 2G\langle n_{in}\rangle + 2(G-1)n_{sp}\Delta f_1 + \\ &4G(G-1)n_{sp}\langle n_{in}\rangle + 2(G-1)^2 n_{sp}^2 \Delta f_2\end{aligned} \tag{14}$$

where σ^2 = output photon number variance, $\langle n_{in}\rangle$ = average number of input photons (s^{-1}), G = cavity gain of the device, n_{sp} = spontaneous emission factor, Δf_1 = equivalent optical noise bandwidth of the spontaneous shot noise, and Δf_2 = equivalent optical noise bandwidth of the spontaneous spontaneous beat noise. The four terms in the variance expression account for signal shot noise, spontaneous shot noise, signal spontaneous beat noise, and spontaneous spontaneous beat noise, respectively. Signal shot noise and spontaneous shot noise arise from the fact that different optical pulses all representing a logical one will contain a varying number of photons. Signal spontaneous beat noise is due to the interference of the input signal at one frequency with spontaneous emission at other frequencies.

Similarly, spontaneous spontaneous beat noise is as a result of the interference of two spontaneous emission components at different frequencies.

The average number of input photons $\langle n_{in} \rangle$ is related to the input optical power by [22]

$$\langle n_{in} \rangle = \frac{\lambda}{hc} P_{in} \tag{15}$$

where P_{in} = input optical power, h = Planck's constant, and λ = input signal peak wavelength.

Yamamoto [34] makes appropriate substitutions for the respective optical noise bandwidths for a Fabry-Perot device which results in

$$\begin{aligned}
\sigma_{out}^2 &= \frac{(1-R_1)(1-R_2)G_s^0}{(1-\sqrt{R_1R_2}G_s^0)^2}\langle n_{in} \rangle + \\
&\sum_m \left[\frac{(1+R_1G_{s,m})(1-R_2)(G_{s,m}-1)n_{sp}}{1-R_1R_2G_{s,m}^2} \frac{c}{2n_{eff}l} \right] + \\
&2\frac{(1+R_1G_s^0)(1-R_1)(1-R_2)^2 G_s^0 (G_s^0-1)n_{sp}}{(1-\sqrt{R_1R_2}G_s^0)^4}\langle n_{in} \rangle + \\
&\sum_m \left[\frac{(1+R_1G_{s,m})^2(1-R_2)^2(G_{s,m}-1)^2 n_{sp}^2(1+R_1R_2G_{s,m}^2)}{(1-R_1R_2G_{s,m}^2)^3} \frac{c}{2n_{eff}l} \right]
\end{aligned} \tag{16}$$

where G_s^o = single pass gain at peak cavity resonance, $G_{s,m}$ = single pass gain at the m^{th} cavity resonance, and the summation is performed over m = all longitudinal cavity modes with net gain.

At this stage it is important to recognize that the variance of the generated signal current in the laser detector is proportional to the variance of the photon number [22]. This can be seen by defining [22]

$$i_{ph}^2 = q^2(\Gamma g_m l)^2 \overline{\sigma_{out}^2} B_e \tag{17}$$

where the bar across the variance in output photons denotes an averaging over the length of the amplifier. This average is easily computed by calculating

$$\overline{\sigma_{out}^2} = \frac{1}{l}\int_0^l \sigma_{out}^2 dl \tag{18}.$$

Substituting (16) into (18) then yields the photon variance averaged over the device length. Unfortunately, a closed form solution does not exist since the single pass gains $G_{s,m}$ and $G_s{}^o$ are both functions of l, so numerical integration must be performed. This result then gives the variance in detected current $i_{ph}{}^2$ due to signal shot noise, spontaneous shot noise, signal spontaneous beat noise, and spontaneous spontaneous beat noise.

The total detector noise can then be computed by summing the variances in the detected current due to the individual noise sources using

$$i_{tot}^2 = i_{ph}^2 + i_{shot}^2 + i_{th}^2 \tag{19}.$$

The signal to noise ratio of the Fabry-Perot detector can now be calculated by using [22]

$$SNR = \frac{i_{sig}^2}{i_{ph}^2 + i_{shot}^2 + i_{th}^2} = \frac{i_{sig}^2}{i_{tot}^2} \tag{20}.$$

The bit error rate of the Fabry-Perot laser detector and the signal to noise ratio are related by [22]

$$BER = \frac{1}{2}\mathbf{erfc}\sqrt{\frac{SNR}{2}} \tag{21}.$$

The relations (12) through (21) form the basis on which the sensitivity of a Fabry-Perot laser diode receiver was calculated.

2.3.2.3 Results

The computer program noisefpa.m listed in Appendix 3 was used to calculate the sensitivity of the Fabry-Perot laser detector. Actual results of the simulations are shown in Figure 17.

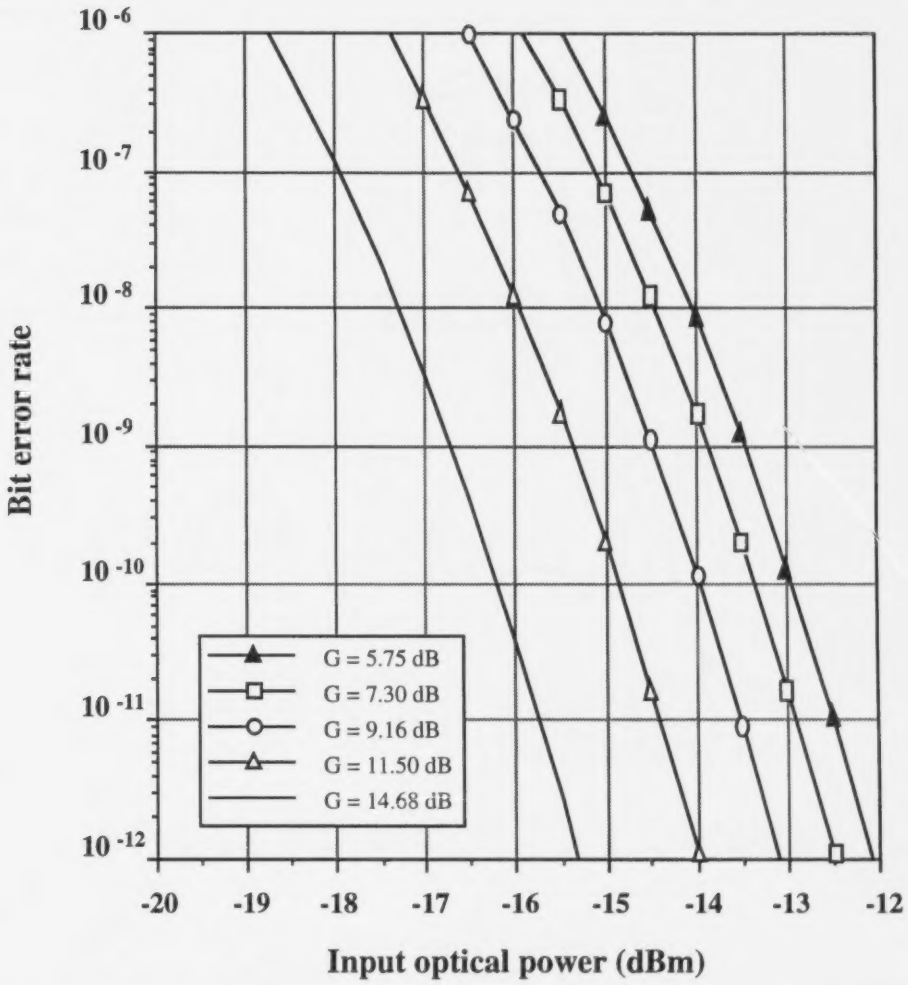

Figure 17A. BER curves for varying cavity gain. G = detector cavity gain. Bandwidth = 30 MHz.

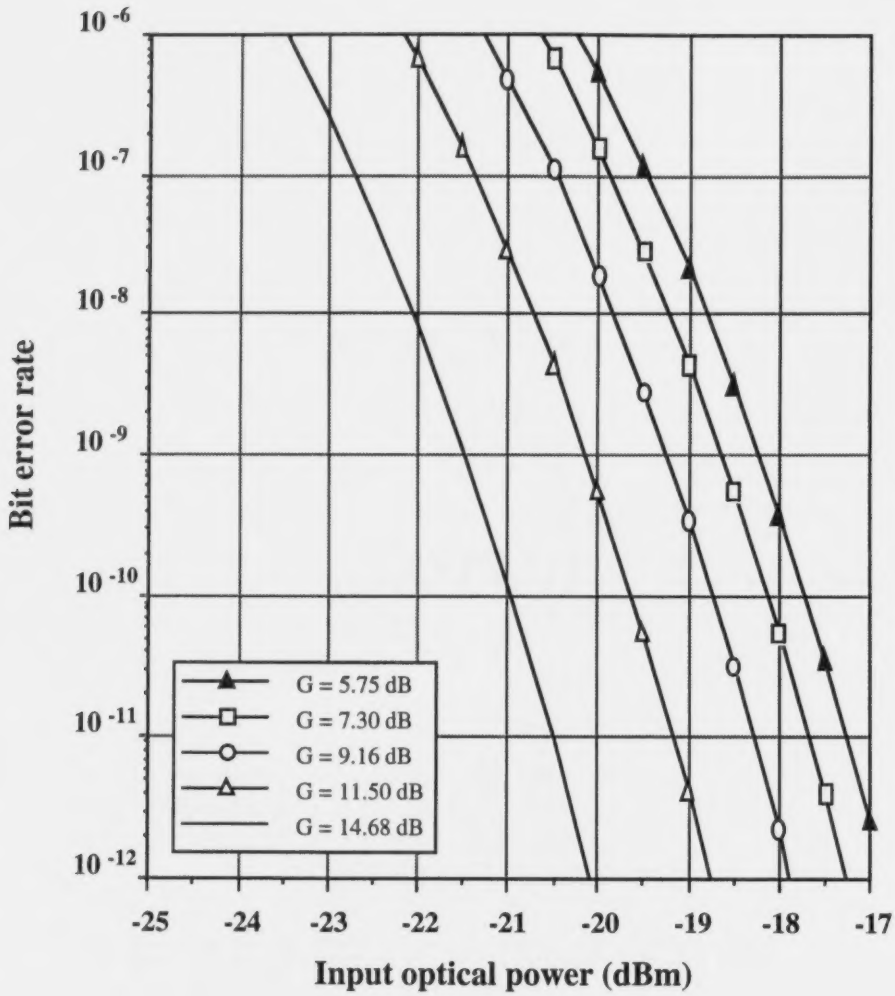

Figure 17B. BER curves for varying cavity gain. G = detector cavity gain. Bandwidth = 10 MHz.

Figure 17A shows the bit error rate as a function of input optical power for different detector cavity gains. Notice that increasing the cavity gain, or moving the detection point closer to lasing threshold, results in an increased detector sensitivity, or less input optical power needed to achieve a giver bit error rate. For this particular case with an electrical bandwidth of 30 MHz the sensitivity ranges from -16.5 dBm to -13.5 dBm. Figure 17B shows the same calculation

with a 10 MHz electrical bandwidth. Notice that the sensitivity range is now from -21.5 dBm to -18.5 dBm. In all cases, the dominant noise contribution limiting detector sensitivity was signal spontaneous beat noise. Figure 17C shows the relative noise contributions from the six individual sources for the cases shown in Figure 17A for a cavity gain of 5.75 dB. Figures 17D and 17E also show noise current contributions for cavity gains of 9.16 dB and 14.68 dB, respectively. The signal spontaneous beat noise and signal shot noise become extremely severe at high input optical power and high laser detector cavity gain.

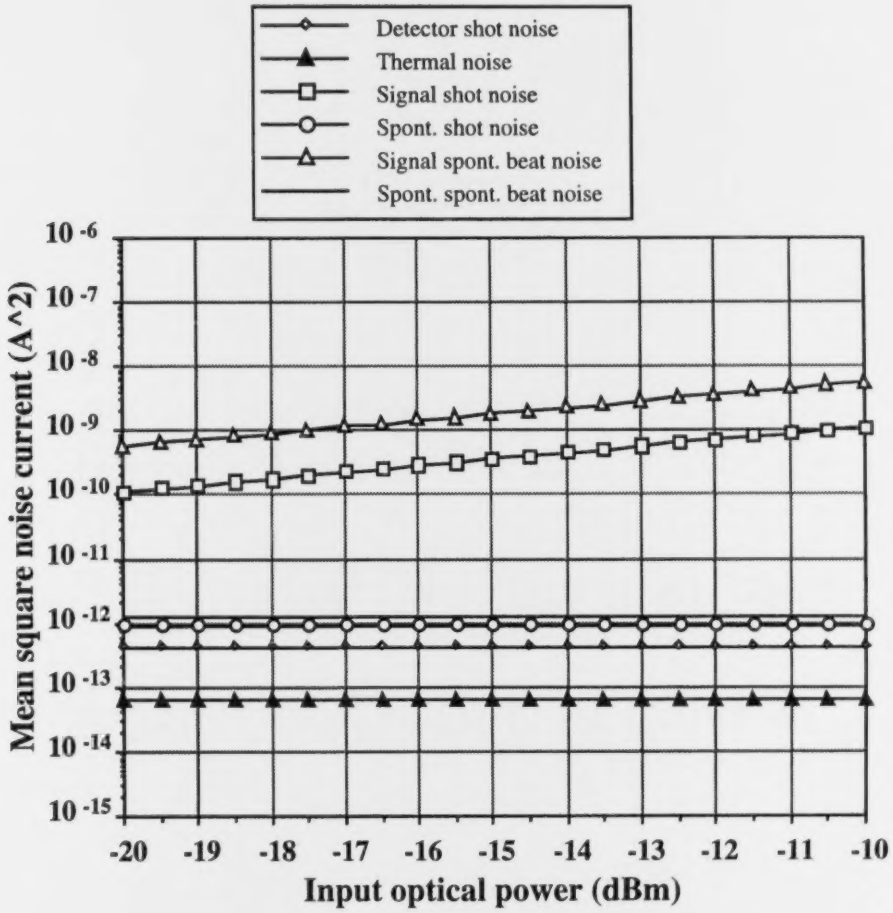

Figure 17C. Mean square noise currents. Cavity gain = 5.75 dB. The spontaneous spontaneous beat noise (solid line) is approximately 10^{-12} A^2 for all input powers.

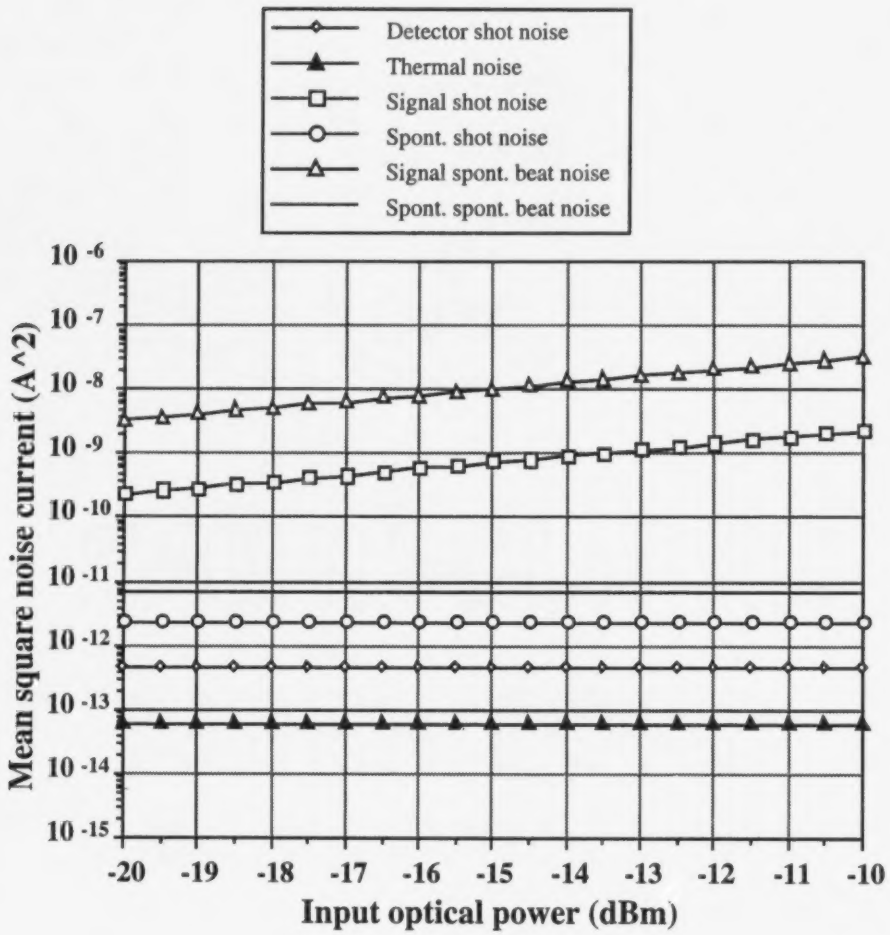

Figure 17D. Mean square noise currents. Cavity gain = 9.16 dB.

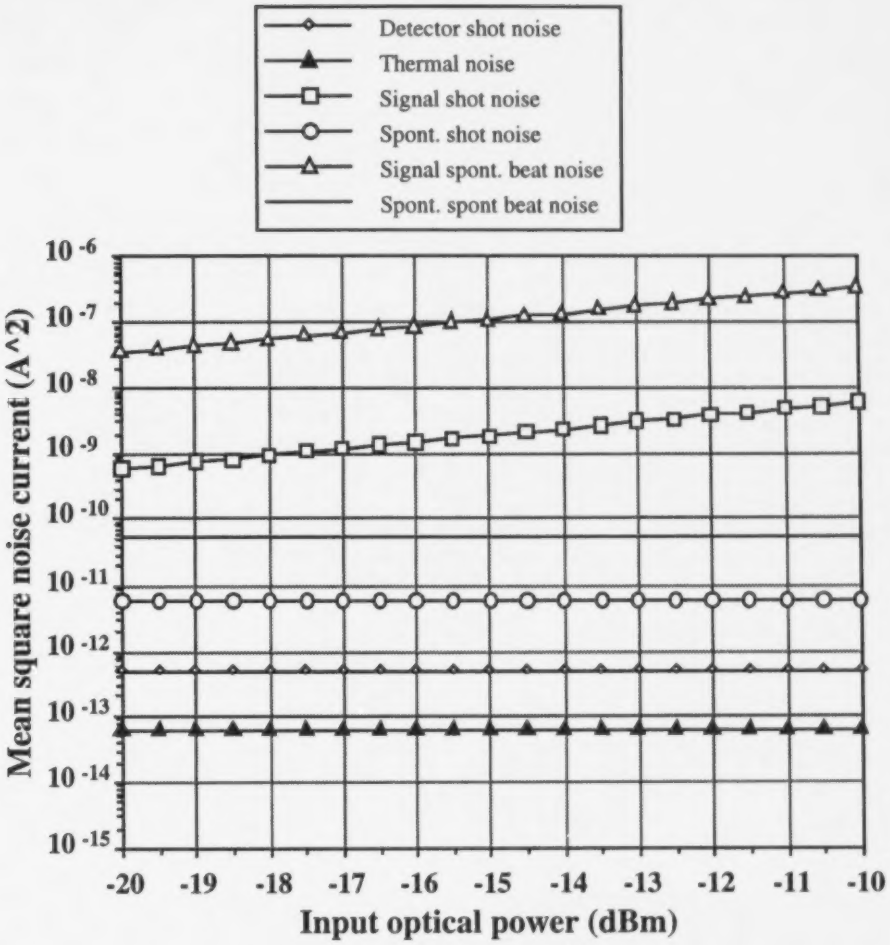

Figure 17E. Mean square noise currents. Cavity gain = 14.68 dB.

Another issue that must be addressed is the effect on sensitivity of the peak input signal wavelength coinciding with a sidelobe Fabry-Perot resonance instead of the peak gain resonance of the detector. This is shown in Figure 18A below, where the bit error rate is plotted versus optical input power for a fixed cavity gain of 14.68 dB and an electrical bandwidth of 30 MHz. Figure 18B shows the BER plot for a cavity gain of 9.16 dB and an electrical bandwidth of 30 MHz, while Figure 18C shows the BER plot for a cavity gain of 14.68 dB and an electrical bandwidth of 10 MHz.

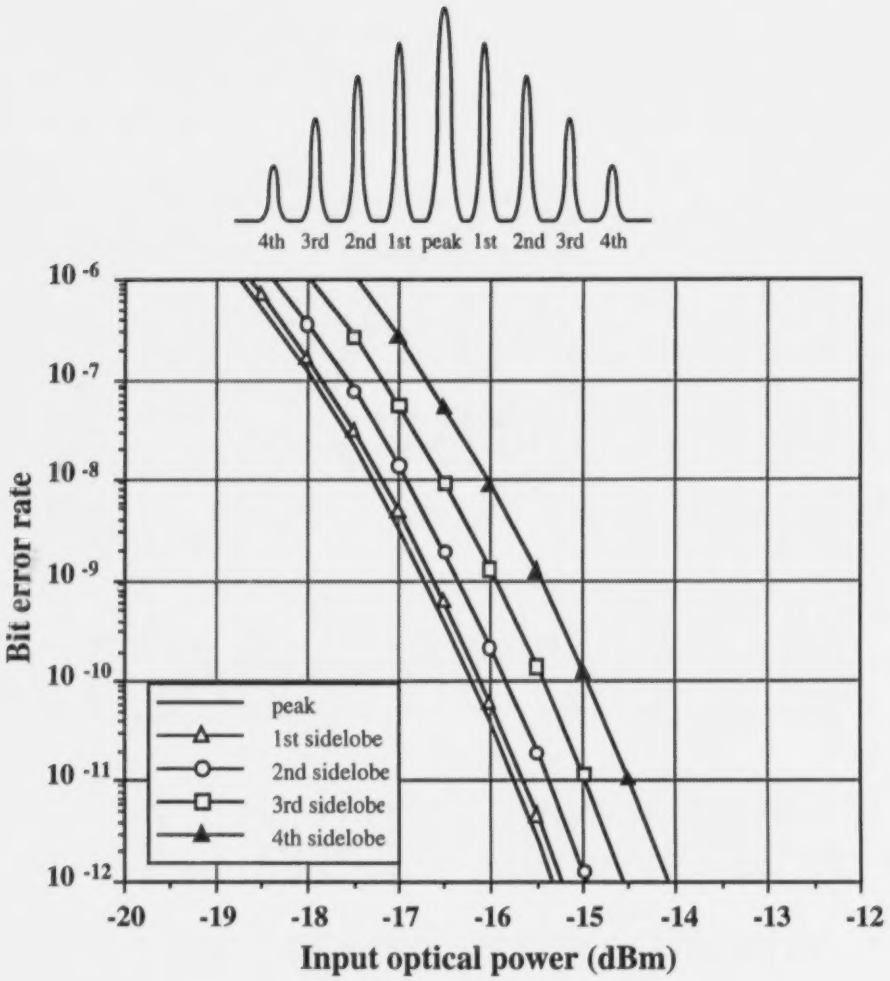

Figure 18A. BER curves for off peak gain resonances. Bandwidth = 30 MHz and cavity gain = 14.68 dB.

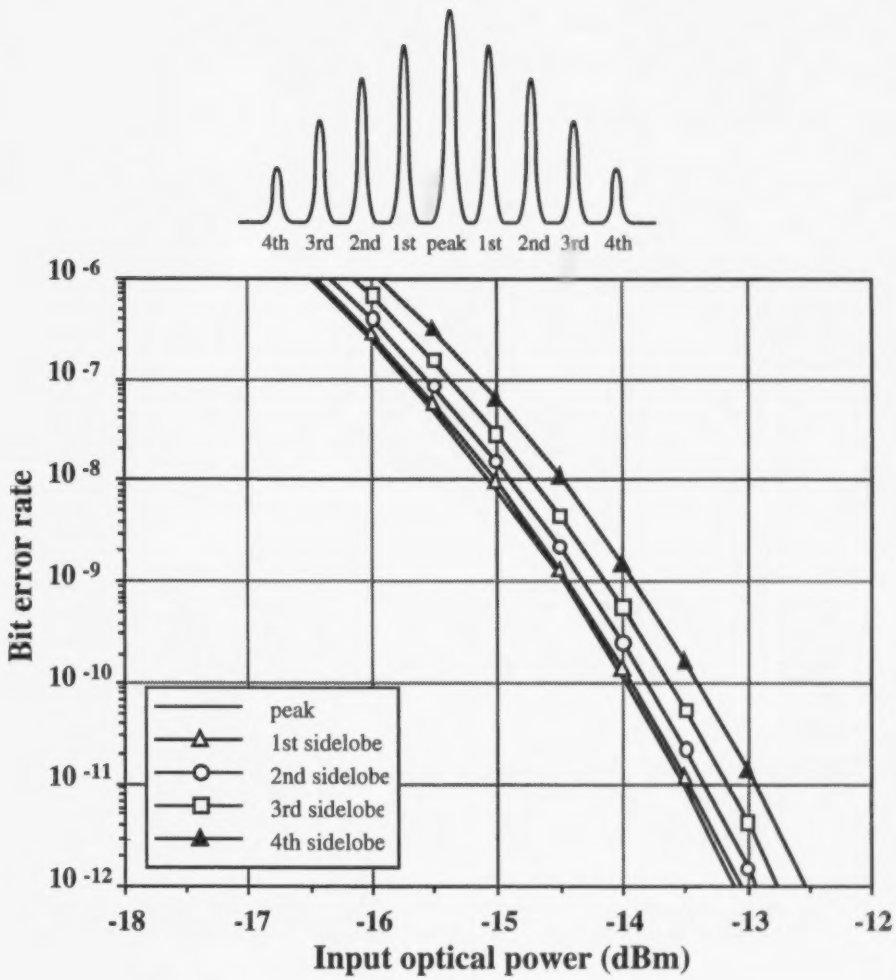

Figure 18B. BER curves for off peak gain resonances. Bandwidth = 30 MHz and cavity gain = 9.16 dB.

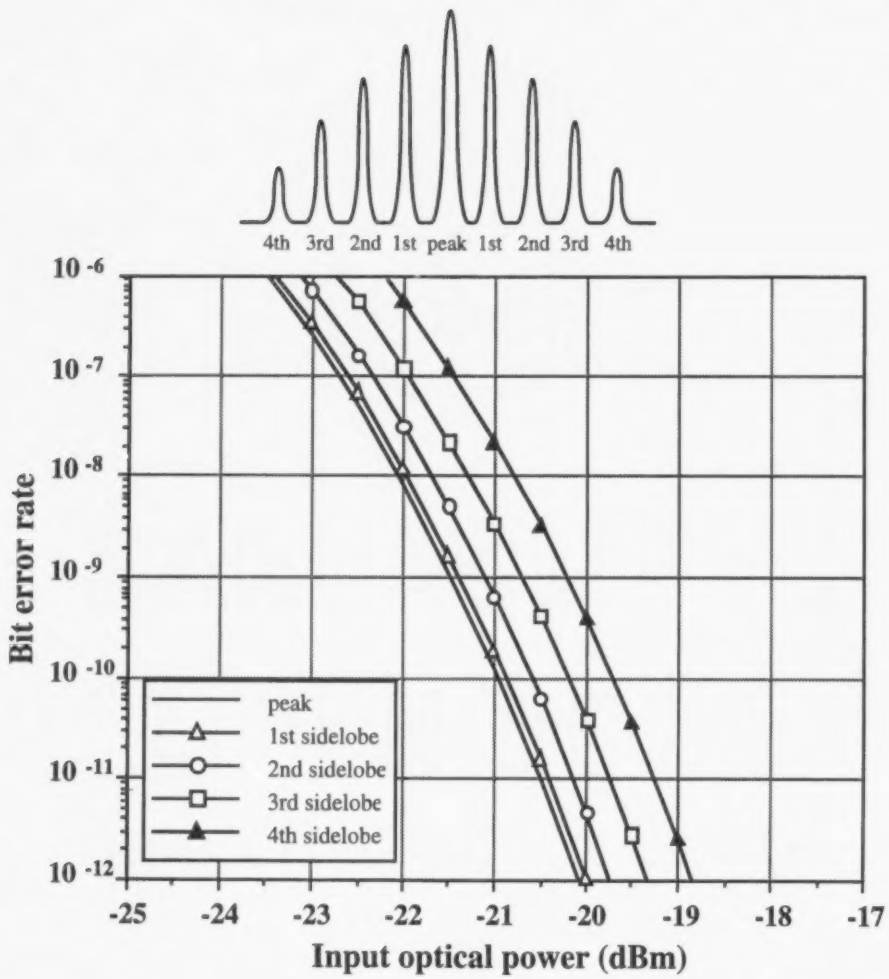

Figure 18C. BER curves for off peak gain resonances. Bandwidth = 10 MHz and cavity gain = 14.68 dB.

Notice that the penalty for coinciding with a Fabry-Perot resonance off peak is small in all three cases. The actual optical gains present at the individual sidelobes are given in Table 3.

Table 3. Cavity gain at various sidelobes			
Figure 18A, 18C: bias point at 95% threshold		**Figure 18B: bias point at 91% threshold**	
peak gain	14.68 dB	peak gain	9.16 dB
1st sidelobe	14.46 dB	1st sidelobe	9.04 dB
2nd sidelobe	13.85 dB	2nd sidelobe	8.70 dB
3rd sidelobe	12.92 dB	3rd sidelobe	8.17 dB
4th sidelobe	11.76 dB	4th sidelobe	7.47 dB

Consider the results in Figures 18A and 18C. The difference in gain between the central peak and the fourth sidelobe is 2.92 dB and the resulting sensitivity degradation is about 1.17 dB for Figure 18A and 1.25 dB for Figure 18C. For Figure 18B, the gain difference between the peak and the fourth sidelobe is 1.69 dB and the sensitivity degradation is about 0.6 dB. From these results it is evident that the sensitivity penalties for signal wavelengths matching the off-peak resonances of the Fabry-Perot laser detector are small. Hence the matching of the peak signal wavelength to the peak Fabry-Perot cavity resonance is not crucial to obtain adequate detector sensitivity since the sensitivity penalty for coinciding with a detector sidelobe off the gain peak is small.

2.4 System considerations

There are many important factors from a systems point of view that have to be addressed in order for the FSHD system to be viable in a widespread commercial application. Factors such as the transition time needed to switch from transmitting to detecting (or detecting to transmitting), response time of the laser detector, synchronization concerns, and four potential causes of system degradation (chromatic dispersion, mode partition noise, longitudinal mode hopping, and light

reflections from optical connectors) will now be discussed along with a power budget calculation to arrive at a bit rate distance product estimate for the FSHD system.

2.4.1 Switching time between states

The switching time of a Fabry-Perot laser diode between transmitting and detecting states is very important in a half-duplex bidirectional system. This switching time is defined as the maximum of the time needed to switch from either transmitting to receiving (turn-off time) or receiving to transmitting (turn-on time). A rate equation model to predict switching times is introduced first, followed by individual discussions on the turn-off time theory and experimental results in Sections 2.4.1.2 and 2.4.1.3 and turn-on time theory in Section 2.4.1.4. Concluding remarks on the switching time analysis are made in Section 2.4.1.5.

2.4.1.1 The rate equations

To properly model either the turn-on time or the turn-off time requires an understanding of the rate equations which govern the dynamic response of a laser diode. The differential equation for the time rate of change of the carrier density in the active region of a laser diode is [35, 36]

$$\frac{dn}{dt} = \frac{i_{inj}}{qlwd} - An - Bn^2 - Cn^3 - \left[\frac{\xi c}{n_{eff} lwd}(n - n_{tr})\right]S \qquad (22)$$

where n = carrier density in active region (m^{-3}), i_{inj} = laser diode injection current (A), l = length of active region (m), w = width of active region (m), n_{eff} = refractive index of active layer, d = depth of active region (m), A = trap or surface recombination coefficient (s^{-1}), B = radiative recombination coefficient ($m^3\ s^{-1}$), C = Auger recombination coefficient ($m^6\ s^{-1}$), c = speed of light ($m\ s^{-1}$), $\xi = \partial g_m/\partial n$ = rate of change of material gain with carrier density (m^2), n_{tr} = carrier density at material transparency (m^{-3}), and S = photon number inside active region. The recombination coefficients A, B, and C are taken from reported values for 1.3 μm wavelength devices. The term An represents nonradiative transitions such as trap

or surface recombination, the term Bn^2 represents radiative transitions and the term Cn^3 represents Auger recombination. Auger recombination cannot be ignored in InGaAsP devices [37, 38] and hence is included in the differential equation. The equation for the time rate of change of photon number follows as [35, 36]

$$\frac{dS}{dt} = \left[\frac{c\alpha}{n_{eff} lwd} - \frac{\xi c}{n_{eff} lwd} (n - n_{tr}) \right] + R_{sp}$$
$$R_{sp} = \beta_{sp} B n^2 lwd \tag{23}$$

where α = total internal scattering and facet losses (m^{-1}), and β_{sp} = fraction of spontaneous emission coupled into lasing mode

Equations (22) and (23) together represent the rate equations of a laser diode. These differential equations can then be solved numerically to arrive at either a turn-on delay time or a turn-off time.

2.4.1.2 Transmitting to receiving turn-off time

The turn-off time of the laser can be substantial and is determined by how fast the carrier density in the active region can be reduced from the threshold carrier density value to the detector bias point carrier density value. The carrier density may be depleted in two ways. The electrons and holes may recombine through an external electrical path or they may recombine internally due to radiative or nonradiative processes. Thus the decay of the carrier density, which translates into an observable decay of the diode junction voltage, can be thought of as having two distinct time constants: an external time constant τ_{ext} and an internal time constant τ_{int}. These two separate decay mechanisms will now be explained individually.

The internal decay process is most easily explained by examining the rate equations of a laser diode, shown in Section 2.4.1.1. At a steady state value, the time rate of change of carrier density and photon number will be zero, which leads to

$$i_{inj} = qlwd\left[An + Bn^2 + Cn^3 + \frac{\xi c}{n_{eff} lwd}(n - n_{tr})S\right] \qquad (24)$$

and

$$S = \frac{\beta_{sp} Bn^2 lwd}{\frac{c\alpha}{n_{eff}} - \frac{\xi c}{n_{eff}}(n - n_{tr})} \qquad (25).$$

The system of equations given by (24) and (25) generate a dc injection current and photon number given a steady state carrier density. When switching from transmitting to receiving, the initial carrier density value will be close to the threshold carrier density value. The final carrier density value, corresponding to the detector bias point, will lie somewhere between the transparency point and the threshold point. This typically results in a detection bias current of between 80% to 98% of the threshold current. Thus by solving the rate equations for an initial and final carrier density and plotting the solution versus time the turn-off time of the laser due to internal recombination can be estimated.

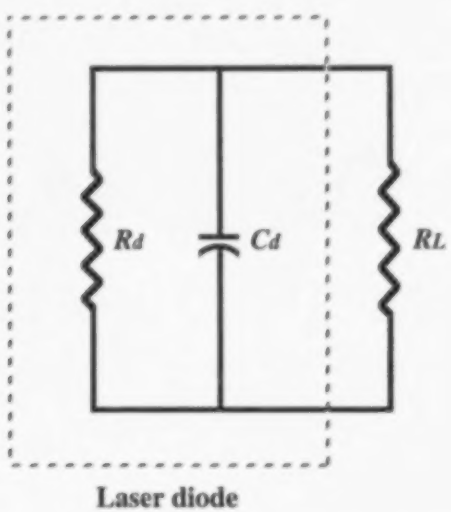

Figure 19. Simple laser diode equivalent circuit from [11].

Another important carrier decay process is due to the external circuitry attached to the laser. A laser diode can be modeled as a circuit element by a diffusion capacitance C_d in parallel with a resistance R_d. When the diode is connected in parallel with a load resistor R_L, the equivalent circuit [11] can then be represented by Figure 19.

The time constant of the circuit in Figure 19, is easily calculated as

$$\tau = C_d \frac{R_L R_d}{R_L + R_d} \tag{26}.$$

Thus Equation (26) provides a means of calculating the laser turn-off time due to external recombination. However, as the laser is switched between states, the diffusion capacitance C_d and diode resistance R_d will vary, which changes the external turn-off time. Harder et al [39] give a relation for the laser diffusion capacitance as

$$C_d = \frac{q}{V_T m} n_o \tag{27}$$

where

$$m = 2 + \frac{n_0}{lwd\,2\sqrt{2}} \left(\frac{1}{N_v} + \frac{1}{N_c} \right) \tag{28}$$

and n_O = bias carrier density, $V_T = kT/q$ = 26 mV at 300 K, N_v = effective valence band carrier density , and N_c = effective conduction carrier density.

N_c and N_v have the values [23]

$$N_c = 2 \left(\frac{2\pi m_c kT}{h^2} \right)^{1.5} \tag{29}$$

and

$$N_v = 2\left(\frac{2\pi m_v kT}{h^2}\right)^{1.5} \tag{30}$$

where m_C = effective electron mass in conduction band and m_V = effective electron mass in valence band. For $m_C = 0.5\ m_e$ and $m_V = 0.07\ m_e$, where m_e is the free electron mass, $N_C = 8.8516\ 10^{24}\ m^{-3}$ and $N_V = 4.6368\ 10^{23}\ m^{-3}$. Using this model, the diffusion capacitance of a typical laser diode with parameters listed ranges from a few picofarads at zero bias to several hundred picofarads at forward bias. The diffusion capacitance of a laser diode versus carrier density using (27) through (30) is shown in Figure 20.

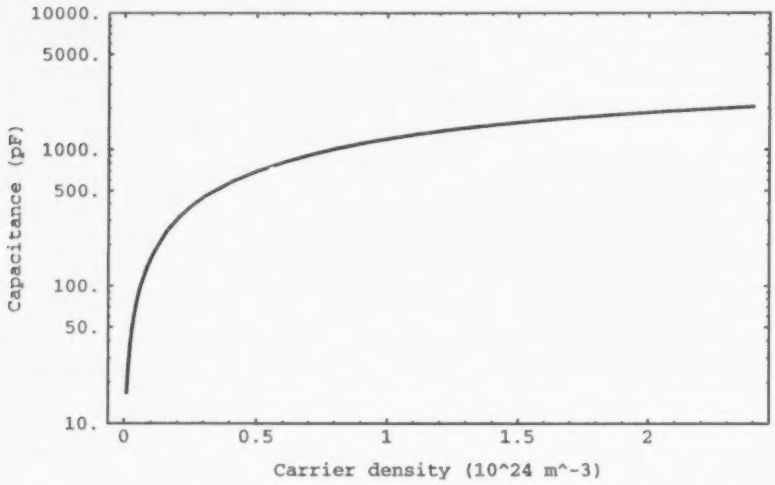

Figure 20. Laser diode capacitance versus carrier density.

It is important to note that the diffusion capacitance of the laser diode increases drastically when the diode becomes forward biased and then starts to level off as the carrier density approaches the transparency and threshold points. Thus switching the laser between two points above and below threshold, has little effect in changing the diffusion capacitance of the laser since both transmitting and detecting points are well above the turn-on voltage of the laser. Moreover, the series resistance of the laser R_S can be taken as constant if the laser diode remains forward biased. Thus the external turn-off time constant relation given in (26) is valid for

switching from a transmitting state to just below threshold since both the laser diffusion capacitance and the series resistance are approximately constant throughout the transition.

2.4.1.3 Experimental turn-off time results

The laser diode was switched between a transmitting state above threshold to zero bias to compare turn-off times with theoretical results from [11]. The experimental setup used to measure the laser turn-off time is shown in Figure 21.

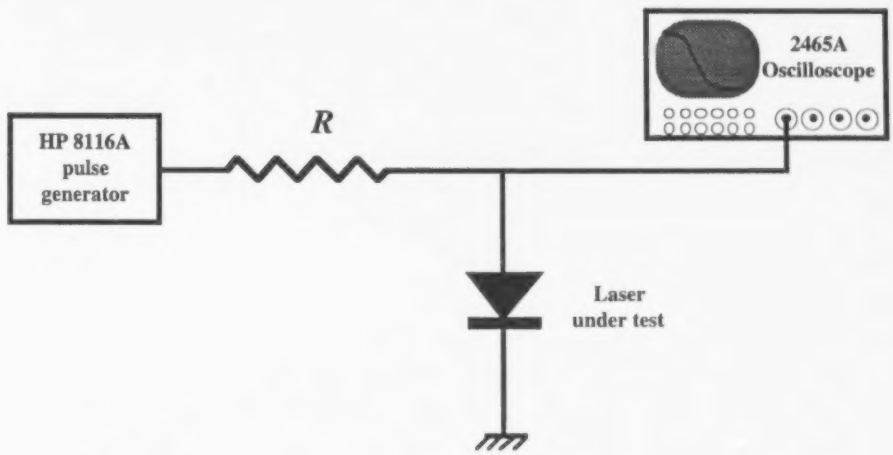

Figure 21. Experimental setup to measure turn-off time.

A Hewlett Packard 8116A function generator was used to drive the laser diode between zero bias to above threshold while the junction voltage was monitored on the oscilloscope. Table 4 shows the experimental results and the values given in [11].

Table 4. Comparison of turn-off times with [11].		
Load resistance R_L	**Turn-off time to 10% (Kashima- [11])**	**Observed turn-off time to 10%**
83 Ω	45 ns	60 ns
119 Ω	80 ns	88 ns
299 Ω	200 ns	222 ns
415 Ω	250 ns	276 ns
549 Ω	300 ns	337 ns
731 Ω	350 ns	418 ns
1000 Ω	400 ns	537 ns

The results in Table 4 are in general agreement. The experimental results are consistently higher than the results reported by Kashima, which may indicate that the capacitance of the laser used in the measurements is slightly higher.

Since turn-off time experiments switching from a transmitting state to zero bias generally agreed with published results, the experiment was expanded to include observing turn-off times between a transmitting state above threshold and a detector bias point just below threshold. The same experimental setup shown in Figure 21 was used with a dc offset added to the laser drive pulse. The function generator was able to produce pulses with 5 ns turn-off times when the laser was switched from above threshold to just below threshold.

Results of turn-off time measurements for a number of bias points and two different external resistances are shown in Figure 22. The observed turn-off times are consistently lower than the predicted times from the rate equation model. The observed turn-off time includes both internal recombination effects and

the external RC time constant decay, and thus it is understandable why the observed turn-off time is consistently smaller than the calculated turn-off time. The discrepancy will become larger as the external resistance is reduced to 100 Ω due to the corresponding reduction in the external RC time constant. This is also observed in Figure 22.

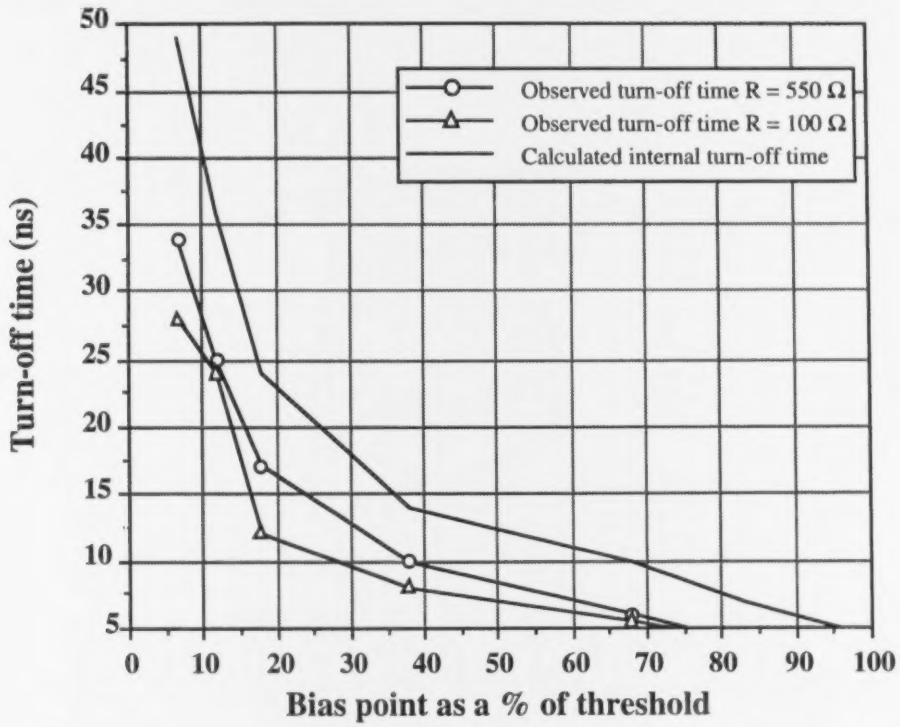

Figure 22. Calculated internal recombination turn-off times and observed turn-off times for different external time constants.

Also notice that the turn-off time for the laser diode for detection points close to threshold is less than 5 ns while the turn-off time to zero bias is as high as 537 ns (Table 4) depending on the external resistance in the laser drive circuit. Thus the turn-off time of the FSHD system is substantially lower than the turn-off time of a conventional half-duplex transceiver system operating at a zero bias detector point.

2.4.1.4 Turn-on delay time and relaxation oscillations

The turn-on delay of a laser diode is due to the finite time needed to build up sufficient carrier density in the active region to achieve enough optical gain to sustain oscillation. After this delay time passes the photon number in the cavity will exhibit underdamped oscillations and finally decay to an equilibrium value. The frequency of this underdamped oscillation is called the relaxation frequency of the laser diode. Typical relaxation oscillations are in the frequency range of 1-5 GHz. To illustrate this phenomenon, a computer program agrawal.m was written for *Mathematica* which solves the coupled differential equations for carrier density and photon number. A result of this calculation is shown in Figure 23.

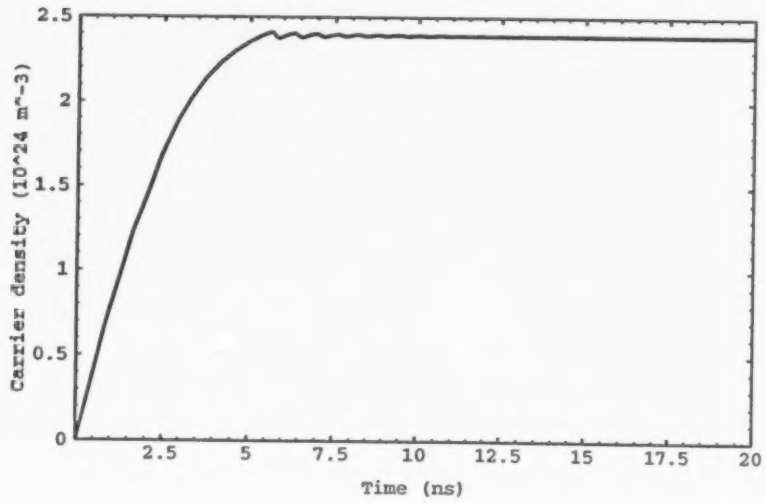

Figure 23A. Carrier density transient as a result of a step increase in injection current from zero to 112% of the threshold current.

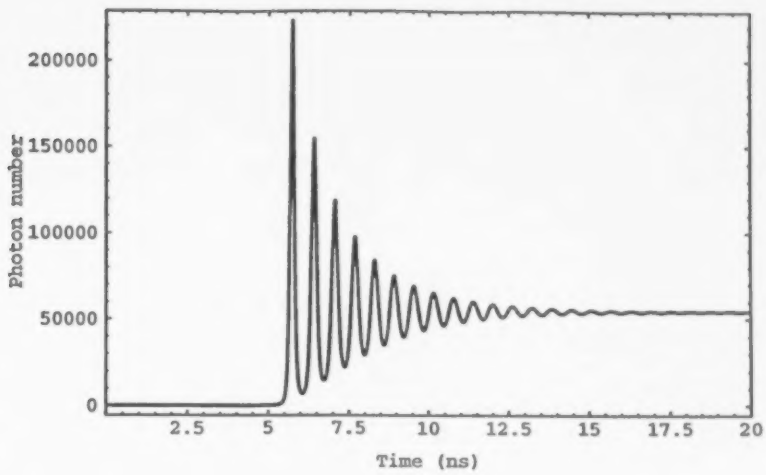

Figure 23B. Photon number transient as a result of a step increase in injection current from zero to 112% of the threshold current.

Notice that in Figure 23 the turn-on time is approximately 5.5 ns and the total time needed for the photon number to arrive within 10% of the final value is about 15 ns. Both these times can be reduced if the laser diode is switched from a bias point just below threshold, as in the FSHD system, rather than from zero bias. This can be observed in Figure 24A and 24B, which shows the carrier density and photon number transients when the laser is turned on from just below threshold. Notice that the turn-on time and the time to 10% of the final value have been reduced to about 0.9 ns and 10 ns, respectively.

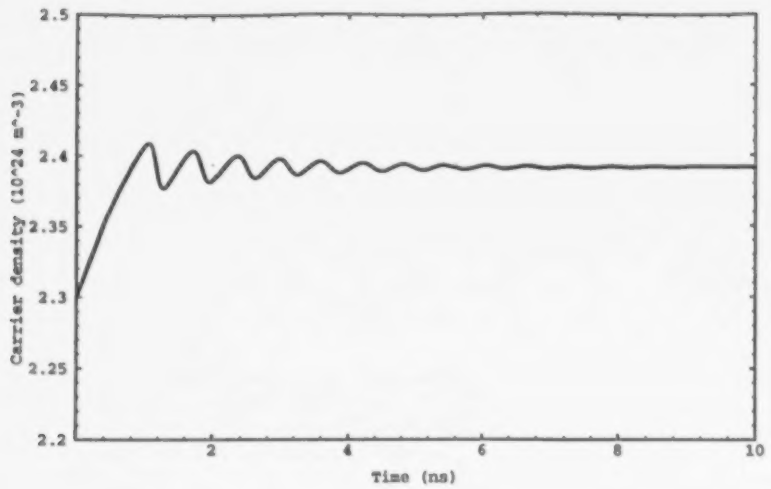

Figure 24A. Carrier density transient as a result of a step increase in injection current from 92% to 112% of the threshold current.

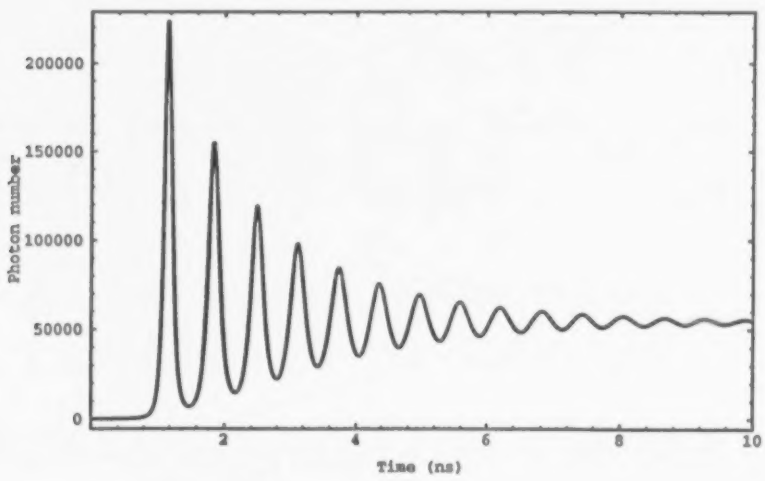

Figure 24B. Photon number transient as a result of a step increase in injection current from 92% to 112% of the threshold current.

To confirm the predictions in Figures 23 and 24 the turn-on time of the laser can be estimated from the rate equations. If the assumption is made that the stimulated emission term in the carrier density rate Equation (22) can be omitted, the differential equation simplifies to

$$\frac{dn}{dt} = \frac{i_{inj}}{qlwd} - An - Bn^2 - Cn^3. \tag{31}$$

Agrawal [23] solves (31) and finds the turn-on delay of a laser diode using:

$$t_d = qlwd \int_{n_0}^{n_{th}} \frac{1}{i_{inj} - qlwd(An - Bn^2 - Cn^3)} dn \tag{32}$$

where i_{inj} = final value of injection current (greater than threshold current), n_O = initial value of carrier density (m^{-3}), and n_{th} = threshold value of carrier density (m^{-3}).

A closed form solution for (32) does not exist, so the turn-on delay time must be solved using numerical integration techniques. Solving (32) for the cases shown in Figures 23 and 24 gives turn-on delays of 5.36 ns and 0.79 ns respectively, which compares favorably with the results obtained by solving the coupled equations for carrier density and photon number.

2.4.1.5 Concluding remarks on switching time

As defined previously, the switching time of the overall FSHD system is the maximum of the turn-off time and the turn-on time. As seen from Section 2.4.1.4, turn-on times for laser diodes biased just below threshold are in the sub-nanosecond range while turn-off times are less than 5 ns for detector bias points just below threshold. Thus the limiting factor on system performance will be the time needed to switch from transmitting to detecting, or the turn-off time.

2.4.2 Response time of a Fabry-Perot laser diode

The response time of a Fabry-Perot laser diode detector is limited by the diffusion capacitance of the laser diode and the resistance R_i in the equivalent

circuit model (see Figure 11). To calculate an actual value for the response time of the Fabry-Perot laser detector, consider Equation (9), which relates the detected junction voltage u to the generated photocurrent i_{sig} due to the input optical power. The frequency at which the responsivity of the device is reduced by 3 dB is given by (10). The value for R_i is given by Equation (8). The value of the diffusion capacitance for a forward biased laser diode can be approximated by (7) which gives $C \approx 1728$ pF if the change in Fermi level separation versus carrier density is assumed constant for points between transparency and threshold. A more accurate diffusion capacitance model is given by Equation (27). Individual 3 dB response time bandwidths are calculated in Table 5 for different detector bias points using both Equations (7) and (27) to arrive at a diffusion capacitance value.

Table 5. Calculated detector bandwidth. Input power = -20 dBm.

Cavity gain (dB)	*C1* (pF) using Equation (7)	*C2* (pF) using Equation (28)	R_i (Ω)	Bandwidth (MHz) using	
				C1	*C2*
3.25	1728	1869	1.064	88.3	86.9
5.75	1728	1889	1.031	91.1	85.9
9.16	1728	1909	0.995	94.3	84.9
14.68	1728	1929	0.932	100.6	84.0

The minimum detector bandwidth using the capacitance *C2* in the model equations is 84 MHz for a cavity gain of 14.68 dB. Recall from Section 2.3.2.3 that the sensitivity of the Fabry-Perot detector is about -16 dBm for the same cavity gain and a bandwidth of 30 MHz. Hence the laser diodes acting as detectors will deliver adequate performance at 30 MHz since the system electrical bandwidth (imposed by noise restrictions) is less than the detection bandwidth of the devices.

2.4.3 Synchronization of the two laser transceivers

Synchronization of the two laser diodes is essential in any half-duplex system. In the case of the FSHD system, it is very important that the transceiver be ready for detection as soon as a group of transmitted bits arrives at the receive laser. To achieve this synchronization, overhead bits must be placed at the beginning and end of each bit group. This way, the drive circuitry of the laser in detection mode will interpret the overhead bits as a signal to switch the laser to the transmission mode. Adding overhead bits at the beginning and end of each transmitted group then allows for many groups or packets of data to be present on the optical link at the same time. In doing so, three important restrictions on the system must be observed. First, the sum of the transmit and receive times for both lasers must be fixed, although the individual transmit and receive times may vary. Second, the system propagation time must be equal to an integer multiple of half of the sum of the transmit and receive times. Third, the individual transmit and receive times must not change more than once in a time frame equal to twice the propagation time. These rules were arrived at using a timing diagram for packet transmission on the system and still allow for the flexibility of dynamic directional bit rates.

2.4.4 System Impairments

Four sources of system degradation in any optical communication system are chromatic dispersion in the fibre, laser mode hopping, mode partition noise, and light reflections from optical connectors or splices. The causes of these system limitations will now be discussed individually.

Chromatic dispersion in silica fibres causes pulse broadening since light at different wavelengths travels at different group velocities down the fibre. The relative time delay through the fibre can be expressed as [40]

$$\tau(\lambda) = a + b\lambda^2 + \frac{c}{\lambda^2} \tag{33}$$

where $\tau(\lambda)$ = time delay as a function of wavelength (ns/km), a = -34.68 (ns/km), b = 10.504 (ns/(km μm^2)), and c = 29.988 ((ns μm^2)/km)

In (33) the time delay τ has the units ns/km if λ is expressed in μm. The dispersion penalty in dB can be calculated as [40]

$$dB_{chr} = B^2 \sigma^2 L^2 D \tag{34}$$

where

$$D = \left[\left(\frac{d\tau(\lambda)}{d\lambda} \right)^2 + \frac{1}{2} \sigma^2 \left(\frac{d^2\tau(\lambda)}{d\lambda^2} \right)^2 \right] \tag{35}$$

and σ = source spectral width (μm), B = bit rate (bits/ns), and L = transmission distance (km). For a bit rate of 60 Mb/s, a transmission distance of 15 km, and a Fabry-Perot laser spectral width of 5 nm at a peak wavelength of 1310 nm, the dispersion penalty given by (34) is very close to zero dB and thus the effects of fibre chromatic dispersion on system performance can be ignored.

Mode hopping occurs in Fabry-Perot laser diodes when the dominant longitudinal mode oscillates over a range of allowable laser modes. This mode hopping then causes pulse jitter at the detect laser due to light of different wavelengths traveling at different group velocities down the fibre. To determine if mode hopping is a factor in the FSHD system, consider the formula for time delay as a function of wavelength (33). Using 1310 nm and 1315 nm as the maximum wavelength deviation occurring due to mode hopping results in pulse jitter of 78 ps after 15 km of transmission. This jitter time is much less than the 16.67 ns bit time at 60 Mb/s. Hence mode hopping effects can also be ignored in the FSHD system.

Mode partition noise is a result of inherent fluctuations in the power in each laser mode varying from bit to bit and causes a system penalty. The theory behind mode partition noise can be found in [41-42]. A previous calculation done for a graduate fibre optics course project using an OC-12 bit rate of 622 Mb/s and a transmission distance of 30 km reveals that the source spectral width must be less than about 10 nm for an allowable mode partition noise penalty of less than 1 dB. Since the FSHD system bit rate is about one tenth of the OC-12 system, mode partition noise can be neglected in the FSHD system.

Back reflection of light from optical connectors can impact the performance of bidirectional systems which use a single fibre. The magnitude and location of the reflections will determine the severity of the degradation. For example, connectors that rely on physical contact (FC- PC and FC- APC) typically reflect -40 to -60 dB of the incident optical power. Thus optical feedback from physical contact connectors will be very small and their effect on system performance can be ignored. Notwithstanding, optical connectors which do not make physical contact (FC- type) reflect about 8 % (-11 dB) of the incident power due to two air glass interfaces. The reflected power in this case would be comparable to the signal power from the other end of the system. Hence FC- type connectors would have a definite impact on performance and thus their use must be avoided in the FSHD system.

2.4.5 Power budget calculation

A power budget calculation yields the maximum allowable transmission distance for the FSHD system. The key parameters in this calculation are transmitter power, optical path loss, coupling and splice losses, and detector sensitivity. As discussed previously, chromatic dispersion, mode hopping and mode partition noise have a negligible impact on system performance and thus can be excluded from the power budget calculation shown in Table 6.

Table 6. Power budget calculation		
Available power from transmitter	0 dBm	
Sensitivity of detector at 10^{-9} BER and an electrical bandwidth of 30 MHz	-16 dBm	
Total system margin available		**16 dB**
Coupling losses	9 dB	
Unallocated margin	3 dB	
Attenuation for 13 km span (0.3 dB / km loss @ 1.3 μm)	4 dB	
Total path loss		**16 dB**

From the results in Table 6 it is clear that a 13 km span is feasible for the FSHD system with an electrical bandwidth of 30 MHz. If the system were never switched, this would correspond to a bit rate of 60 Mb/s. However, with the dead time incurred by switching the devices and overhead bits to maintain synchronization, the user bit rate in a typical application is reduced to about 50 Mb/s. The user bit rate distance product of the system would then be 650 Mb km/s, which meets the minimum performance requirement stated previously in Section 1.3.

CHAPTER 3. POSSIBLE IMPROVEMENTS TO THE FSHD SYSTEM

Throughout the discussion of the proposed FSHD system the transceivers have been Fabry-Perot type laser diodes. This section will consider the use of other types of laser diodes as transceivers to see if any improvement in system performance can be realized. In addition, the potential for ultrafast switching is discussed along with a possible feedback control circuit to keep the transceiver biased for optimal detector performance.

3.1 Use of different laser diodes for transceiver elements

One of the most attractive features of the proposed fast switching half-duplex system is its low cost compared to other more elaborate short-haul bidirectional systems. The cost savings is realized by using relatively inexpensive Fabry-Perot laser diodes for transceiver elements and by reducing the number of components needed at each end of the link. The effects of using different laser diodes for transceivers will now be discussed to determine if enhanced responsivity or sensitivity is possible while still preserving the economic viability of the FSHD system.

3.1.1 The effect of using a different laser diode on responsivity

The responsivity of a laser diode biased below threshold is mainly a function of the device cavity gain as seen in Section 2.3.1.2. The use of devices with antireflection coatings, or traveling wave devices, allows for higher unsaturated cavity gains than is available for uncoated amplifiers. Hence the responsivity of traveling wave devices can be larger due to an increased unsaturated cavity gain. In addition, the responsivity of traveling wave devices is relatively insensitive to small input wavelength changes, unlike Fabry-Perot laser detectors, and the choice of traveling wave devices as transceivers allows for the system to operate in full duplex mode.

The cavity gain of uncoated devices with different geometries (such as DFB, ridge waveguide, or transverse junction stripe laser diodes) should be roughly equal for

the same bias conditions. Thus responsivities for all other uncoated laser diodes should not differ for the same input power and device cavity gain.

3.1.2 The effect of using a different laser diode on sensitivity

A possible sensitivity improvement lies in the utilization of a distributed feedback (DFB) laser instead of a Fabry-Perot laser as the transceiver element for the system. Since the DFB laser has only one significant longitudinal mode, the signal spontaneous beat noise and the spontaneous spontaneous beat noise would be less than what is observed in multi longitudinal mode Fabry-Perot lasers. Therefore it is conceivable that a DFB laser transceiver can improve noise performance and hence improve detector sensitivity. However, there are two negative aspects of choosing DFB lasers for the FSHD system transceivers. First, since DFB lasers operate in a single longitudinal mode, it would be more difficult to overlap two single mode DFB laser peak wavelengths than two multimode Fabry-Perot resonances. Second, the cost of DFB laser modules is much higher than the cost of Fabry-Perot lasers. Thus the improved detector sensitivity by using DFB lasers would be offset by biasing problems and increased cost.

Another sensitivity improvement comes from making the Fabry-Perot device a traveling wave amplifier by applying antireflection coatings on the laser facets. This would result in sensitivities of -36 dBm to -30 dBm at 200 Mb/s [22] instead of the -16 dBm sensitivity at 60 Mb/s seen for the Fabry-Perot devices.

Excluding DFB lasers and traveling wave amplifiers, other types of laser diodes (such as ridge waveguide or transverse junction stripe laser diodes) will give no improvement in detector sensitivity, since the sensitivity is mainly a function of the optical gain spectrum of the device and is limited by signal spontaneous beat noise. However, if the detector bias voltage is lowered to zero volts and detection takes place by absorption rather than by stimulated emission, it is possible that an increase in detector sensitivity can be realized. Reported sensitivity is -36 dBm at a bit rate of 3.5 Mb/s [11]. However, this increase in sensitivity obtained by lowering the detector bias voltage will increase the turn-off time needed between transmitting and detecting states for the system.

3.2 Ultrafast switching potential

A significant decrease in turn-off time can be realized by the application of an appropriate fast pulse to the laser diode that has an amplitude which is less than the detector bias voltage. The effect of this "interim" or "accelerator" pulse on turn-off time is shown in Figure 25.

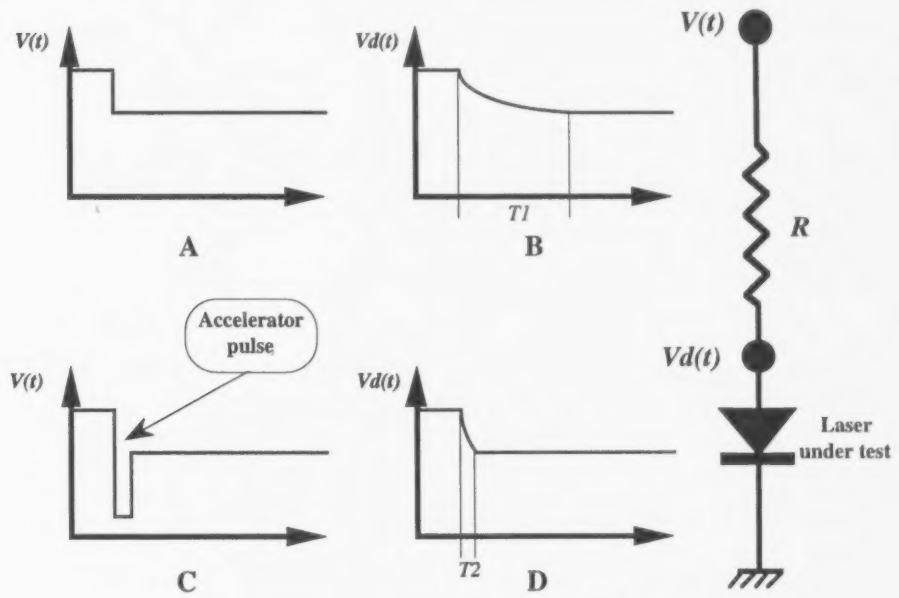

Figure 25. Ultrafast switching of laser diodes.

In Figure 25A, a voltage pulse *V(t)* is applied to the laser to switch it from transmitting to receiving. The actual voltage across the diode in Figure 25B decays to the final value after a turn-off time delay of *T1* seconds. In Figure 25C, a different voltage pulse with an interim value lower than the final value is applied to switch the laser. The voltage across the laser in Figure 25D will decay towards a final value which is lower than the desired final value, but will reach and stay at the desired final value if the accelerator drive pulse is of optimal height and duration. The turn-off time is thus reduced to *T2* seconds by the application of an accelerator pulse with a lower amplitude than that of the desired detector bias point.

The ultrafast switching potential of laser diodes was confirmed using the rate equation model program agrawal.m in Appendix 4. Turn-off times of more than 10 ns could be reduced to less than 1 ns by the application of an optimum accelerator pulse.

At present, the overall system switching time is limited by the time needed to switch from transmitting to detecting (the laser turn-off time). If this turn-off time were to be made smaller than one nanosecond, the time needed to switch the laser from detecting to transmitting (the turn-on time) would then become the limiting factor for the overall switching time. Recall from Section 2.4.1.4 that a typical turn-on time for lasers biased just below threshold is about 0.8 ns. Thus efforts to reduce device turn off times below the turn-on time of the laser are in vain since the turn-on time represents the ultimate switching time limit of the FSHD system. Therefore this ultrafast switching concept could be used to equalize the turn-on delay and turn-off time of the lasers and thus minimize the overall switching time of the FSHD system.

3.3 Thermal stability problems and possible solutions

The Fabry-Perot resonant gain peaks of a laser diode biased below threshold are sensitive to changes in device temperature. To keep a Fabry-Perot resonance of the detect laser at a fixed frequency, temperature stabilization of the laser becomes desirable, since a slight temperature fluctuation will cause a shift in resonant frequency. The magnitude of this shift varies, but one estimate of this shift for InGaAsP material is 0.35 nm per degree Celsius at forward bias [8]. From this, it is evident that even a small temperature change of 0.5 °C is enough to shift the detector resonance away from the signal peak and destroy the responsivity of the device. In fact, O'Mahony [43] states that to maintain the cavity gain of a Fabry-Perot amplifier within ± 1 dB the temperature of the device must be controlled within ± 0.1 °C. Thus if the FSHD system is designed to operate in a hostile environment where temperature changes are substantial, the detector must be temperature stabilized within a small temperature range to avoid sudden drops in responsivity. Conventional temperature stabilization using a thermistor and a feedback control loop has a thermal time constant of several hundred microseconds. Thus all the transmitted bits would be lost in error if the temperature change was

drastic enough to impair detector responsivity. To quickly stabilize the detect laser requires a feedback control mechanism that can act much faster than thermal compensation so that transmitted bits at the start of a detect sequence would not be lost. One approach to accomplish this is to make use of existing packaging in commercially available laser diodes. Most laser chip packages contain a photodiode to monitor the light output from the back facet of the laser diode. This back facet monitor could be used in a feedback loop to adjust the injection current and hence the cavity resonances of the detector.

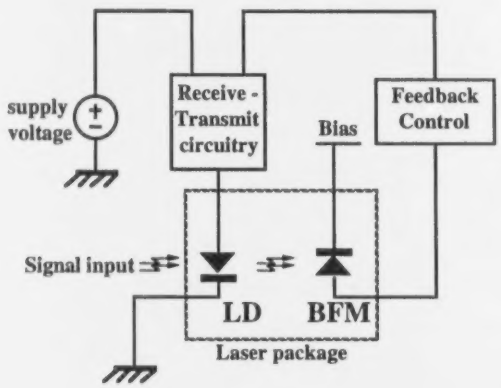

Figure 26. Possible feedback control system to stabilize laser detector responsivity. LD = laser diode, BFM = back facet monitor.

Consider the block diagram of the proposed feedback control mechanism shown in Figure 26. At the beginning of a receive session for laser #2, laser #1 would start by sending a dc light output impressed with a very small amplitude sine wave. The frequency of this sine wave should be lower than the reciprocal of the response time of the laser diode calculated in Section 2.4.2. After the detect laser amplifies this combined dc and ac signal, the signal is detected by the back facet monitor. A circuit could be constructed that would compare the relative intensity values detected at the bottom and top of one cycle. This information will allow a compensation circuit to increase or decrease the detector injection current as necessary until the detect laser peak would coincide exactly with the signal peak. At this point, the detected intensities at the top and bottom of the

signal would be equal, and no further compensation would be necessary. The detect laser would then be ready to receive information since the detection bias point has been optimally set to maximize the responsivity of the receive laser.

Although the possibility of implementing a feedback control system to set the optimum detector bias point appears feasible, there is an undesirable feature in doing so. If the feedback control mechanism limits the turn-off time to around 20 ns or greater, the turn-off time of the FSHD system using feedback then becomes roughly equivalent to turn-off times of conventional half-duplex systems between zero bias and above threshold. Since a laser detector at zero bias has better responsivity and sensitivity than a detector biased just below threshold, adding the feedback control might make the FSHD system unnecessarily complicated and inferior to existing systems. Therefore both switching time and detector performance considerations must be addressed before a detector bias point feedback mechanism is put into place for the FSHD system.

CHAPTER 4. COMPARISON WITH OTHER BIDIRECTIONAL SYSTEMS

This chapter will compare the performance of the FSHD system with other more popular schemes for bidirectional optical communication. These systems are bidirectional communication using directional couplers (System #2), switching between a transmitting state and a zero bias detection state (System #3), and full duplex bidirectional communication using traveling wave laser amplifiers (System #6).

4.1 A comparison of the FSHD system with the directional coupler system

A bidirectional system using one single mode fibre, two directional couplers, two lasers and two photodetectors as described in Section 1.1.2 represents one option for bidirectional optical transmission over a single fibre. Compared to the FSHD system, this system has the potential for faster bit rates over longer transmission distances. Typical pin photodetector sensitivities would range from -40 dBm to -30 dBm depending on the actual system bit rate. This represents a 15 to 25 dB improvement in detector sensitivity as compared to the FSHD system. Moreover, this directional coupler system can operate in full duplex mode, and there is no need for the two laser transmitters to retain any form of synchronization with each other. However, the cost of the extra components needed for the directional coupler system can be substantial. This includes extra single mode fibre couplers and extra photodetectors at each end. In addition, the directional couplers introduce extra loss in the system since the signal is split between the photodetection branch and the transmission branch. Thus the increased path loss and the expensive addition of extra couplers and photodetectors in the directional coupler system gives the FSHD scheme a major advantage for short-haul cost sensitive optical links.

4.2 A comparison of the FSHD system with switching between a transmitting state and a zero bias detection state

The half-duplex bidirectional optical link where the lasers are switched between a transmitting state and a zero bias detection state (system #3) is also an option for bidirectional optical communication. Instead of switching to a detecting state just below laser threshold as in the FSHD system, the laser is switched to a zero bias detection state to improve responsivity. Increased responsivity and better noise performance are the main factors why detect lasers biased at zero volts have a sensitivity of about -36 dBm at a 5 Mb/s bit rate [11]. However, the turn-off time incurred by switching the laser from transmitting above threshold to zero bias can be very substantial as noted in Section 2.4.1.3.

Another important difference between the FSHD system and this half-duplex system lies in the synchronization of the two remote lasers. Most half-duplex systems transmit such that only one "packet" or group of data is present on the fibre link at a given time. This packet of data then "bounces" between the two remote ends of the link, where data is received and new data transmitted. Thus in this "ping pong" type of half-duplex arrangement synchronization of the two lasers is not a problem. The FSHD system approach differs in that many packets of information are present on the link at a given time, and synchronization is achieved by the addition of overhead bits at the end of every information packet. By adding overhead bits to account for the synchronization, the FSHD system dead time can then be made independent of the total length of the link. In contrast, the performance of the ping pong system is limited by the signal propagation time, which can amount to several hundred nanoseconds for transmission distances of 5 - 15 km. Thus by having many packets of information on the link at a given time, the FSHD system capacity is greatly increased over the capacity of a comparable ping pong transmission system.

4.3 A comparison of the FSHD system with the full duplex traveling wave laser amplifier system

The laser amplifier detector scheme described in Section 1.1.5 is unique in that it is the only bidirectional optical communication system to operate in full duplex mode needing just one major component at each end. Other bidirectional systems such as the directional coupler system can operate in full duplex mode but require additional fiber couplers and photodetectors. Using

traveling wave devices instead of Fabry-Perot devices results in significant performance increases. First, the traveling wave device sensitivity (-30 to -36 dBm at 200 Mb/s) is much higher than the Fabry-Perot sensitivity (-16 dBm at 60 Mb/s). In addition, the traveling wave detector gain profile is insensitive to small input wavelength changes or changes in device temperature, while the Fabry-Perot device gain is highly input wavelength and temperature dependent. The relatively stable gain versus wavelength profile of traveling wave amplifiers combined with the fact that a suitable feedback control circuit to stabilize the wavelength and temperature dependent Fabry-Perot cavity gain may significantly increase the switching time of the lasers gives the traveling wave amplifier system both a stability and performance advantage over the FSHD system.

A potential drawback of the traveling wave amplifier system is that the increased source spectral width due to spontaneous emission would impact the transmission distance severely due to chromatic dispersion. Indeed, [18] has found that chromatic dispersion limits the maximum transmission distance to 5.5 km at 50 Mb/s when operating at a peak wavelength of 1.55 μm. The chromatic dispersion penalty at 1.3 μm can be estimated from Equations (33) and (34). For a source spectral width of 30 nm, a bit rate of 200 Mb/s and a transmission distance of 30 km, the chromatic dispersion penalty is calculated to be about 0.1 dB. Thus a traveling wave device acting as the source will not limit the transmission distance due to chromatic dispersion when operating at the fibre dispersion minimum wavelength.

Another point favoring the traveling wave amplifier system is the less polarization dependent traveling wave device gain. The facet reflectivities of any device are polarization dependent, but the AR coating on traveling wave device facets reduces the gain difference between TE and TM polarization as compared to uncoated Fabry-Perot devices [43]. Since the gain and responsivity of traveling wave amplifiers are less sensitive to input signal polarization, this gives the traveling wave amplifiers an advantage over uncoated Fabry-Perot transceivers.

Both the FSHD system and the traveling wave detector system suffer from the relatively high reflections that can take place from non-physical

contact optical connectors. Hence physical contact optical connections must be used for both systems to meet all performance goals.

One issue not addressed in detail in the thesis is the cost of the Fabry-Perot devices versus the cost of traveling wave devices. The application of antireflection coatings on the laser facets is very expensive to achieve extremely low reflectivities, as mentioned previously in Section 1.1.5. Hence this additional cost would be prohibitive in making the traveling wave amplifier system acceptable for mass deployment. It remains to be seen that single layered coatings of higher, yet still acceptable reflectivity be achieved at a low cost [44]. If a low cost AR coating technique can be realized, the full duplex traveling wave amplifier system operating at 1.3 μm may prove to be more attractive for widespread short-haul applications.

CHAPTER 5. CONCLUSIONS

A novel bidirectional optical transmission system utilizing Fabry-Perot lasers as transceivers has been analyzed. The results of this investigation have indicated three important conclusions on the feasibility of implementing the FSHD system for cost sensitive short-haul optical communication.

First, the performance of the FSHD system meets the minimum goals specified for short-haul applications. The overall system was found to have a 16 dB link margin which allowed for 60 Mb/s bidirectional transmission over 13 km of fibre at a 10^{-9} error rate. Turn-off times for the laser diodes (< 5 ns typical) were far better than any other switched half-duplex transceiver system due to the placement of the detection bias current just below threshold.

Second, it was determined that in comparison to other laser diode types (e.g. DFB, ridge waveguide, and transverse junction stripe) without antireflection coating, Fabry-Perot lasers served as the best transceivers for the FSHD system. Some of these different laser types can offer improved performance but will also introduce added difficulties in other parts of the system

Third, it was determined that the traveling wave amplifier transceiver system outlined in [18] and [22] was superior to the FSHD system in two distinct areas: device performance characteristics and device gain stability as a function of wavelength. The traveling wave amplifier detectors offered increased sensitivity and responsivity compared with Fabry-Perot laser detectors. Moreover, the gain (and hence responsivity) of a traveling wave amplifier detector is much less sensitive to signal wavelength and temperature changes than Fabry-Perot type detectors. Although a possible feedback circuit was discussed to maximize Fabry-Perot device responsivity, the implementation of such a feedback circuit will significantly increase the switching time needed between transmitting and receiving. Overall, it remains to be seen if the cost of applying antireflection coatings on the device facets can be lowered to make the traveling wave amplifier system more attractive for cost sensitive applications.

The author would like to recommend further study on traveling wave amplifier transceiver systems operating at 1.3 μm. Since results have been published on such systems operating at 1.55 μm, but no results have yet been published in the literature on systems operating at 1.3 μm, an opportunity exists for extending the research into bidirectional short-haul systems. This research could run concurrently with an in-depth study on cost effective ways of applying AR coatings to achieve optimum performance from traveling wave amplifier transceivers.

REFERENCES

[1] B. S. Kawasaki, K. O. Hill, D. C. Johnson, A. U. Tenne-Sens, "Full Duplex Transmission Link over Single Strand Optical Fiber", *Optics Letters*, Vol. 1, No. 3, pp. 107 - 108, 1977.

[2] Y. Sasaki, K. Tajima, I. Yokohama, "Bidirectional Optical Transmission Using Polarized Light Waves", *Electronics Letters*, Vol. 23, No. 13, pp. 692 - 693, 1987.

[3] R. D. Hall, R. A. Betts, J. P. Moss, "Bidirectional Transmission Over 11 km of Single Mode Optical Fibre at 34 Mb/s Using 1.3 μm LEDs and Directional Couplers", *Electronics Letters*, Vol. 21, No. 14, pp. 628 - 629, 1985.

[4] A. Reichelt, H. Michel, W. Rauscher, "Wavelength Division Multi Demultiplexers for Two Channel Single Mode Transmission Systems", *Journal of Lightwave Technology*, Vol. LT-2, No. 5, pp. 675 - 681, 1984.

[5] G. P. Coombs, "565 Mb/s Duplex Transmission at 1300 nm Over 50 km of Single Mode Optical Fibre", *Electronics Letters*, Vol. 22, No. 15, pp. 821 - 822, 1986.

[6] P. J. Duthie, M. J. Wale, I. Bennion, J. Hankey, "Bidirectional Fibre Optic Link Using Reflective Modulation", *Electronics Letters*, Vol. 22, No. 10, pp. 517 - 518, 1986.

[7] A. Alping, R. Tell, S. T. Eng, "Photodetection Properties of Semiconductor Laser Diode Detectors", *Journal of Lightwave Technology*, Vol. LT-4, No. 11, pp. 1662 - 1668, 1986.

[8] J. P. VanDerZiel, "Characteristics of 1.3 μm Lasers Used as Detectors", *Journal of Lightwave Technology*, Vol. 7, No. 2, pp. 347 - 352, 1989.

[9] J. P. VanDerZiel, R. M. Mikulyak, R. A. Logan, "7.5 km Bidirectional Single Mode Optical Fiber Link Using Dual Mode InGaAsP / InP 1.3 μm Laser Detectors", *Electronics Letters*, Vol. 21, No. 11, pp. 511 - 512, 1985.

[10] A. Alping, R. Tell, "100 Mbit/s Semiduplex Optical Fiber Transmission Experiment Using GaAs / GaAlAs Laser Transceivers", *Journal of Lightwave Technology*, Vol. LT-2, No. 5, pp. 663 - 667, 1984.

[11] N. Kashima, "Properties of Commercial 1.3 μm Fabry-Perot Laser Modules in a Time Compression Multiplexing System", *Journal of Lightwave Technology*, Vol. 9, No. 7, pp. 918 - 923, 1991.

[12] N. Kashima, "Time Compression Multiplex Transmission System Using a 1.3 μm Semiconductor Laser as a Transmitter and a Receiver", *IEEE Transactions on Communications*, Vol. 40, No. 3, pp. 584 - 590, 1992.

[13] R. A. Linke, K. C. Reichmann, T. L. Roch, U. Koren, "Full Duplex Optical Transmission Using Self-Heterodyne Laser Transceivers", *IEEE Photonics Technology Letters*, Vol. 1, No. 9, pp. 278 - 280, 1989.

[14] G. R. Hadley, "Injection Locking of Diode Lasers", *IEEE Journal of Quantum Electronics*, Vol. QE-22, No. 3, pp. 419 - 426, 1986.

[15] R. Lang, "Injection Locking Properties of a Semiconductor Laser", *IEEE Journal of Quantum Electronics*, Vol. QE-18, No. 6, pp. 976 - 983.

[16] H. Kawaguchi, K. Inoue, T. Matsuoka, K. Otsuka, "Bistable Output Characteristics in Semiconductor Laser Injection Locking", *IEEE Journal of Quantum Electronics*, Vol. QE-21, No. 9, pp. 1314 - 1317, 1985.

[17] H. Kawaguchi, "Multiple Bistability and Multistability in a Fabry-Perot Laser Diode Amplifier", *IEEE Journal of Quantum Electronics*, Vol. QE-23, No. 9, pp. 1429 - 1433, 1987.

[18] P. A. Andrekson, N. A. Olsson, "Optical Full Duplex Transmission with Diode Laser Amplifiers", *Journal of Lightwave Technology*, Vol. 9, No. 6, pp. 737 - 740, 1991.

[19] M. Okada, H. Kikuchi, K. Takizawa, H. Fujikake, "Optical Bistability and Set Reset Operation of a Fabry-Perot Semiconductor Laser Amplifier with Two

Detuned Light Injections", *IEEE Journal of Quantum Electronics*, Vol. 27, No. 8, pp. 2003 - 2015, 1991.

[20] M. J. Adams, H. J. Westlake, M. J. O'Mahony, I. D. Henning, "A Comparison of Active and Passive Optical Bistability in Semiconductors", *IEEE Journal of Quantum Electronics*, Vol. QE-21, No. 9, pp. 1498 - 1504, 1985.

[21] K. Otsuka, S. Kobayashi, "Optical Bistability and Nonlinear Resonance in a Resonant Type Semiconductor Laser Amplifier", *Electronics Letters*, Vol. 19, No. 7, pp. 262 - 263, 1983.

[22] M. Gustavsson, A. Karlsson, L. Thylen, "Traveling Wave Semiconductor Laser Amplifier Detectors", *Journal of Lightwave Technology*, Vol. 8, No. 4, pp. 610 - 617, 1990.

[23] B. E. A. Saleh, M. C. Teich, *Fundamentals of Photonics*, New York: John Wiley and Sons, Inc., 1991.

[24] T. Mukai, Y. Yamamoto, "Gain, Frequency Bandwidth, and Saturation Output Power of AlGaAs DH Laser Amplifiers", *IEEE Journal of Quantum Electronics*, Vol. QE-17, No. 6, pp. 1028 - 1034, 1981.

[25] S. Kobayashi, T. Kimura, "Automatic Frequency Control in a Semiconductor Laser and an Optical Amplifier", *Journal of Lightwave Technology*, Vol. LT-1, No. 2, pp. 394 - 401, 1983.

[26] J. S. Cohen, F. Wittgrefe, M. D. Hoogerland, J. P. Woerdman, "Optical Spectra of a Semiconductor Laser with Incoherent Optical Feedback", *IEEE Journal of Quantum Electronics*, Vol. QE-26, No. 6, pp. 982 - 990, 1990.

[27] D. Lenstra, B. H. Verbeek, A. J. Den Boef, "Coherence Collapse in Single Moded Semiconductor Lasers Due to Optical Feedback", *IEEE Journal of Quantum Electronics*, Vol. QE-21, No. 6, pp. 674 - 679, 1985.

[28] N. Schunk, K. Petermann, 'Noise Analysis of Injection Locked Semiconductor Injection Lasers", *IEEE Journal of Quantum Electronics*, Vol. QE-22, No. 5, pp. 642 - 650, 1986.

[29] J. S. Cohen, D. Lenstra, "Spectral Properties of the Coherence Collapsed State of a Semiconductor Laser with Delayed Optical Feedback", *IEEE Journal of Quantum Electronics*, Vol. QE-25, No. 6, pp. 1143 - 1151, 1989.

[30] K. Petermann, *Laser Diode Modulation and Noise*, Dordrecht: Kluwer Academic Publishers, 1988.

[31] N. Schunk, K. Petermann, "Numerical Analysis of the Feedback Regimes for a Single Mode Semiconductor Laser with External Feedback", *IEEE Journal of Quantum Electronics*, Vol. 24, No. 7, pp. 1242 - 1247, 1988.

[32] C. H. Henry, R. F. Kazarinov, "Instability of Semiconductor Lasers Due to Optical Feedback from Distant Reflectors", *IEEE Journal of Quantum Electronics*, Vol. QE-22, No. 2, pp. 294 - 301, 1986.

[33] R. Lang, K. Kobayashi, "External Optical Feedback Effects on Semiconductor Injection Laser Properties", *IEEE Journal of Quantum Electronics*, Vol. QE-16, No. 3, pp. 347 - 355, 1980.

[34] Y. Yamamoto, "Noise and Error Rate Performance of Semiconductor Laser Amplifiers in PCM-IM Optical Transmission Systems", *IEEE Journal of Quantum Electronics*, Vol. QE-16, No. 10, pp. 1073 - 1080, 1980.

[35] G. P. Agrawal, N. K. Dutta, *Long Wavelength Semiconductor Lasers*, New York: Van Nostrand Reinhold Company, 1986

[36] J. O. Binder, *Semiconductor Lasers with Optical Feedback*, Ph. D. Thesis, University of Alberta, Edmonton, Alberta, Fall 1989.

[37] J. Wang, H. Olesen, K. E. Stubkjaer, "Recombination, Gain and Bandwidth Characteristics of 1.3 μm Semiconductor Laser Amplifiers", *Journal of Lightwave Technology*, Vol. LT-5, No. 1, pp. 184 - 189, 1987.

[38] R. Olshansky, C. B. Su, J. Manning, W. Powazinik, "Measurement of Radiative and Nonradiative Recombination Rates in InGaAsP and AlGaAs Light Sources", *IEEE Journal of Quantum Electronics*, Vol. QE-20, No. 8, pp. 838 - 854, 1984.

[39] C. Harder, J. Katz, S. Margalit, J. Shacam, A. Yariv, "Noise Equivalent Circuit of a Semiconductor Laser Diode", *IEEE Journal of Quantum Electronics*, Vol. QE-18, No. 3, pp. 333 - 337, 1982.

[40] J. L. Gimlett, N. K. Cheung, "Dispersion Penalty Analysis for LED/Single Mode Fiber Transmission Systems", *Journal of Lightwave Technology*, Vol. LT-4, No. 9, pp. 1381 - 1391, 1986.

[41] K. Ogawa, "Analysis of Mode Partition Noise in Laser Transmission Systems", *IEEE Journal of Quantum Electronics*, Vol. QE-18, No. 5, pp. 849 - 855, 1982.

[42] G. P. Agrawal, P. J. Anthony, T. M. Shen, "Dispersion Penalty of 1.3 μm Lightwave Systems with Multimode Semiconductor Lasers", *Journal of Lightwave Technology*, Vol. 6, No. 5, pp. 620 - 625, 1988.

[43] M. J. O'Mahony, "Semiconductor Laser Optical Amplifiers for Use in Future Fiber Systems", *Journal of Lightwave Technology*, Vol. 6, No. 4, pp. 531 - 544, 1988.

[44] C. Janz, Private communication.

[45] B. G. Streetman, *Solid State Electronic Devices*, Englewood Cliffs: Prentice Hall, 3rd Ed., 1990.

[46] D. M. Fye, "Relationship Between Carrier Induced Index Change and Feedback Noise in Diode Lasers", *IEEE Journal of Quantum Electronics*, Vol. QE-18, No. 10, pp. 1675 - 1678, 1982.

[47] L. Glimmer, E. Goobar, L. Thylen, M. Gustavsson, "Semiconductor Laser Amplifier Optimization: An Analytical and Experimental Study", *IEEE Journal of Quantum Electronics*, Vol. 25, No. 8, pp. 1822 - 1827, 1989.

APPENDIX 1

RELATIONSHIP BETWEEN DIODE VOLTAGE AND CARRIER DENSITY

To begin with the derivation linking laser diode junction voltage and carrier density, we start with the Fermi Dirac distribution function. This function states that under thermal equilibrium at an absolute temperature T, the probability $f(E)$ that an electron is in a state of energy E is given by [23, 45]

$$f(E) = \frac{1}{e^{(E-E_f)/kT} + 1} \tag{A.1}$$

where E_f = Fermi energy or Fermi level and k = Boltzmann's constant. The probability of a hole in a state of energy E follows as $1-f(E)$.

Now consider that electrons and holes are only allowed to occupy certain energy states in a semiconductor material. Allowed states are above the conduction band edge E_C and below the valence band edge E_V. In between these two energy levels, called the energy gap E_g, there are no energy states for an electron or hole to occupy. The density of allowable energy states in the conduction and valence bands $\rho_C(E)$ and $\rho_V(E)$ as a function of energy are

$$\rho_c(E) = \frac{4\pi(2m_c)^{1.5}}{h^3}\sqrt{E - E_c}, \; E \geq E_c \tag{A.2}$$

and

$$\rho_v(E) = \frac{4\pi(2m_c)^{1.5}}{h^3}\sqrt{E_v - E}, \; E \leq E_v \tag{A.3}$$

where m_C = effective electron mass in conduction band, m_V = effective electron mass in valence band, and h = Planck's constant.

It can be seen from (A.2) and (A.3) that the density of states obeys a square root law as energy is increased from the conduction band edge or decreased from the

valence band edge. To find the density of electrons n_O in the conduction band, the product of the density of states function and probability of occupancy function is integrated over all energies in the conduction band by calculating

$$n_O = \int_{E_c}^{\infty} \rho_c(E) f(E) dE \qquad \text{(A.4).}$$

A similar integration is performed for the hole density p_O in the valence band using

$$p_O = \int_{-\infty}^{E_v} \rho_v(E)[1 - f(E)] dE \qquad \text{(A.5).}$$

Now consider a steady state electron injection taking place in the active region of a laser diode. The excess injected carriers n modify the location of the Fermi level. Instead of a single Fermi level E_f to calculate the probability of electron or hole occupancy of a particular energy state, separate probability functions are defined for the conduction band and valence band. The conduction band Fermi function f_C and valence Fermi function f_V are defined as

$$f_c(E) = \frac{1}{e^{(E-E_{fc})/kT} + 1} \qquad \text{(A.6)}$$

and

$$f_v(E) = \frac{1}{e^{(E-E_{fv})/kT} + 1} \qquad \text{(A.7)}$$

respectively, where E_{fC} = conduction band Fermi level and E_{fV} = valence band Fermi level.

These separate Fermi functions are now used to calculate the carrier density in the active region by using the new distributions in (A.6) and (A.7) in place of the single Fermi function (A.1) to give

$$n + n_o = n = \int_{E_c}^{\infty} \rho_c(E) f_c(E, E_{fc}) dE \qquad \text{(A.8)}$$

and

$$n + p_o = n = \int_{-\infty}^{E_v} \rho_v(E)[1 - f_v(E, E_{fv})] dE \qquad \text{(A.9).}$$

In (A.8) and (A.9) the value of the injected carrier density n will be much larger than the intrinsic concentrations n_O or p_O, so the sum of the two quantities is approximately equal to the value of the injected carrier density. Expanding (A.8) and (A.9) gives

$$n = \frac{4\pi(2m_c)^{1.5}}{h^3} \int_{E_c}^{\infty} \frac{\sqrt{E - E_c}}{e^{(E - E_{fc})/kT} + 1} dE \qquad \text{(A.10)}$$

and

$$n = \frac{4\pi(2m_v)^{1.5}}{h^3} \int_{-\infty}^{E_v} [\sqrt{E_v - E} - \frac{\sqrt{E_v - E}}{e^{(E - E_{fv})/kT} + 1}] dE \qquad \text{(A.11)}$$

respectively. Unfortunately two integral equations (A.10) and (A.11) do not have a closed form solution. A numerical integration must be performed to solve for E_{fc} and E_{fv} when given a value for the injected carrier density n.

Finally, the voltage present across the junction of a semiconductor laser diode (below the threshold point)v is given by [22]:

$$v = \frac{E_{fc} - E_{fv}}{q} \qquad \text{(A.12)}$$

where q = electronic charge and E_{fc} and E_{fv} are in units of Joules. Equations (A.1) through (A.12) provide an analytical means of calculating the quasi-Fermi levels and hence diode junction voltage as a function of carrier density.

APPENDIX 2

LISTING OF MATHEMATICA PROGRAM MODEL.M

The following *Mathematica* program model.m uses equations from the paper written by Okada et al [19]. The program outputs data to a file which can then be plotted using any available plotting routine. Comment statements within the program are contained in the star brackets. Periodic explanations are given throughout the program to describe the function of individual sections.

```
(*PROGRAM model.m    June 10/ 93*)

(*Constants*)
```

The first part of the program defines all the constants needed for subsequent equations. The physical quantity represented by individual constants are described in the star brackets.

```
c = 3 10^8;                          (* speed of light: m/sec  *)
q = 1.6 10^-19;                      (* electronic charge: C  *)
nr = 3.8;                            (* index of refraction of active layer *)
gamma = 0.46;                        (* mode confinement factor for TE *)
neffn = 1.25;                        (* ratio of effective index to actual index *)
dwcdn = 2.14 10^-12;

(* change in resonant frequency with respect to carrier density: m^3/sec  *)

v = 2 10^-9;                         (* effective carrier lifetime: sec *)
smallg = 0.856 10^-12;

(* change in material gain (per second) with respect to carrier density: m^3/sec *)

taup =1.65 10^-12;                   (* photon lifetime: sec *)
beta = 10^-5;                        (* spontaneous emission factor *)
taunot = 2 10^-12;

(* effective time constant from spontaneous emission to contribute to stimulated
emission- see [16]: sec *)
```

The next section defines important parameters such as the threshold carrier density ("nth"), input wavelength ("lambda"), bias carrier density ("nnot"), and the fraction of normalized optical power coupled into the amplifier ("x1").

```
nth = 1.873;                          (* threshold carrier density: m^-3  *)
lambda = 1.310 10^-6;                 (* peak input wavelength: m *)
w1 = 2 Pi c / lambda;                 (* peak input optical frequency: rad/sec *)
nnot = 1.7;                           (* bias carrier density value: m^-3 *)
x1 = 0.5;

(* fraction of normalized optical power coupled into amplifier *)
```

The facet reflectivity ("R") and the dimensions of the active region of the device are now defined.

```
R = 0.32;                             (* facet reflectivity of device *)

(*Volume*)

l = 270 10^-6;                        (* length of device: m *)
w = 10 10^-6;                         (* width of active region: m *)
d = 0.2 10^-6;                        (* depth of active region: m *)
vol = l w d;                          (* volume of active region: m^3 *)

(* Definitions  *)
```

The next section starts defining equations from [19] which will generate the asymmetric responsivity curves. The constant "tauc" is the photon lifetime and the equation for "wnot" is Equation (3) from [19].

```
ith = q vol (nth 10^24 / taus);       (* threshold current: A*)
tauc = nr l / (c (1 - R));            (* time constant : sec *)
wnot[nnot_] := w1 + dwcdn (nnot 10^24 - 1.6 10^24);
```

The next three equations define "Y00", the power at frequency "wnot", and "Y10", the power at frequency "w1", all at a bias carrier density. The injection current as a function of carrier density ("iinj[nnot]") is also defined. . These three equations correspond to (7) (8) and (9) from [19].

```
Y00[nnot_] := (beta / (smallg taunot)) nnot 10^24 / (nth 10^24 - nnot 10^24)^2;

Y10[nnot_] := Y00[nnot] / (1 + 4 neffn^2 (w1 - wnot[nnot])^2 / (gamma^2
smallg^2 (nth 10^24 - nnot 10^24)^2));

iinj[nnot_] := q vol ((nnot 10^24 / taus) + 1 / (smallg taus) (1 / (gamma taup) +
smallg (nnot 10^24 - nth 10^24)) (Y00[nnot] + Y10[nnot]));
```

Calculate the power at frequency w1 ("Y1") and at frequency wnot ("Y0") and resolve rate equation for a new lower carrier density.

```
(* Simultaneous solution of 3 steady state equations *)

Y1[n_, nnot_] := (gamma Sqrt[beta smallg n 10^24 / taunot] + x1/tauc)^2 /
(gamma^2 smallg^2 (nth 10^24 - n 10^24)^2 + 4 (neffn (wnot[nnot] - w1) +
dwcdn (n 10^24 - nnot 10^24))^2);

Y0[n_, nnot_] := (gamma^2 beta smallg n 10^24 / taunot) /(gamma^2 smallg^2
(nth 10^24 - n 10^24)^2 + 4 dwcdn^2 (n 10^24  - nnot 10^24)^2);

(* State output file *)
```

The output is then written to an output file for plotting with an x-y plot routine. Two columns of data are written to the output file: frequency detuning ("v0 - v1") and the change in carrier density as a result of the optical injection ("diff1").

```
OpenWrite["/home/decs/corazza/Mathemat/data.1", FormatType -> TextForm];

(* Equations *)

count = -0.1;

deltan[count_] := 1.6 + count;

While[count <= 0.1, count +=0.005;
        sol1 = FindRoot[{iinj[deltan[count]] == q vol ((n 10^24 / taus) + 1 /
        (smallg taus) (1 / (gamma taup) + smallg (n 10^24 - nth 10^24)) (Y0[n,
        deltan[count]] + Y1[n, deltan[count]]))}, {n, 1, 2} ];

        sol2 = FindRoot[{iinj[deltan[count]] == q vol ((n 10^24 / taus) + 1 /
        (smallg taus) (1 / (gamma taup) + smallg (n 10^24 - nth 10^24)) Y0[n,
        deltan[count]])}, {n, 1, 2} ];
```

```
        off = n /. sol2;
        on = n /. sol1;
        diff1 = off - on;
        Write["/home/decs/corazza/Mathemat/data.1", N[(wnot[deltan[count]] -
        w1)/(2 Pi 10^12), 6], "          ", diff1];
];
```

Close the output file.

```
Close["/home/decs/corazza/Mathemat/data.1"]
```

APPENDIX 3

LISTING OF MATHEMATICA PROGRAM NOISEFPA.M

The following *Mathematica* program noisefpa.m uses equations from the paper written by Gustavsson et al [22] along with the theory from [34]. The program outputs the bit error rate of the detector as a function of input optical power. Comment statements in the program are contained in the star brackets. Periodic explanations are given throughout the program to describe the function of the individual sections.

```
(* PROGRAM noisefpa.m  June 22 / 93  *)

(* This program takes equations 18, 19, 26, 27, 29, 30, 31, 32, and 33 from
Gustavsson's TWA paper and makes necessary modifications for a FP amplifier by
using equation (44) from Yamamoto instead of using equation (31) from
Gustavsson.  Equation (44) must be integrated over the cavity length l and
substituted in Gustavsson equation (30) to calculate i2ph[pin].  Result is BER
curves vs. input power with peak amplifier gain as a parameter. *)

(* Constants *)
```

The first part of the program defines all the constants needed for the program.

```
c = 3. 10^8;                    (* speed of light: m/s*)
h = 6.6262 10^-34;              (* Planck's constant: J s*)
temp = 300.;                    (* temperature: K*)
k = 1.38 10^-23                 (* Boltzmann's constant: J/K*)
q = 1.6 10^-19;                 (* electronic charge: C*)

l = 270. 10^-6                  (* length of active region: m*)
w = 10. 10^-6;                  (* width of active region: m*)
d = 0.2 10^-6;                  (* depth of active region: m*)

R1 = 0.32;                      (* facet 1 power reflectivity *)
R2 = 0.32;                      (* facet 2 power reflectivity *)

gamma = 0.3;                    (* mode confinement factor *)
neff = 3.6;                     (* refractive index of active region *)
biga = 7. 10^7;                 (* recombination coefficient from [47] *)
```

```
bigb = 4. 10^-17;                (* recombination coefficient from [47] *)
bigc = 2.5 10^-41;               (* recombination coefficient from [47] *)
vol = l w d;                     (* volume of active region: m^3 *)
```

The threshold current ("ith") was empirically located by finding the point where the dc light output rapidly increased with injection current. This resulted in ith ≈ 53 mA. The value of other constants are deemed appropriate for InGaAsP.

```
ith = 0.053038;                  (* threshold current approx. *)
betasp = 1. 10^-4;               (* sp. emiss. coupled into lasing mode [35]*)
df =c / (2. neff l);             (* frequency sep. of F-P long. modes: Hz*)
nsp = 1.7;                       (* spontaneous emission factor from [35]*)
kappa = 2.7 10^19;

(* change in material gain with respect to lambda parameter: m^-3*)

dlpdn = 2.0 10^-32;

(* change in carrier density with respect to lambda: m^4*)

a =1.8 10^-20;

(* change in material gain with respect to carrier density: m^2*)

lambdanot = 1.300;               (* peak wavelength: um*)
```

Define input optical power ("p1[pin]"), bandwidth ("bnot"), material loss ("alpha") and other important constants.

```
(* Input Power  *)

p1[pin_] := 10^((pin - 30.) / 10);   (* input optical power: dBm*)

(* Electrical BW, F, and cct R *)

bnot = 30 10^6;                  (* electrical bandwidth: Hz*)
f =6.3;                          (* noise figure of electrical amplifier: 8 dB*)
res = 50;                        (* external load resistance: ohms*)

(* Carrier density and current *)

nnot = 1.85                      (* transparent carrier density: 10^24 m^-3*)
alphas = 2000;                   (* scattering loss in active region: m^-1*)
alphaf = -1 / (2 l) Log[R1 R2];  (* facet loss: m^-1*)
```

```
alpha = alphas + alphaf;                (* total material loss per unit length: m^-1*)
nth = nnot + alpha / a 10^-24;          (* threshold carrier density: 10^24 m^-3  *)

(* Carrier density at bias point *)

(*G = 3  dB deltan =                    2.026 @ 83%  *)
(*G = 6  dB deltan =                    2.074 @ 88%  *)
(*G = 10 dB deltan =                    2.118 @ 92%  *)
(*G = 13 dB deltan =                    2.142 @ 90%  *)
(*G = 15 dB deltan =                    2.152 @ 95%  *)
```

Define bias carrier density ("deltan"), calculate steady state photon number ("sa") and solve for steady state injection current ("iinj").

```
deltan = 2.152;                         (* bias carrier density : 10^24 m^-3 *)

(* Calculate photon number from carrier density - from [35] *)

sa = betasp bigb (deltan 10^24)^2 vol / (c alpha / neff - a c / neff (deltan - nnot)
10^24);

(*Calculate iinj from carrier density and photon number - Agrawal*)

righta = ( a c / neff / vol (deltan - nnot)) sa;
sola = FindRoot[0 == ix / (q vol) 10^-24 - biga deltan - bigb deltan^2 10^24 - bigc
deltan^3 10^48 - righta, {ix, 0, 0.2}, AccuracyGoal -> 6, WorkingPrecision ->
60, MaxIterations -> 400]

(* Solution *)

iinj = (ix /. sola);
```

Define input wavelength ("lambdain"), peak cavity gain wavelength ("peakl"), material gain ("peakgm"), single pass gain ("peakG"), envelope cavity gain ("env" and "envdb"), and cavity gain ("peakcavityg").

```
(* Solve for material gain peakgm *)

lambdain = 1944. / 1495.;               (* input wavelength: um*)

peakl = 1944. / 1495.;                  (* peak gain wavelength: um*)

peakgm[lambdain_] :=  (a(deltan - nnot) 10^24 - kappa (lambdain 10^-6 - peakl
10^-6)^2) / gamma;
```

```
peakG[lambdain_] := Exp[(gamma peakgm[lambdain] - alphas) l];
envelope[lambdain_] := (1 - R1) (1 - R2) peakG[lambdain] / (1 - Sqrt[R1 R2]
peakG[lambdain])^2;

envdb[lambdain] := 10 Log[10, envelope[lambdain]];

peakcavityg[lambdain_] := (1 - R1) (1 - R2) peakG[lambdain] / ((1 - Sqrt[R1 R2]
peakG[lambdain])^2 + 4 Sqrt[R1 R2] peakG[lambdain] Sin[2 Pi l neff / (lambdain
10^-6)]^2);
```

Print results

```
(*Print["lambdain = ", N[lambdain, 5], " , peakcavityg[lambdain, -20] = ",
N[peakcavityg[lambdain, -20], 5], "  iinj = ", N[iinj, 5]];*)
```

Calculate "nquantum"- equation (19) from [22].

```
nquantum[lambdain_] := N[(1- R2) (1 + R1 peakG[lambdain]) (peakG[lambdain] -
1) / ((1 - Sqrt[R1 R2] peakG[lambdain])^2 + 4 Sqrt[R1 R2] peakG[lambdain]
(Sin[2 Pi neff l / (lambdain 10^-6)])^2) gamma peakgm[lambdain] / (gamma
peakgm[lambdain] - alphas)];

(* Print output *)

Print["peakcavitygain@ -20 = ", N[10 Log[10, envelope[peakl]],5], "  dB. "];
Print["carrier density = ", deltan, " at i = ", N[100 iinj / ith, 5], " % ith."];

(* Check responsivity *)
```

Calculate responsivity. Change in Fermi level separation with respect to carrier density = "dufdn", "drdn" = change in recombination rate with respect to carrier density, "isig" = equivalent signal current, "ssignot" = Equation (3) from [22], "ri" = Equation (21) from [22], "resp" = Equation (11) from thesis.

```
dufdn = 5. 10^-26;

drdn[deltan_] := biga + 2 bigb deltan 10^24 + 3 bigc deltan^2 10^48;

isig[pin_] := q lambdain / (h c) p1[pin] nquantum[lambdain] 10^-6;
```

```
ssignot[pin_] := N[(1 - R1) (1 + R2 peakG[lambdain]) (peakG[lambdain] - 1) / ((1
- Sqrt[R1 R2] peakG[lambdain])^2 + 4 Sqrt[R1 R2] peakG[lambdain] Sin[2 Pi
neff l / (lambdain 10^-6)]^2) lambdain 10^-6 p1[pin] neff / (h c vol (gamma
peakgm[lambdain] - alphas))];

ri[pin_] := dufdn / (q vol (drdn[deltan] + gamma a ssignot[pin]));

resp[pin_] := isig[pin] ri[pin] 50 / (53 + ri[pin]) / p1[pin]; Print["responsivity -20 =
", resp[-20]];
```

Start sensitivity calculation.

```
(* PART 2: CALCULATION OF THE AVERAGE OF THE VARIANCE OF THE
NUMBER OF PHOTONS OVER THE AMPLIFIER LENGTH l  *)
```

Single pass gain as a function of length x (x in um) = "GS[x]". "GSlong" is single pass gain for other longitudinal modes.

```
(* Single pass gain *)

GS[x_] := Exp[(gamma peakgm[lambdain] - alphas) x 10^-6];

GSlong[x_, inc_] := Exp[(gamma peakgm[1944./ inc] - alphas) x 10^-6];
```

The following loop looks for the range of longitudinal modes that have a net gain. These modes will then be used later to solve for noise contributions. Constants "inc" and "stop" are the minimum and maximum modes that have net gain.

```
(* Test for # of longitudinal modes *)

small = 1470.;
large = 1530.;

test1[small_] := peakgm[1944. / small]; test2[small_] := peakgm[1944. / (small +
1.)]; test3[large_] := peakgm[1944. / large]; test4[large_] := peakgm[1944. / (large
- 1.)];

For[small = 1470., Sign[test1[small]] == Sign[test2[small]], small++1];
For[large = 1530., Sign[test3[large]] == Sign[test4[large]], large--1];

inc = small + 1.;
stop = large - 1.;
```

```
(* Expressions to be integrated *)
```

Set up equations to be integrated. Comes from Equation (16) in thesis.

```
expr1[x_] := (1 - R1) (1 - R2) GS[x] / (1 - Sqrt[R1 R2] GS[x])^2;

expr2[x_,inc_] := (1 + R1 GSlong[x, inc]) (1 - R2) (GSlong[x, inc] - 1) nsp df / (1
- R1 R2 (GSlong[x, inc])^2);

expr3[x_] := (1 + R1 GS[x]) (1 - R1) (1 - R2)^2 GS[x] (GS[x] - 1) nsp / (1 -
Sqrt[R1 R2] GS[x])^4;

expr4[x_,inc_] := (1 + R1 GSlong[x, inc])^2 (1 - R2)^2 (GSlong[x, inc] - 1)^2
nsp^2 (1 + R1 R2 (GSlong[x, inc])^2) df / (1 - R1 R2 (GSlong[x, inc])^2)^3;

(* Integrate *)
```

Average quantities over amplifier length "l" (Equation 18 from thesis) and calculate total noise current variance (Equation 17 from thesis). "sol1" = signal shot noise term, "sol2" = spont. shot noise term, "sol3" = signal spont. beat noise term, "sol4" = spont. spont. beat noise term.

```
sol1 = NIntegrate[q^2 gamma^2 peakgm[lambdain]^2 expr1[x], {x, 0, l 10^6}]
Print ["Done #1:  ", sol1];

(* Sum over longitudinal modes: sol2 -> spontaneous shot noise term *)

subtot2 = 0.;
While[inc <= stop,
        pass2 = NIntegrate[q^2 gamma^2 peakgm[1944. / inc]^2 expr2[x, inc], {x,
        0, l 10^6}]; subtot2 += pass2;
        inc += 1.;
];
sol2 = subtot2;
Print ["Done #2:  ", sol2];

sol3 = NIntegrate[q^2 gamma^2 peakgm[lambdain]^2 expr3[x], {x, 0, l 10^6}]
 Print ["Done #3:  ", sol3];

(* Sum over longitudinal modes: sol4 -> spont spont beat noise term *)

inc = small + 1.;
stop = large - 1.;
```

```
subtot4 = 0.;
While[inc <= stop,
        pass4 = NIntegrate[q^2 gamma^2 peakgm[1944. / inc]^2 expr4[x, inc], {x,
        0, l 10^6}]; subtot4 += pass4;
        inc += 1.;
];
sol4 = subtot4;
Print ["Done #4:  ", sol4];
```

Calculate individual noise current contributions. "i2shot" = detector shot noise, "i2th" = thermal noise, "i2sshot" = signal shot noise, "i2spshot" = spont. shot noise, "i2ssp" = signal spont. beat noise, "i2spsp" = spont. spont. beat noise, "i2ph" = sum of the last four noise currents, "itot" = sum of all noise currents.

```
i2shot = 2 q iinj bnot;

i2th = (1 / res + (f - 1) / res) 4 k temp bnot;

i2sshot[pin_] := l lambdain 10^-6 p1[pin] / (h c) sol1 bnot;

i2spshot =  l sol2 bnot;

i2ssp[pin_] := l 2 lambdain 10^-6 p1[pin] / (h c) sol3 bnot;

i2spsp =  l sol4 bnot;

i2ph[pin_] := i2sshot[pin] + i2spshot + i2ssp[pin] + i2spsp;

itot[pin_] := i2shot + i2th + i2ph[pin];
```

Signal to noise ratio calculation- Equation (20) from thesis.

```
dbsnrone[pin_] := 10 Log[10, Abs[isig[pin]^2 / (i2shot + i2th + i2ph[pin])]];

snrone[pin_] := N[Abs[isig[pin]^2 / (i2shot + i2th + i2ph[pin])]];

testp = -20;

Print[" Signal equivalent current              = ",isig[testp]];
Print[" Detector shot noise                    = ",i2shot];
Print[" Thermal noise                          = ",i2th];
Print[" Signal shot noise                      = ",i2sshot[testp]];
Print[" Spontaneous shot noise                 = ",i2spshot];
Print[" Signal spontaneous beat noise          = ",i2ssp[testp]];
```

```
Print[" Spont spont beat noise                    = ",i2spsp];
```

Bit error rate calculation- Equation (21) from thesis.

```
ber[pin_] := 0.5 (Erf[Sqrt[snrone[pin]/2], Infinity]);
```

Bit error rate plot as a function of input power in Mathematica

```
LogPlot[ber[pin], {pin, -30, -10}, Frame -> True, FrameLabel -> {"Input optical
power (dBm)", "Bit error rate"}, AspectRatio -> 1, PlotRange -> {-12,-4},
PlotLabel -> {deltan, envdb[lambdain], bnot}]
```

Individual noise current plot as a function of input power in Mathematica.

```
LogPlot[{i2th,i2shot,i2sshot[pin],i2spshot,i2ssp[pin],i2spsp}, {pin, -30, -10},
PlotLabel -> {deltan, envdb[lambdain], bnot}, AspectRatio -> 1, PlotRange -> {-
14, -4}, Frame -> True, FrameLabel -> {"Input optical power (dBm)", "Noise
current density (A^2/Hz)"}]
```

APPENDIX 4

LISTING OF MATHEMATICA PROGRAM AGRAWAL.M

The following *Mathematica* program agrawal.m uses the rate equations in Section 2.4.1.1 and simulates the differential equation for carrier density for a step change in injection current.. The program can then plot the result to identify the turn-off time of the laser due to internal electron hole recombination. In addition, the program can be used to arrive at a turn-on time for the laser diode by modifying the initial and final values for carrier density in the active region. Comment statements in the program are contained in the star brackets. Periodic explanations are given in boxes throughout the program to describe the function of the individual sections.

```
(*PROGRAM agrawal.m  Apr 7/ 93*)

(* This program solves the rate equations for a laser diode and plots the result
versus time. The program can be used to solve for a turn-on time where startn <
endn or for a turn-off time due to internal recombination where startn > endn.
*)
```

The first part of the program defines constants to be used in later equations.

```
(*Constants*)

c = 3 10^8;                          (* speed of light: m/s *)
h = 6.6262 10^-34;                   (* Planck's constant: J s *)
dgdn = 1.2 10^-12;

(* change in material gain (per second) with respect to carrier density: m^3/sec *)

nr = 3.6;                            (* refractive index of active layer *)
l = 270 10^-6;                       (* length of active layer : m *)
w = 10 10^-6;                        (* width of active layer: m *)
d = 0.2 10^-6;                       (* depth of active layer: m *)
R = 0.32;                            (* facet reflectivity of device *)
```

```
(*Effective total loss *)

alphai = 2000;                    (* material loss in active layer: m^-1 *)
alphaf = -1 / (2 l) Log[R R];     (* facet loss: m^-1 *)
alpha = alphai + alphaf;          (* total losses in active layer: m^-1 *)

(* A, B, and C coefficients *)

biga = 7 10^7;                    (* recombination coefficient: sec^-1 [47]*)
bigb = 4 10^-17;                  (* recombination coefficient: m^3/sec [47]*)
bigc = 2.5 10^-41;                (* recombination coefficient: m^6/sec [47]*)

(*Other constants *)

q = 1.6 10^-19;                   (* electronic charge: C *)
vol = l w d;                      (* volume of active layer: m^3*)
nth = 2.39174;                    (* threshold carrier density: 10^24 m^-3*)
```

"vt" and "idark" are values that are fitted to experimental data. Experimental data of diode voltage versus current was fitted to the equation I = idark (Exp[V/vt] - 1) to obtain an estimate of the diode I-V characteristic.

```
vt = 0.048;                       (* I-V parameter fitted to exp. data*)

idark = 0.1 10^-10;               (* I-V parameter fitted to exp. data*)

betasp = 10^-4;                   (* spontaneous emission factor: from [23]*)
```

Calculate transparency point and steady state values for injection current ("iinj") and diode voltage ("volt").

```
(* Compute transparency point *)

ntr = nth - c alpha / (nr dgdn 10^24);  (* transparent carrier density: m^-3 *)

(*Calculate iinj from carrier density and photon number - Agrawal*)

right[deltan_] := betasp bigb deltan^2 10^48 dgdn (deltan - ntr) 10^24 / (c alpha /
nr - dgdn (deltan - ntr) 10^24);

sdc[deltan_] := betasp bigb deltan^2 10^48 vol / (c alpha / nr - dgdn (deltan 10^24 -
ntr 10^24));
```

```
iinj[deltan_] := q vol ( biga deltan 10^24 + bigb deltan^2 10^48 + bigc deltan^3
10^72 + right[deltan]);

volt[deltan_] := vt Log[q vol / idark (biga deltan 10^24 + bigb deltan^2 10^48 +
bigc deltan^3 10^72 + right[deltan]) + 1];

(* Global parameters *)
```

Define initial, intermediate and final conditions. "startn" = initial carrier density, "intern" = intermediate carrier density (interim or accelerator pulse), "endn" = final carrier density, "cuttime" = duration of interim or accelerator pulse, "plottime" = time range for plot. Note that if the interim pulse response is not desired (when calculating turn-on time), "cuttime" should be set to zero.

```
startn = 2.3917;
intern = 1.3.;
endn = 2.2;

cuttime = 0.27 10^-9;

lowlim = 0;
uplim = 2.4;

plottime = 80 10^-9;
```

Solve the differential equation for carrier density for the interim or accelerator drive pulse (for the interval of time from t= 0 to t = cuttime)

```
(* NDSolve - Part 1 of double plot *)

nnot1 = startn;

snot1 = sdc[startn];

ifinal1 = iinj[intern];

sol1 = NDSolve[{n'[t] == ifinal1 / (q vol) 10^-24 - biga n[t] - bigb (n[t])^2 10^24
- bigc (n[t])^3 10^48 -dgdn / vol (n[t] - ntr) s[t], s'[t] == (dgdn (n[t] - ntr) 10^24 -
c alpha / nr) s[t] + betasp bigb (n[t])^2 vol 10^48, n[0] == nnot1, s[0] == snot1},
{n,s}, {t, 0, 0.000001}, WorkingPrecision -> 15, AccuracyGoal -> 9, MaxSteps
-> 5000];
```

Solve the differential equation for carrier density for after the interim pulse (for the interval of time from t = cuttime on). Note that the final values obtained for the interim pulse in the previous section become the initial conditions for this section.

```
(* NDSolve - Part 2 of double plot *)

nnot2 = Evaluate[n[cuttime] /. sol1] [[1]];

snot2 = Evaluate[s[cuttime] /. sol1] [[1]];

ifinal2 = iinj[endn];

sol2 = NDSolve[{n'[t] == ifinal2 / (q vol) 10^-24 - biga n[t] - bigb (n[t])^2 10^24
- bigc (n[t])^3 10^48 -dgdn / vol (n[t] - ntr) s[t], s'[t] == (dgdn (n[t] - ntr) 10^24 -
c alpha / nr) s[t] + betasp bigb (n[t])^2 vol 10^48, n[0] == nnot2, s[0] == snot2},
{n,s}, {t, 0, 0.000001}, WorkingPrecision -> 15, AccuracyGoal -> 9, MaxSteps
-> 5000];
```

Solve the differential equation for carrier density with no interim pulse (from t = 0 on).

```
(* NDSolve - Part 3 single plot only *)

nnot3 = startn;

snot3 = sdc[startn];

ifinal3 = iinj[endn];

sol3 = NDSolve[{n'[t] == ifinal3 / (q vol) 10^-24 - biga n[t] - bigb (n[t])^2 10^24
- bigc (n[t])^3 10^48 -dgdn / vol (n[t] - ntr) s[t], s'[t] == (dgdn (n[t] - ntr) 10^24 -
c alpha / nr) s[t] + betasp bigb (n[t])^2 vol 10^48, n[0] == nnot3, s[0] == snot3},
{n,s}, {t, 0, 0.000001}, WorkingPrecision -> 15, AccuracyGoal -> 9, MaxSteps
-> 5000];

(* Call comparison plot *)
```

Call Mathematica plot to show the difference between the response with and without a lower interim pulse. The command superimposes the original response and the ultrafast response.

```
Show[Plot[Evaluate[n[t] /. sol1], {t, 0, cuttime}, PlotRange -> {{0, plottime},
{lowlim, uplim}}, Frame -> True ], Plot[Evaluate[n[t - cuttime] /. sol2], {t
,cuttime , plottime}, PlotRange -> {{0, plottime}, {lowlim, uplim}}, Frame ->
True ], Plot[Evaluate[n[t ] /. sol3], {t ,0 , plottime}, PlotRange -> {{0, plottime},
{lowlim, uplim}}, Frame -> T
rue ], PlotLabel -> "Concatenated plots "]
```

Plot the voltage decay in Mathematica from the calculated carrier density decay as a function of time.

```
Plot[volt[Evaluate[n[t] /. sol3]], {t, 0, 200 10^-9}, PlotRange -> {0.75, 1.2},
PlotLabel -> " Turn-off time to Zero "]
```

Note: this program can also be used to calculate the theoretical turn-on delay of the laser. By making the starting carrier density zero and the final carrier density above threshold and eliminating the sections that use an interim pulse to calculate turn-off time, this program can output plots of carrier density and photon number like those in Figures 23 and 24.